This is to certify that the
dissertation entitled

DESIGN AND CHARACTERIZATION OF
NANOSTRUCTURED BIOMIMETIC INTERFACES
CONTAINING BILAYER LIPID MEMBRANES

presented by

SACHIN RAMANLAL JADHAV

has been accepted towards fulfillment
of the requirements for the

Ph.D. degree in Chemical Engineering

Robert Mark Worden

Major Professor's Signature

9/30/2009

Date

DESIGN AND CHARACTERIZATION OF NANOSTRUCTURED BIOMIMETIC INTERFACES CONTAINING BILAYER LIPID MEMBRANES

By

Sachin Ramanlal Jadhav

A DISSERTATION

Submitted to
Michigan State University
in partial fulfillment of the requirements
for the degree of

DOCTOR OF PHILOSOPHY

Chemical Engineering

2009

ABSTRACT

DESIGN AND CHARACTERIZATION OF NANOSTRUCTURED BIOMIMETIC INTERFACES CONTAINING BILAYER LIPID MEMBRANES

By

Sachin Ramanlal Jadhav

Cell membranes carry out several molecular recognition, communication, transport, and catalytic functions to maintain cellular homeostasis. Various membrane proteins and other biomolecules embedded in the cell membrane contribute specific physiological functions and often require a lipid bilayer environment to express their activities. Biomimetic interfaces containing artificial bilayer lipid membrane (BLM) with embedded membrane proteins can effectively reproduce functions of biological cell membranes *in vitro*. These interfaces have many potential applications in fundamental and applied research. BLM-containing interfaces can be used in functional proteomics research to characterize novel membrane proteins, to investigate receptor-drug interactions for high-throughput drug screening, and in development of biosensor systems that exploit specific interactions between membrane proteins and analytes.

The central theme of this work is to develop robust, model membrane interfaces that are easy to fabricate, directly addressable by various analytical techniques, and suitable for advanced research and commercial applications. Three different BLM interfaces, namely planar unsupported BLMs, supported BLMs (sBLM), and tethered BLMs (tBLM), were fabricated and characterized using electrochemical techniques. Planar BLM and tBLM interfaces were used for functional characterization of ion channel membrane proteins. PorB class II (PorBII), a transmembrane pore-forming protein from *Neisseria meningitidis*, was incorporated in a tBLM interface and the ion

transport mediated by porin was measured using electrochemical impedance spectroscopy (EIS). EIS study of PorBII porin incorporated in a tBLM interface showed that the porin's conductance decreases with increase in applied DC potential. The porin conductance values were restored after returning to lower potentials. Parallel single channel studies conducted using planar BLMs revealed that PorBII forms a trimeric pore in BLM that undergoes a reversible, voltage-dependent closure at high transmembrane potentials, corroborating tBLM findings. In addition to measuring proteins' activities, novel methods were developed to incorporate membrane proteins into an interface. A tBLM interface was fabricated using membrane fractions derived from *Schizosaccharomyces pombe* yeast cells. The approach will facilitate a direct incorporation of recombinant membrane proteins overexpressed in *S. pombe* into BLM interfaces without the need to separate the proteins from the membrane, purify the proteins, and then deposit the resulting proteoliposomes.

A sBLM interface was developed to characterize interactions between polymeric nanoparticles and cell membranes. This interface provided a rapid and convenient way to screen nanoparticles' ability to disrupt BLMs, thereby helping assess nanoparticles' toxicity and suitability for commercial applications (e.g., gene delivery into cells). Finally, BLM containing interfaces were formed on microelectrode arrays to provide a cost-effective, high-throughput platform that allows a rapid and simultaneous electrochemical characterization of proteins for functional proteomics research or nanoparticle characterization.

DEDICATED

TO

MY FAMILY

TABLE OF CONTENTS

LIST OF TABLES

LIST OF FIGURES

NOMENCLATURE

Chemicals

Ag/AgCl	Silver/silver chloride
ATP	Adenosine triphosphate
C8E4	Tetraoxyethylene mono-*n*-octylether
$CaCl_2$	Calcium chloride
DMPC	1,2-dimyristoyl-*sn*-glycero-3-phosphocholine
DOPC	1,2-dioleoyl-*sn*-glycero-3-phosphocholine
DPhytPC	1,2-diphytanoyl-*sn*-glycero-3-phosphocholine
DPPTE	1,2-dipalmitoyl-*sn*-glycero-3-phosphothioethanol
DTT	Dithiothreitol
EDTA	Ehtylenediamine tetraacetic acid
GCE	Glassy carbon electrode
HEPES	4-(2-hydroxyethyl)-1-piperazineethanesulfonic acid
IPTG	Isopropyl-β-D-thiogalactopyranoside
KCl	Potassium chloride
$MgCl_2$	Magnesium chloride
NBD-PC	1-oleoyl-2-[6-[(7-nitro-2-1,3-benzoxadiazol-4-yl)amino]hexanoyl]-*sn*-glycero-3-Phosphocholine
NEST	A catalytically active fragment of NTE

NHS	N-hydroxysuccinimide
NP	Nanoparticles
NTA	Nitrilotriacetic acid
NTE	Neuropathy target esterase
OP	Organophosphorus
PAH	Poly(allylamine hydrochloride)
PAMAM	Polyamidoamine
PDAC	Poly(diallyldimethylammonium chloride)
PEG	Polyethylene glycol
PLL	Poly-L-lysine
PMSF	Phenylmethanesulfonyl fluoride
POPC	1-palimotoyl, 2-oleoyl -*sn*-glycero-3-phosphocholine
PorBII	PorB class II porin from *Neisseria meningitidis*
PorBIII	PorB class III porin
SPS	Sulfonated polystyrene
TMAC	Tetramethylammonium chloride

Symbols

A	Electrode area
a	Stripe periodicity
C_{BULK}	Bulk concentration of redox species

C_{DL}	Double layer capacitance
C_{DEFECT}	Capacitance of defects in sBLM
C_F	Faradaic capacitance
C_M	Membrane capacitance
CPE	Constant phase element
D	Diffusion coefficient
F	Faradays constant
f(0)	Pre-bleach fluorescence intensity ($t < 0$)
f(t)	Post-bleach fluorescence intensity ($t > 0$)
G	Conductance
G_{MAX}	Maximum open conductance
G_{MIN}	Voltage independent conductance
I_C	Charging current
I_M	Current amplitude
i_P	Peak faradaic current
m	Mobile fraction of sBLM

n	Number of electrons transferred
NR_M	Normalized membrane resistance
Q	Charge transferred during oxidation/reduction
R	Gas constant
R_{CT}	Charge transfer resistance
R_M	Membrane resistance
R_S	Solution resistance
t	Time
T	Temperature
v	Scan rate
V	Applied potential
V_0	Voltage at which the channel has equal probability of being in open or closed state
Y	Admittance
Z	Impedance
Z_I	Imaginary part of impedance
Z_R	Real part of impedance

Z_W	Warburg impedance
θ_M	Phase delay
ω	Frequency

Terminologies

BLM	Bilayer lipid membrane
LBL	Layer-by-layer
SAM	Self assembled monolayer
sBLM	Supported BLM
tBLM	Tethered BLM

Instrumentation

AFM	Atomic force microscopy
CV	Cyclic voltammetry
CHI	CH Instruments
CPA	Constant potential amperometry
DLS	Dynamic light scattering
EIS	Electrochemical impedance spectroscopy
FRAPP	Fluorescence recovery after pattern photobleaching
IDC	Impedance extraction and digitization circuit
JEOL	Japan electronic optics laboratories
QCM	Quartz crystal microbalance

QCM-D	Quartz crystal microbalance with dissipation monitoring
TEM	Transmission electron microscopy

1. INTRODUCTION

1.1. Overview and objectives

The cell membrane carries out many molecular recognition, communication, transport, and catalytic functions needed to maintain cellular homeostasis. The primary structural component of a cell membrane, the bilayer lipid membrane (BLM), is formed by spontaneous self assembly of amphiphilic lipid molecules. Various membrane proteins and other biomolecules embedded in the lipid bilayer contribute specific physiological functions and often require a lipid bilayer environment to express their activities. Artificial BLMs, formed using synthetic amphiphilic lipids, can effectively mimic the structure and function of biological cell membranes, and thus allow membrane processes to be studied in a well-defined system. For example, a membrane protein can be incorporated into a BLM of known lipid composition and the protein's functional properties can be characterized. These interfaces offer a powerful research tool for carrying out biophysical investigations, as components can be added as desired to better mimic the natural cellular environment. The ability of different macromolecules to interact and change the structure of cell membranes can also be studied using BLM interfaces. BLM-containing interfaces can be used in functional proteomics research to characterize novel membrane proteins, develop membrane protein interfaces for high-throughput drug screening studies, to investigate receptor-drug interactions, for investigating interactions between nanoparticles and cell membranes, and in developing biosensor systems that exploit specific interactions between membrane proteins and analytes.

Development of biosensors based on membrane proteins poses several challenges. Membrane proteins are difficult to purify, often less stable than soluble proteins and may need a lipid bilayer environment to express their activities. In some cases, special methods are required for reconstituting membrane proteins in artificial BLMs. Hence, there is a need for improved experimental tools that will allow the membrane proteins to be reconstituted in BLMs and the proteins' activities to be simultaneously expressed and measured *in vitro*. These tools will allow a functional characterization of membrane proteins and the effect of different environmental variables on protein activity to be studied.

BLM-containing interfaces can be used to study the interactions of macromolecules, such as charged nanoparticles (NPs), with cell membranes. Nanoparticles have proven to be of great value in many commercial applications, including their use as gene and drug delivery agents. Charged polymeric NPs, in particular, are highly effective in disrupting lipid bilayers, thereby mediating the internalization of molecular cargos into the host cell. This property of NPs raises a concern that NP-mediated defect formation in cell membranes might lead to cytotoxicity. BLM interfaces provide a rapid and convenient way to screen NPs for their interactions with lipid bilayers, thereby helping assess nanoparticles' toxicity and suitability for commercial applications.

Electrochemical techniques offer a powerful and convenient way of monitoring BLM-related phenomena. Electrochemical data can be acquired and analyzed online to provide quantitative and meaningful information in real time about bilayer-associated

physical processes, including molecular function of membrane proteins or BLM-NP interactions.

The objective of the present research was to develop robust, dynamic model membrane interfaces that have several desirable properties: (1) can be deposited using molecular self assembly, (2) are easily analyzed by analytical techniques, and (3) are suitable for carrying out membrane protein assays and other biophysical studies. Toward this end, the proposed research focused on the following research tasks: (1) develop a tethered BLM (tBLM) interface for measuring the ion transport activity of PorB class II (PorBII) outer membrane protein from *Neisseria meningitidis*, (2) investigate the voltage dependence of PorBII activity in tethered and planar BLM interface, (3) develop high impedance tBLMs using the membrane fractions, (4) study the effect of an NP's physical properties on its interaction with supported BLMs (sBLM), and (5) adapt BLM interfaces to an array platform designed for high-throughput electrochemical characterization of proteins.

This research focused on development of a tBLM interface for PorBII porin that would facilitate the design of biosensors for ion transporting membrane proteins, and would provide a stable BLM system for functional characterization of membrane proteins. For example, it will allow study of voltage-gated channel proteins using impedance spectroscopy. Depositing tBLMs using membrane fractions will allow a facile incorporation of membrane proteins in BLM interfaces. Potential gene delivery agents can be screened using sBLM interface, while also providing understanding of membrane-nanoparticle interactions. sBLM interface will also facilitate the design of novel gene or drug delivery agents. Finally, integrating BLM interfaces with array microsystem will

provide a high-throughput platform for studying various membrane related processes. While each chapter in this dissertation focuses on unique issue, the underlying theme is designing improved biomimetic architectures for studying cell membrane processes and developing novel interfaces that express protein activities. The interfaces were designed such that they are easily adaptable to high-throughput screening platforms and will facilitate development of other protein biosensors.

1.2. Dissertation Outline

Chapter 2 of this dissertation presents the architectures and fabrication of different BLM-containing interfaces. The use of planar unsupported BLM and tethered BLM (tBLM) interfaces to measure activities of small ion transporting molecules is discussed. In Chapter 3, a tBLM-containing biomimetic interface for a transmembrane pore-forming membrane protein, PorB class II (PorBII) porin from *Neisseria meningitidis*, is presented. Chapter 4 presents the functional characterization of voltage dependent conductance properties of PorBII using planar BLM and tBLM interfaces. In Chapter 5, fabrication of tBLM interface using the membrane fractions from *Schizosaccharomyces pombe* yeast cells is presented. Chapter 6 presents the development of a novel supported BLM (sBLM) interface for screening BLM-nanoparticle interactions. In Chapter 7, adaptation of tBLM interface and other protein interfaces to gold electrode arrays is presented.

1.3. Background

1.3.1. Biomimetic interfaces containing bilayer lipid membranes

Ion channels, a class of membrane proteins that control ion transport across membranes, are involved in critical physiological functions such as generation of action

potential in nervous tissue, regulation the heartbeat cadence, and muscle contraction. Ion-channel malfunction is responsible for many cardiac and neuronal diseases. Hence, ion channels are important drug targets. High-throughput methods are needed to screen compounds for activity against ion channels and thereby identify new lead drug candidates. However, studying ion channel activity *in vitro* is a very challenging task because ion channels express their activities under specialized amphiphilic environments.

The functions of membrane proteins can be reproduced in laboratory using biomimetic interfaces that consist of artificial BLMs embedded with membrane proteins. The conventional methods to characterize ion channel activity include patch clamp technique, and planar BLM. Patch clamp technique can be carried out using whole cells or cell membrane fractions. Though sensitive to measure single channel activity, patch clamp technique is laborious, highly skill-demanding and has a very low throughput. Unsupported planar BLMs offer an easy and powerful alternative to patch clamp technique. Planar BLMs can be painted across small apertures. A single channel activity of ion channel proteins can be measured. However, planar BLMs are fragile and difficult to adapt to high-throughput platforms. Solid supported BLMs offer a chemically and mechanically stable BLM system compared to conventional BLMs that can be investigated using range of analytical techniques. However, supported BLMs provides less sensitive measurements than conventional BLMs. In this chapter, the design and characterization of different BLM interfaces is discussed. Three membrane interfaces, namely planar unsupported BLMs, supported BLMs (sBLM), and a tethered BLM (tBLM) are presented. Fabrication and characterization of these interfaces using electrochemical techniques is discussed. Model ion transporting peptide, gramicidin, was

used to demonstrate the measurement of ion channel activity using a planar BLM and a tBLM interface.

1.3.2. Biomimetic interface for PorB class II porin from *Neisseria meningitidis*

tBLM approach has been widely used to study small molecules such as ionophore valinomycin, and gramicidin peptides. However, incorporation of full-length transmembrane protein in tBLM interface and measurement of its ion transport activity still remains a challenging task. In this chapter, we present the incorporation of a transmembrane porin channel in a tBLM interface and the characterization of protein's activity using electrochemical techniques. PorBII is a pore-forming outer membrane protein from *Neisseria sp.* The possible role of PorBII in mediating *Neisserial* infection makes this protein a potential target for therapeutic drug development. Recombinant PorBII from *N. meningitidis* was expressed in *E. coli* and purified from inclusion bodies. PorBII was found to get rapidly incorporated in tBLM and transported ions across tBLM. PorBII activity in the presence of different ionic species was measured using electrochemical impedance spectroscopy (EIS). Though the interface was developed for measuring PorBII activity, the interface can be easily extended to other pore-forming proteins such as outer membrane protein A (OmpA), α-hemolysin, and others. PorBII was provided by Yi Zheng and Dr. R. M. Garavito from the Department of Biochemistry and Molecular Biology at Michigan State University (MSU).

1.3.3. Investigation of voltage dependent closure of PorBII porin using planar BLM and tBLM interfaces

Porins allow transport of ions and other nutrients across cell membranes of bacteria. The porin-mediated transport processes can be regulated by binding of a chemical molecule, by transmembrane potential, or by a mechanical stimulus. The understanding of ion channel gating mechanisms is important for design of targeted therapies. Additionally, ion channel safety pharmacology has been an important area in drug discovery. In this chapter, we studied the voltage dependent conductance properties of PorBII porin using planar BLM and tBLM interfaces. EIS was used to show a reversible, voltage dependent closure of PorBII porin incorporated in a tBLM. Single channel studies were conducted in parallel using planar BLMs to confirm tBLM results. The approach involving tBLM and EIS can be easily automated and adapted for a rapid preliminary screening of compounds that modulate activity of voltage-gated proteins. After identification of possible hits, a detail characterization can be followed using planar BLM technique. This work was conducted in collaboration with Yi Zheng and Dr. R. M. Garavito from the Department of Biochemistry and Molecular Biology at MSU. Planar BLM experiments were carried out in collaboration with Dr. Sreenivasarao Kota at Department of Chemical Engineering and Materials Science (CHEMS) at MSU.

1.3.4. Fabrication of tBLMs using membrane fractions of *Schizosaccharomyces pombe* yeast cells

Yeast cells are often used as host cells for expressing recombinant eukaryotic proteins that require post-translational modifications. In most membrane biosensor

studies, purified recombinant membrane proteins are utilized. Membrane proteins are often difficult to purify and may lose activity during the downstream processing of the protein. After purification, most membrane proteins need to be reconstituted in liposomes to restore protein's activity. In this study, we described an approach to reconstitute membrane proteins in their native BLM environment on an interface without need of purification and subsequent reconstitution in liposomes. Membrane fractions derived from *S. pombe* yeast cells were used to simultaneously deposit the upper leaflet of tBLM and the membrane proteins of *S. pombe*. Electrochemical and optical techniques were used to monitor BLM formation. Highly insulating tBLMs were obtained using the membrane fractions, which were found suitable for measuring the ion transport activity of gramicidin peptides. This approach could streamline efforts to characterize novel proteins and screen drug candidates for activity against membrane proteins. This work was carried out in collaboration with Dr. Dexin Sui and Dr. R. M. Garavito from the Department of Biochemistry and Molecular Biology at MSU. Fluorescence recovery after pattern photobleaching (FRAPP) experiments were performed in collaboration with Aaron Greiner and Dr. R.Y. Ofoli from Department of Chemical Engineering and Materials Science at MSU.

1.3.5. Interaction of nanoparticles with supported BLMs

Since last decade, nanoparticles have been introduced in myriad of commercial applications including cosmetics, paints, textiles and others. Nanoparticles also have tremendous application in biosensor development. Incorporation of nanoparticles greatly enhances the surface area, thereby increasing the sensitivity of biosensor by several folds. The small size of nanoparticles provides them unique properties such as low

immunogenicity. This property has been exploited in medical applications wherein nanoparticles are being used as gene and drug delivery vehicles. Recent research has suggested that the increasing use of nanoparticles in commercial products poses significant health risks. Therefore, a detail understanding of molecular mechanisms that causes nanoparticle induced cellular toxicity is required.

It has been hypothesized that nanoparticles disrupt cell membranes to transport materials inside the cell. Damage to cell membranes could also induce cytotoxic effects in host cells. In this study, a supported BLM interface was developed for studying the interaction of nanoparticles with BLMs. Monodisperse positively charged polyamidoamine (PAMAM) nanoparticles of different size and generation number were used to study the effect of nanoparticles' physical properties on their ability to disrupt BLMs. To understand the effect of surface functionality, novel synthetic nanoparticles were designed and screened for their interaction with sBLMs. This work was carried out in collaboration with Dr. G. Baker from the Department of Chemistry at MSU.

1.3.6. Integration of biomimetic interfaces with gold electrode arrays

With completion of Human Genome Project, the focus has now shifted towards structural and functional characterization of proteins encoded by newly discovered gene sequences. Novel soluble and membrane proteins are being identified and expressed using recombinant DNA technology. There is a need for development of tools that will allow a rapid, cost-effective, multi-parameter, parallel, and high-throughput characterization of multiple classes of proteins. In this study, gold electrode arrays were designed and fabricated using photolithography. The microelectrode array platform was used to deposit different protein interfaces. High impedance tBLMs were deposited on

microelectrodes ranging in size from 3 mm in diameter down to 50 μm in diameter. Gramicidin peptide was incorporated in tBLMs and the ion transport across BLM was measured using EIS. Further, tBLM interface was used to study the effect of temperature on bilayer fluidity and gramicidin activity.

In addition to tBLMs, a biosensor interface for measuring the esterase activity of NEST, a catalytically active fragment of a membrane protein Neuropathy Target Esterase (NTE), was fabricated on microelectrode arrays. NTE is found in human neurons, and its malfunction or inhibition by organophosphorus (OP) compounds leads to several neurological diseases including organophosphate induced delayed neuropathy and Lou Gehrig's disease. A NEST biosensor was used to measure the esterase activity of NEST, the hydroxylation activity of tyrosinase, and NEST inhibition by phenylmethylsulfonyl fluoride (PMSF). Further, NEST sensor was utilized to study the temperature dependence of NEST and tyrosinase activity. This work was carried out in collaboration with Dr. Andrew Mason from the Department of Electrical and Computer Engineering at MSU.

2. BIOMIMETIC INTERFACES CONTAINING BILAYER LIPID MEMBRANES

2.1. Abstract

The biological functions of cell membranes can be reproduced in the laboratory using biomimetic interfaces that consist of artificial bilayer lipid membranes (BLM). In this chapter, the design and characterization of conventional, and modern biomimetic interfaces containing BLMs is discussed. Electrophysiological methods such as patch clamp technique and the planar BLM techniques are the 'gold standard' techniques used for measuring a single channel activity of ion channel proteins. However, these techniques are labor intensive, less stable and have low throughput. Solid supported artificial BLMs (sBLM) offer stable BLM interfaces that can be self assembled on variety of substrates and are readily addressable by several analytical techniques. Tethered BLMs (tBLM) are specialized solid supported BLMs that provide necessary molecular architecture for carrying out ion channel assays. In a tBLM approach, BLM is decoupled from electrode surface using a hydrophilic chemical spacer thereby creating an ion reservoir. The electrical properties of the tBLM and ion passage mediated through the incorporated ion channels can be measured using electrochemical impedance spectroscopy (EIS). The design and characterization of planar BLM, sBLM, and tBLM interfaces is described. Planar BLM and tBLM interfaces were used to measure the ion transport activity of gramicidin peptides.

2.2. Introduction

Ion channels are transmembrane proteins that allow conduction of different ions across the hydrophobic lipid bilayer of a cell membrane (Miller, C., 1986). Ion channels are involved in various physiological processes such as generation of action potential in excitable cells like muscle cells, cardiac cells and neurons. Ion channels also control the physiological processes in non-excitable cells such as release of hormone vasopressin from posterior pituitary gland. Ion channels can be selective or non-selective towards ion transport. Depending on the controlling factor, ion channels can be classified as

1. Ligand-gated channels: A chemical molecule (ligand) binds to the ion channels and causes a change in the conformation that may open or close the channel.
2. Voltage-gated channels: A change in membrane potential can cause opening or closing of the channel.
3. Mechano-sensitive channels: A mechanical stimulus such as shear stress acts as an activator for opening of an ion channel.

Due to their critical physiological role in human body, ion channels are of immense importance to the pharmaceutical and biotechnology industry. Drugs acting on the ion channels have an annual sale of more than $6 billion (Wang, X. B. and Li, M., 2003). The major therapeutic indications include the heart diseases like cardiac arrhythmias and hypertension, neuronal diseases such as epilepsy and anxiety, pain and diabetes. Also, some drugs may have undesired interactions with the ion channels leading to fatal side effects. Therefore, ion channel safety pharmacology has been equally important area in drug discovery. There is a tremendous need for development of high throughput techniques for measuring ion channel activities in drug discovery process.

2.2.1. Patch clamp technique

In 1978, biophysicists Erwin Neher and Bert Sakmann revolutionized the field of electrophysiology when they successfully measured the electric current through ion channels in cell membrane (Neher, E. *et al.*, 1978; Sigworth, F. J. and Neher, E., 1980). The technique was called patch clamp method which won them the Nobel Prize for medicine in 1991. Conventional patch clamping (Wang, X. B. and Li, M., 2003) was completely carried out under the microscope using a glass micropipette which has a conducting solution and a microelectrode in it. The cells were taken on a glass slide; micropipette tip was moved towards a cell surface using a micromanipulator and pressed gently against cell membrane. A small suction was then applied to pull a patch of membrane into the opening of pipette tip and create a seal. The seal resistance was monitored by applying the test voltage pulses. A seal resistance of order gigaohms, thus called 'gigaseal', was required for accurate recordings with low noise signal and formation of a stable seal. Formation of gigaseal is very much dependent on the surface characteristics of pipette tip. Smooth surfaces are required for the formation of gigaseal which allows the low interferences by avoiding the leakage currents. Once the gigaseal is formed, the activity of the channel through the patch of cell membrane can be measured. Whole cell measurements of ion channel activity can be done by applying additional suction to rupture a membrane patch. The effect of drug on channel activity can be measured by adding the drug in external solution and measuring the ion currents. Voltage can be manipulated to control the current across the whole cell membrane. Though sensitive, patch clamp technique have critical disadvantages. The technique is very labor intensive and skill demanding. Highly skilled and experienced electro physiologist would

be required for successful measurements. It has a very low throughput. Conventional patch clamp can allow only 7-8 cell measurements per day even by a highly skilled professional.

2.2.2. Planar unsupported BLMs

The planar unsupported BLM is an alternative 'standard' technique used to study ion-transporting membrane proteins. The approach involves forming a BLM across an aperture in a teflon or delrin partition that separates two aqueous solutions [Figure 2.1] (Miller, C., 1986; Ottovaleitmannova, A. and Tien, H. T., 1992; Tien, H. T. and Ottova, A. L., 2000; Tien, H. T. and Ottova, A. L., 2001). BLM is formed by painting a phospholipid solution across the aperture (100 μm - 2 mm in diameter) and then allowing the lipid film to gradually thin into a bilayer membrane. A surfactant-solubilized membrane protein can then be added to one of the solutions, resulting in incorporation of the protein into the BLM. The activity of the protein can then be measured electrochemically. Planar BLM technique shares the advantages of patch clamp technique. It is very sensitive and can resolve the ion channel function at single channel level. Single channel measurements can be used to characterize the channel's conductance states, open probability, and gating properties (Miller, C., 1986). Kinetic behavior of ion channels can be accurately determined in time resolution of tens of microseconds. Membrane potential is controlled at specific voltages which allow ion currents to be measured under well defined conditions, giving accurate results. The tight control over the transmembrane potential allows the investigation of voltage dependence of the channel conductance, as well as the channel closure.

The major limitation of the planar BLMs is that they are very fragile lasting only a hour before breaking. Also, the technique is not well-suited for high-throughput studies, due to the relative low stability of the BLM and issues related to the scaling up of the system. Attempts are being made to develop high-throughput planar bilayer methodologies using silicon substrates that are etched to create micrometer holes (Pantoja, R. *et al.*, 2004) and then using polydimethoxylsilane (PDMS) polymer framework to fabricate microfluidic channels to create two aqueous compartments of bilayer chamber (Klemic, K. G. *et al.*, 2002a; Klemic, K. G. *et al.*, 2002b; Wang, X. B. and Li, M., 2003).

2.2.3. Solid supported BLMs

Supported BLMs (sBLM) provide more stable and mechanically robust system than planar BLMs (Sackmann, E., 1996). sBLM can be deposited on various hydrophilic substrates such as metals (e.g., platinum) (Snejdarkova, M. *et al.*, 1997), glass (Cremer, P. S. and Boxer, S. G., 1999), silica, mica (Radler, J. *et al.*, 1995; Richter, R. P. and Brisson, A. R., 2005) and gold (Peng, Z. Q. *et al.*, 2002). Small unilamellar liposome vesicles made of synthetic phospholipids fuse and rupture (vesicle fusion technique) over the hydrophilic surfaces (such as silica, glass) due to electrostatic interactions between the surface groups of substrate and the head group charges of the phospholipids [Figure 2.2A]. On gold substrates, a self assembled monolayer (SAM) of alkanethiols is first deposited to create the lower leaflet of sBLM and then the liposome vesicles were used to deposit the upper leaflet of BLM using vesicle fusion technique [Figure 2.2B]. sBLMs are suitable to study several classes of membrane processes, including redox proteins and those that involve simple receptor-analyte binding. sBLMs also offer a suitable platform

for electrochemical investigation of BLM disruption by nanoparticles. However, sBLMs are less suitable for studying protein-mediated ion transport, due to the lack of a hydrophilic ion reservoir between the sBLM and the underlying substrate. Various approaches have been used to create an ion reservoir, including depositing the sBLM onto a polymeric cushion [Figure 2.2C] (Mauro, A. *et al.*, 1988; Naumann, C. A. *et al.*, 2002; Fortig, A. *et al.*, 2004) or polyelectrolyte multilayer (Kugler, R. and Knoll, W., 2002), and attaching biotinylated vesicles to the surface using avidin-biotin interaction followed by fusion of liposomes to form a BLM (Berquand, A. *et al.*, 2003). Formation of freely suspended sBLMs on anodized alumina membranes is also reported, wherein the freely suspended BLM essentially acts as planar BLM having infinite ion reservoir on both sides of membrane [Figure 2.2D]. These approaches have been met with limited success, in part, because defects in the BLM allow ion leakage and preclude formation of an insulating membranes (Richter, R. P. *et al.*, 2006).

The tethered BLM (tBLM) architecture [Figure 2.3] (Lang, H. *et al.*, 1992; Lang, H. *et al.*, 1994; Cornell, B. A. *et al.*, 1997; Raguse, B. *et al.*, 1998; Krishna, G. *et al.*, 2003; Terrettaz, S. *et al.*, 2003) overcomes the drawbacks associated with sBLM by simultaneously providing a highly insulating BLM and an ion reservoir between the BLM and an underlying electrode. The approach uses custom tethering lipids, whose architecture includes one terminal group (such as thiol-) that binds to the electrode (gold), another terminal group that anchors into the BLM, and an intermediate hydrophilic region (e.g., a polyethylene glycol (PEG) moiety). Cornell and coworkers prepared synthetic tethered lipids with a phytanoyl lipidic core and a hydrophilic spacer group composed of tetraethylene glycol and hemisuccinate ester (Cornell, B. A. *et al.*, 1997;

Raguse, B. *et al.*, 1998; Woodhouse, G. *et al.*, 1999; Krishna, G. *et al.*, 2001). Similarly, Knoll and coworkers (Bunjes, N. *et al.*, 1997; Krishna, G. *et al.*, 2001; Sinner, E. K. and Knoll, W., 2001; Atanasov, V. *et al.*, 2005; Atanasov, V. *et al.*, 2006; Vockenroth, I. K. *et al.*, 2007) have synthesized thiolipids which have a thioctyl- group as a surface binding residue, a tetraethylene glycol chain as a hydrophilic spacer group and phytanoyl chains as hydrocarbon tail. Vogel and coworkers have also reported synthesis of thiolipids with similar chemical composition (Lang, H. *et al.*, 1992; Lang, H. *et al.*, 1994; Terrettaz, S. *et al.*, 2003). Though gold is the most widely used substrate in tBLM studies, Beccuci and coworkers have used mercury surface to deposit tBLMs (Moncelli, M. R. *et al.*, 2004; Becucci, L. *et al.*, 2005a; Becucci, L. *et al.*, 2005b; Becucci, L. *et al.*, 2006; Becucci, L. and Guidelli, R., 2007). First, a self assembled monolayer (SAM) of the tethering lipids is deposited on gold surface. After SAM formation, remaining lipids needed to establish the bilayer are deposited, usually by the vesicle fusion technique [Figure 2.4] (Atanasov, V. *et al.*, 2005). An ideal tBLM possesses a well defined ion reservoir, is mechanically and biochemically stable, is accessible to electrical measurements, and retains the fluid nature of BLM. Cornell and coworkers successfully demonstrated the use of tBLM interface as ion channel immunosensor wherein the change in the ion transport through antibody-modified-gramicidin channels was used to identify and detect the antigen concentration in test solution (Cornell, B. A. *et al.*, 1997).

2.2.4. Electrochemical characterization of BLM

2.2.4.1. Electrochemical impedance spectroscopy (EIS)

The functional characterization of tBLM can be performed using electrochemical impedance spectroscopy. Absence of redox reactions in normal tBLM measurements

prevents the use of amperometric techniques. In impedance spectral analysis, a small sinusoidal potential is applied in addition to a biased DC potential, and the resulting current is measured as a function of frequency (Bard, A. and Faulkner, L., 2001). The frequency sweep is generally carried out between 0.01 to 10000 Hz for lipid bilayer measurements. Impedance represents the net resistance to current flow offered by the interface at applied potential. Impedance data can be modeled using a suitable equivalent circuit which is an arrangement of electrical components such as capacitors, resistors and inductors. Impedance is defined as the ratio of applied voltage to the resulting current.

$$Z(\omega) = \frac{1}{Y(\omega)} = \frac{V_M}{I_M}\left(\cos(\theta_M) - i\sin(\theta_M)\right) = Z_R + iZ_I \quad \text{.....(Eq. 2.1)}$$

where, Z_R = real part of impedance, Z_I = imaginary part of impedance, Y = admittance, V_M = amplitude of voltage, I_M = amplitude of the current, θ_M = phase delay and ω = the radial frequency. The plot of real and imaginary part of impedance is called the 'Nyquist plot' whereas the plot of absolute value of impedance as a function of frequency is called 'Bode plot'.

tBLM's impedance can be modeled using a Randles equivalent circuit shown in Figure 2.5. The electrical elements can be roughly attributed to the specific components of the interface. In an equivalent circuit shown in Figure 2.5, resistance of solution (R_S) represents the ohmic drop across the electrolyte solution; capacitance (C_M), and resistance of membrane (R_M) represent the electrochemical properties of BLM, and the capacitance of double layer (C_{DL}) is a characteristic of the electrical double layer at the

electrode surface. tBLM formation is characterized from the values obtained for the electrochemical properties associated with BLM namely the capacitance (0.5 - 0.8 μFcm^{-2}) and the resistance (1 - 100 $M\Omega cm^2$) of the membrane (Raguse, B. *et al.*, 1998; Atanasov, V. *et al.*, 2005).

2.2.4.2. Cyclic voltammetry (CV)

CV is a powerful technique to characterize the electron transfer reactions at electrode surface (Bard, A. and Faulkner, L., 2001). In a typical CV experiment, the potential of the electrode is cycled between two values of potential at specified scan rate and the current produced due to electron transfer is measured. The redox couple present in the solution (or immobilized on the surface) get oxidized or reduced at the standard redox potential for that particular redox reaction. CV measurements can be used to determine the diffusion coefficient of the redox species in the solution, to determine the effective electrode area available for the electron transfer, and to provide insights into the mechanism of the reaction (such as multiple electron transfer reactions). Multiple redox reactions having different standard redox potentials can also be interrogated.

Before taking BLM's CV measurement, the first step is to record cyclic voltammograms of a bare electrode of known area at different scan rates in an electrolyte solution (usually, 100 mM NaCl) containing a redox couple (1 mM of potassium ferricyanide and 1 mM of potassium ferrocyanide). A duck shaped cyclic voltammogram with well defined reduction and oxidation current peaks around the standard redox potential (220 mV vs Ag/AgCl) is obtained. Either reduction or oxidation peak current value is plotted against the square root of scan rate and the slope of the curve is used to

obtain the diffusion coefficient of redox species according to the following Randles-Sevcik equation (Bard, A. and Faulkner, L., 2001)

$$i_P = (2.69 \times 10^5)\, n^{3/2} A\, C_{BULK}\, (Dv)^{1/2} \quad \text{.....(Eq. 2.2)}$$

where, i_P is the peak current (μA), n is the number of electrons transferred (1), A is electrode area exposed, C_{BULK} is the bulk concentration of redox species (1×10^{-6} molcm^{-3}), D is the diffusion coefficient (cm^2/s) and v is the scan rate (V/s). In a tBLM interface, BLM forms an insulating dielectric film that hinders the electron transfer at the electrode surface. For an insulating BLM that is free of major defects, no reduction or oxidation currents are obtained. Defects in BLM would provide the redox species an access to electrode surface. The magnitude of the redox currents is directly proportional to the defect area of BLM.

2.3. Materials and methods

2.3.1. Chemicals

The phospholipids 1,2-dipalmitoyl-*sn*-glycero-3-phosphothioethanol (DPPTE), 1,2-diphytanoyl-*sn*-glycero-3-phosphothioethanol (DPhytPC), and 1,2-dioleoyl-*sn*-glycero-3-phosphocholine (DOPC) were obtained from Avanti Polar Lipids Inc., Alabaster, AL. All other chemicals including chloroform, *n*-decane, ethanol, NaCl, KCl, 4-(2-hydroxyethyl)-1-piperazineethanesulfonic acid (HEPES) were obtained from Sigma Aldrich, St. Louis, MO. Deionized (DI) water (18.2 MΩcm^2) was supplied by a Nanopure-UV four-stage purifier (Barnstead International, Dubuque, IA). All aqueous solutions are prepared in DI water.

2.3.2. Planar bilayer lipid membrane measurements

Planar BLMs were painted across a 250 μm diameter aperture in a delrin cup (Warner Instruments, Hamden, CT) using a solution of DPhytPC lipids in *n*-decane (20 mg/mL). 10 mM HEPES buffer, pH 7.4 containing 1 M potassium chloride was used as electrolyte solution in *cis* and *trans* sides of BLM chamber (1 mL each). After painting the BLM, the BLM stability was tested by holding the potential at +100 mV and -100 mV for 10 min each. Ethanol stock solution of gramicidin was diluted and added to *cis* side of BLM chamber to achieve the required concentration.

The *cis* compartment (voltage command) was connected to the head stage input, and *trans* compartment was held at ground using a pair of Ag/AgCl reference electrodes immersed in both sides of BLM chamber. Unitary currents were recorded using a bilayer-clamp BC-535 amplifier (Warner Instruments, Hamden, CT) and digitized using an analog-to-digital converter (Digidata 1440A; Axon Instruments, Sunnyvale, CA). Data were filtered through eight-pole low pass Bessel filter (LPF-8; Warner Instruments, Hamden, CT) and analyzed using pClamp10 software (Axon Instruments, Sunnyvale, CA).

2.3.3. sBLM formation on glassy carbon electrodes

Glassy carbon electrodes (GCE) (Bioanalytical Systems, West Lafayette, IN) were sequentially polished with 1000, 300 and 50 nm alumina slurry, followed by washing with DI water and methanol. The electrode was ultrasonicated for 2 min in DI water to remove physically adsorbed alumina, given final rinses with methanol and DI water, and then dried under a nitrogen stream. The GCE was placed in 100 mM NaCl solution and oxidized at a potential of +1500 mV for 3 min (Du, L. W. *et al.*, 2006). It

was then washed with DI water and dried under a nitrogen stream. Five μL of DOPC lipid solution (5 mg/mL in chloroform) was applied to the electrode surface, and the electrode was immediately immersed in an electrolyte solution (100 mM sodium phosphate buffer, pH 7.4, containing 1 mM of potassium ferrocyanide and 1 mM of potassium ferricyanide). CV was used to monitor changes in the sBLM's electrochemical properties until a steady-state situation was observed.

2.3.4. Preparation of liposomes

A chloroform solution of DOPC phospholipids was dried in a test tube under a slow stream of nitrogen to yield a thin lipid film that was freeze dried for at least 5 h to evaporate residual organic solvent. The dried lipid was hydrated at 22°C using 0.01 M HEPES buffer, pH 7.4, containing 150 mM NaCl to obtain multilamellar vesicles, which were then ultrasonicated using a bath sonicator to yield small unilamellar vesicles. The liposome solution was subjected to 20 cycles of sonication for 1 min followed by cooling on ice for 1 min. The solution was then diluted with HEPES buffer to give 1 mM lipid concentration, and the liposomes' size distribution was immediately measured using dynamic light scattering (Brookhaven Instruments Corporation, Holtsville, NY).

2.3.5. Fabrication of tethered bilayer lipid membrane on gold substrate

The gold substrates were fabricated by Lans Goddard Associates, Foster City, CA, by deposition of a 15 nm adhesion layer of chromium over a silicon wafer, followed by deposition of a 100 nm layer of gold using e-beam evaporation. These substrates were cleaned in piranha solution (7 parts concentrated sulfuric acid and 3 parts 30% hydrogen peroxide) for 30 s and washed with DI water and ethanol [Caution: Piranha solution is a vigorous oxidant and should be used with extreme caution]. Cleaned gold electrodes

were dried in nitrogen and immersed in chloroform solution containing 1 mM DPPTE tethering lipids and 0.5 mM DOPC mobile lipids for 24 h. DPPTE has a terminal thiol group that forms a covalent bond gold surface, thus creating a SAM. The SAM formation is usually rapid for the first hour of incubation but it takes several hours to give a uniform monolayer (Diao et al., 2001). After SAM formation, the electrodes were washed with chloroform to remove weakly attached lipids and dried in a nitrogen stream. The electrodes were transferred to an electrochemical cell with 0.2 cm^2 of electrode area exposed to the electrolyte solution. The upper tBLM leaflet was deposited using the vesicle fusion technique. Small, unilamellar DOPC liposomes were added to a final concentration of 0.25 mM lipids. DOPC was chosen because of its low phase transition temperature, which obviates the need for temperature control during the experiments. Bilayer formation was allowed to proceed for 24 h, after which the liposome solution was replaced with fresh 100 mM NaCl solution. EIS and CV data were collected. For valinomycin experiments, 5 μM of valinomycin was added to electrolyte solution (100 mM NaCl) and impedance was recorded. After 1 h of incubation, the a stock solution of KCl was added to give a 100 mM KCl concentration in electrolyte solution. For gramicidin experiments, 1 μM peptide was added to an electrolyte solution (100 mM NaCl) and the protein incorporation into tBLM was allowed to proceed for an hour, and then EIS and CV were recorded.

2.3.6. Instrumentation

Dynamic light scattering experiments were performed at 25°C using a 90 Plus Nanoparticle Size Analyzer (Brookhaven Instruments Inc., Holtsville, NY). Measurements were obtained at an angle of 90° after appropriate sample dilution. Ten

runs were performed for each sample. Ellipsometric measurements were carried out using rotating analyzer ellipsometer (Model M-44; J.A. Woollan Co. Inc., Lincoln, NE) running WVASE32 software. The SAM's thickness value was determined using 44 wavelengths between 414.0 nm and 736.1 nm. The angle of incidence was 75°, and the SAM's refractive index was assumed to be described by n = 1.5 and k = 0. The advancing contact angle for the tethering lipid SAM was measured by pendant drop shape analysis using a software-controlled SEO Contact Angle Analyzer (Phoenix 450, Surface Electro Optics Corporation Ltd., Korea). Electrochemical measurements were performed using a CHI660B electrochemical workstation (CH Instruments Inc., Austin, TX). The three-electrode electrochemical cell consisted of an Ag/AgCl reference electrode, platinum wire as auxiliary electrode and a gold or GCE as working electrode. EIS was carried out in 100 mM NaCl solution using a 0 V DC potential and a 5 mV sinusoidal potential across the frequency range of 0.01 to 10,000 Hz. Electrochemical parameters were calculated by fitting an appropriate equivalent circuit to the impedance data, using Z-view software (Scribner Associates, Southern Pines, NC). CV was performed in 100 mM NaCl solution containing 1 mM potassium ferricyanide as a redox species. The potential was cycled in a range of 500 mV to -200 mV relative to an Ag/AgCl reference electrode at a scan rate of 50 mV/s.

2.4. Results and discussion

2.4.1. Planar BLMs measurements of gramicidin activity

Planar BLMs were painted using DPhytPC phospholipids. The stability of the BLM was tested by applying a potential of +100 mV and -100 mV for 10 min each.

Gramicidin was added to the *cis* compartment of BLM chamber at a concentration of 1 pg/mL. A single channel current of 25 pS was obtained [Figure 2.6A]. Incorporation of multiple channel units resulted in proportional increase in the channel currents. The current-voltage relationship was linear in a potential range of -110 mV to +110 mV [Figure 2.6B]. The channel current-voltage relationship was symmetric for positive and negative potentials.

2.4.2. Characterization of sBLM interface

sBLMs have been deposited on hydrophilic supports such as mica and silica and on the conductive materials such as platinum (Sackmann, E., 1996). sBLM formation on metal surfaces requires cutting the metal while it is immersed in the lipid solution, to ensure that the lipids contact a fresh metal surface (Sackmann, E., 1996; Tien, H. T. and Ottova, A. L., 2000). GCE provides a convenient and cost-effective alternative to metal electrodes such as platinum, offering good conductivity, a wide potential window, and the possibility of chemical functionalization (Niwa, O. and Tabei, H., 1994). To increase the hydrophilicity of the surface, we oxidized the GCE at 1.5 V for 3 min in a 100 mM NaCl solution. The resulting formation of carboxylate ions imparts a net negative charge to the surface of electrode, which associates with the positively charged choline moiety of the DOPC lipids.

Upon cooling, lipid bilayers undergo a phase transition from a highly fluid, liquid-crystalline phase (L_α) to a more viscous, gel phase (L_β). Mecke et al (Mecke, A. *et al.*, 2005a; Mecke, A. *et al.*, 2005b) reported that polycationic polymers selectively interact with the lipid bilayers in the liquid-crystalline phase (i.e., above the transition

temperature). To ensure that the sBLM was fully fluid during the room-temperature studies, unsaturated phospholipid DOPC (phase transition temperature = -4°C) was chosen. In contrast, saturated phospholipid having 14 carbon hydrocarbon chains (myristyl-) has a phase transition temperature of about 28°C. sBLM formation was monitored using CV and EIS. Figure 2.7 shows the CV curves for bare GCE and DOPC sBLM. The bare GCE curve exhibited the classic duck shaped profile, with well-defined peaks for ferrocyanide oxidation and ferricyanide reduction. The cathodic and anodic peak currents were 43.5 and 44.2 $\mu A/cm^2$, respectively [Figure 2.7]. The peak splitting of 70 mV was indicative of a reversible electron transfer. The sBLM curve was essentially flat, with no redox peaks, indicating that the sBLM forms an effective dielectric barrier that prevents redox species from reaching and transferring electrons at the electrode surface [Figure 2.7].

Figure 2.8 shows EIS curves of the bare GCE and the DOPC sBLM. An equivalent circuit shown in Figure 2.9 was used to fit impedance data and obtain the values of electrochemical parameters. The bare GCE showed a very small charge transfer resistance (R_M in the equivalent circuit) (6 Ωcm^2), and most of the impedance spectrum was representative of Warburg impedance, indicating mass transfer resistance. In the absence of sBLM, the defect capacitance in equivalent circuit is equal to the bare GCE capacitance ($C_{DEFECT} = C_{GCE}$) which was obtained to be 35 $\mu F/cm^2$. A membrane resistance of sBLM (R_M in the equivalent circuit), which is equal to the charge transfer resistance, was found to be 85 $k\Omega cm^2$. R_M values greater than 1 $M\Omega cm^2$ have been reported for tethered lipid bilayer systems, suggesting that the sBLM formed on the GCE

has pin-hole defects. Nevertheless, the sBLM still effectively shields the electrode from the ferricyanide. An equivalent circuit assumed for the sBLM involves a parallel arrangement of capacitors: one corresponding to the membrane (C_M), and the other corresponding to membrane defects (C_{DEFECT}). The overall capacitance is the sum of both capacitances. At the defects, where the electrolyte can contact the electrode surface, the capacitance per area of defect should be similar to C_{GCE}. Before nanoparticle addition, the overall capacitance was determined to be 0.75 $\mu F/cm^2$, a value typical of those reported for sBLM-coated electrodes (Gao, H. *et al.*, 2001). Under these conditions, the fraction of the total area occupied by defects, and thus the C_{DEFECT} term, is negligibly small.

2.4.3. Fabrication of tBLM on gold electrode

A variety of electrode materials have been used for tBLM studies, including gold (Sinner, E. K. and Knoll, W., 2001; Schiller, S. M. *et al.*, 2003; Atanasov, V. *et al.*, 2005; Kohli, N. *et al.*, 2006a; Jadhav, S. R. *et al.*, 2008b) and mercury (Moncelli, M. R. *et al.*, 2004; Becucci, L. *et al.*, 2005a; Becucci, L. *et al.*, 2005b). The choice of substrate is governed by factors including surface smoothness, availability of tethering molecules that bind to the surface, and electrical conductivity. Gold has been the most popular substrate for tBLM experiments because of its chemical stability, high conductivity, facile thiol chemistry to couple tethering lipids, and compatibility with microfabrication methods for eventual application in electrode arrays.

2.4.3.1. Characterization of a tethering lipid monolayer

We have deposited a tBLM on gold surface by slight variations of published procedures (Raguse, B. *et al.*, 1998; Naumann, R. *et al.*, 2003a; Naumann, R. *et al.*, 2003b; Atanasov, V. *et al.*, 2005). The inner leaflet of the BLM was deposited by dipping a gold substrate in a chloroform solution of DPPTE tethering lipids. A self assembled monolayer (SAM) of tethering lipids was formed after 24 h, which was characterized using contact angle measurement, ellipsometry, EIS and CV. Ellipsometry indicated that the tethering lipid SAM had a thickness of 2.7 ± 0.1 nm, which is comparable to the length of tethering lipid molecule. The SAM exhibited advancing and receding contact angles of 109 ± 3° and 105 ± 3° respectively, consistent with formation of a uniform, ordered, hydrophobic SAM film on the gold substrate. This finding is reasonable, because binding between the thioethanol end group and the gold should orient the tethering lipid molecules so that the hydrophobic dipalmitoyl tails face outward. A Bode plot showing EIS results for the SAM is shown in Figure 2.10 (curves marked with triangles). Fitting a Randles equivalent circuit model [Figure 2.5] to impedance data gave a monolayer capacitance of 1.12 $\mu F/cm^2$ and a monolayer resistance of 68 $k\Omega cm^2$. In contrast, the capacitance of the bare gold surface was 25 $\mu F/cm^2$. The large drop in capacitance value suggested that most of the gold surface was covered with the SAM (Diao, P. *et al.*, 1999). The CV data obtained in the presence of potassium ferricyanide showed that SAM formation decreased the redox peak current by 96%, confirming formation of uniform insulating barrier on the gold (Diao, P. *et al.*, 1999).

2.4.3.2. Characterization of a tBLM

The outer leaflet of tBLM was deposited using the vesicle fusion technique in which the liposomes made of DOPC lipids were allowed to fuse over tethering lipid SAM. EIS results taken at various times after addition of vesicles to the SAM indicated membrane resistance value (R_M) increased rapidly during the first few hours and then approached an asymptotic value after about 10 h. This trend is consistent with the mechanism of sBLM formation on planar glass surfaces, in which vesicles initially fuse onto the surface at random locations, forming bilayer patches, and then gaps are gradually filled (Cremer, P. S. and Boxer, S. G., 1999). The electrochemical properties of BLM were obtained by fitting the Randles equivalent circuit to impedance data using Z-view software [Figure 2.10]. The fitting gave a capacitance value of 0.709 $\mu F/cm^2$ for tBLM, which is in agreement with the reported capacitance value of 0.5 – 0.8 $\mu F/cm^2$ for BLM (Schiller, S. M. *et al.*, 2003). The resistance value of 5.98 $M\Omega cm^2$, indicated formation of an insulating tBLM that is impermeable to sodium and chloride ions. CV of the tBLM in the presence of ferricyanide lacked redox peaks [Figure 2.11], further confirming formation of a defect-free tBLM that is impermeable to ferricyanide anions.

2.4.3.3. Characterization of valinomycin and gramicidin activity using tBLM interface

In an electrolyte solution bathing the preformed tBLM, an aliquot of ethanolic stock solution containing the ionophore valinomycin (5 μM) or gramicidin peptide (1 μM) was added and the incorporation of the ionophore or protein was allowed for an hour. Partitioning of valinomycin or gramicidin into the tBLM in a functional

conformation was confirmed by EIS. Valinomycin ionophores selectively transported potassium ions across the BLM. In a 100 mM NaCl electrolyte solution, incorporation of valinomycin did not change the membrane resistance. Addition of 100 mM KCl to the solution (bathing valinomycin incorporated tBLM) decreased the R_M value from 5.98 $M\Omega cm^2$ to 0.98 $M\Omega cm^2$ [Figure 2.12], indicating the transport of potassium ions across tBLM. The results also confirmed the ion selectivity of valinomycin ionophores. Gramicidin is a penta decapeptide that forms a dimeric ion channel in BLMs. The monomers of gramicidin peptide gets partitioned in the lower and the upper leaflet of BLM and are free to diffuse in a fluid bilayer environment. Gramicidin peptides are selective towards alkali metal ions for transporting ions across BLM. Incorporation of gramicidin peptides in tBLM decreased the membrane resistance from 3.08 $M\Omega cm^2$ to 0.34 $M\Omega cm^2$ [Figure 2.13]. CV results showed a slight increase in charging current after gramicidin incorporation in tBLM and no redox peaks were obtained [Figure 2.14]. It suggested that gramicidin did not allow ferricyanide ion transport across tBLM. Replacing the NaCl solution to 100 mM tetramethylammonium chloride or 50 mM barium chloride results in the recovery of the tBLM membrane resistance observed before gramicidin addition, suggesting the larger cations such as tetramethylammonium and barium ions are not transported across BLM by gramicidin [Figure 2.15]. These results provide evidence for the ion selectivity of gramicidin peptide. Additionally, the effect of ion concentration and the protein concentration on membrane resistance was studied. At a fixed concentration of gramicidin peptides, a larger drop in the membrane resistance was obtained when an ionic strength of the electrolyte solution was increased

[Figure 2.16]. Increasing the protein concentration had the similar effect due to partitioning of higher number of protein molecules inside BLM [Figure 2.16].

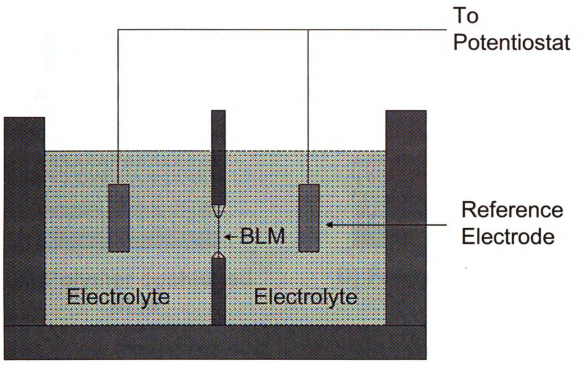

Figure 2.1: Planar BLM set-up. Lipids were painted across a small aperture in a partition that separates two compartments of BLM chamber. The ionic current mediated by ion transport across BLM through the ion channel proteins was measured by a pair of Ag/AgCl reference electrodes.

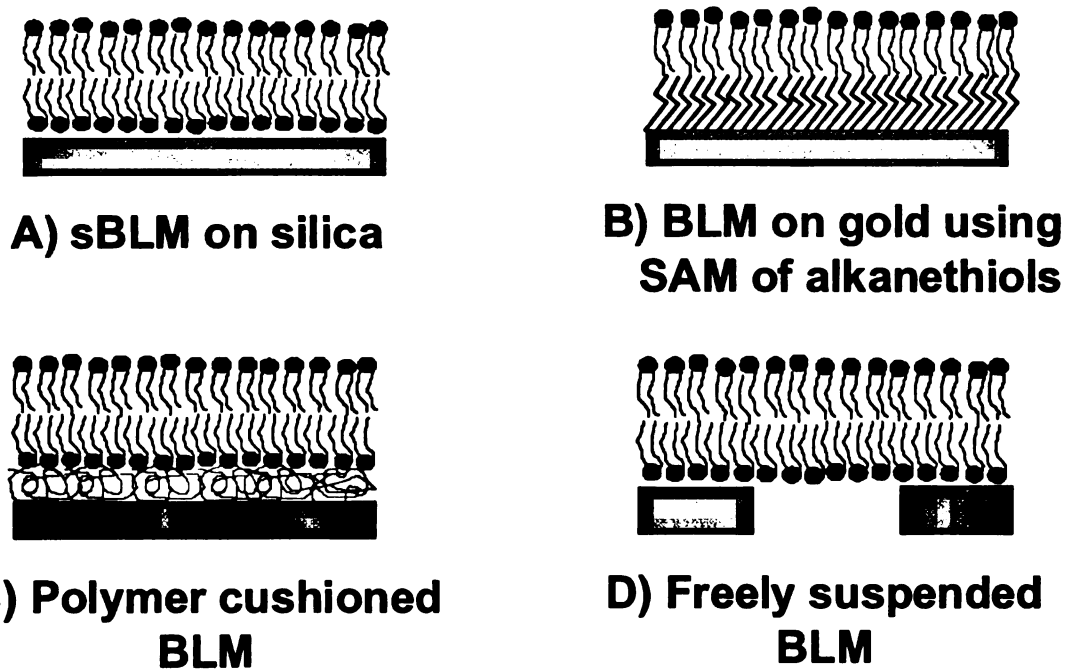

Figure 2.2: Supported BLM interfaces. (A) sBLM deposited on a silica or glass surface. A thin layer of water separates the BLM from the surface of substrate. (B) sBLM can be deposited on gold surface by forming a SAM of alkanethiols followed by depositing the upper leaflet of sBLM using liposome vesicles. (C) Charged polymers and polyelectrolytes have been used as polymeric cushions to separate sBLM from electrode surface and create ion reservoir. (D) Freely suspended BLMs are deposited on anodized alumina membranes to create sBLM architecture that mimics planar BLMs. [(Richter, R. P. *et al.*, 2006)]

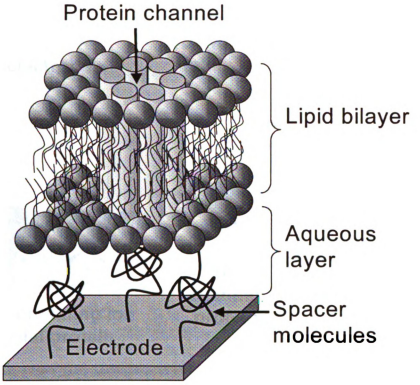

Figure 2.3: A tethered BLM (tBLM) architecture showing the decoupling of BLM from electrode surface using hydrophilic spacer molecule creating an ion reservoir beneath BLM. The ion reservoir also provides space to accommodate the bulky extramembraneous domains of transmembrane proteins. tBLM offers a stable BLM interface that is suitable for studying ion channel proteins using electrochemical impedance spectroscopy.

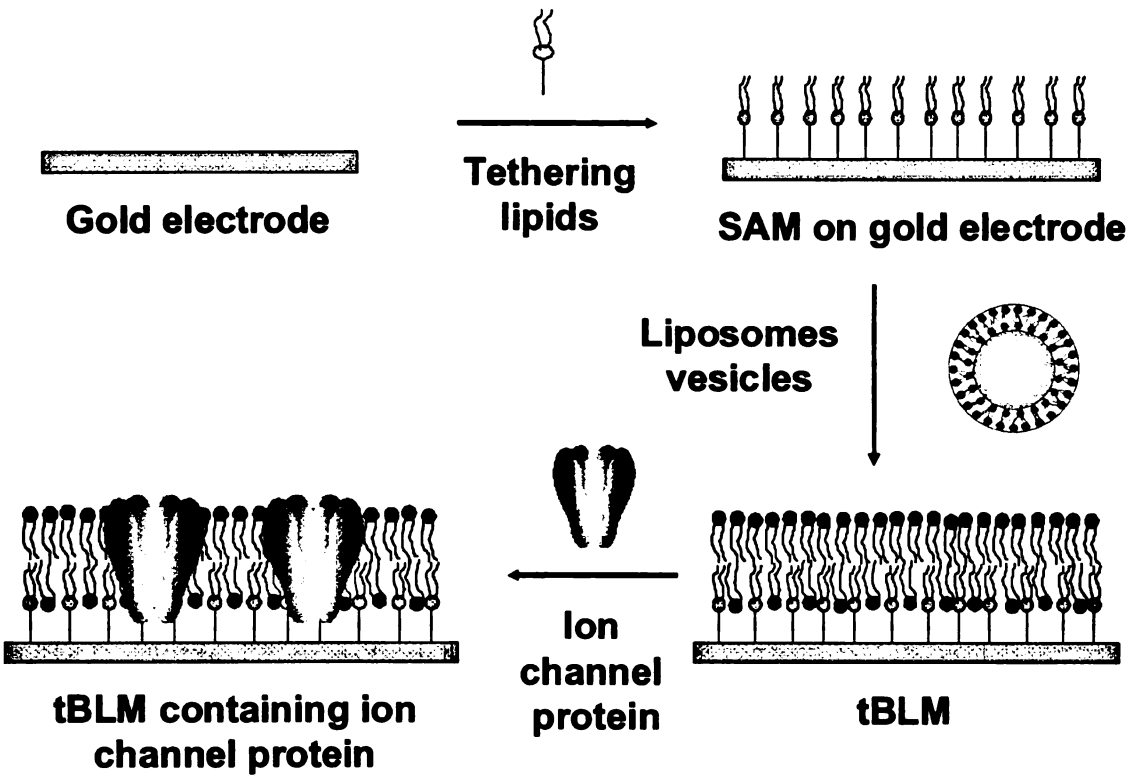

Figure 2.4: A scheme for fabrication of a tBLM. A self assembled monolayer (SAM) of tethering lipids was first deposited on gold electrodes. After SAM formation, liposomes made of DOPC lipids were used to deposit the upper leaflet of tBLM using vesicle fusion technique. tBLM formation was characterized using EIS and CV. Ion channel protein was then be added to the electrolyte solution to allow its incorporation in tBLM. [Figure not to scale]

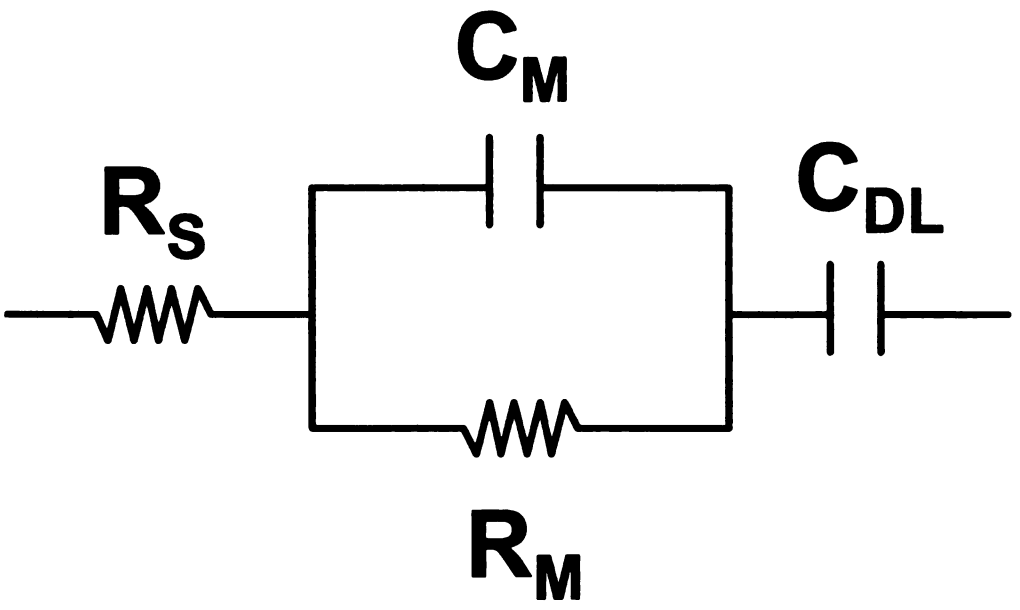

Figure 2.5: A Randles equivalent circuit model was fitted to tBLM impedance data to calculate the values of electrochemical properties. R_S represents the solution resistance, C_M represents the capacitance of the membrane, R_M represents the resistance of membrane and C_{DL} represents the double-layer capacitance, which includes the Hemholtz capacitance.

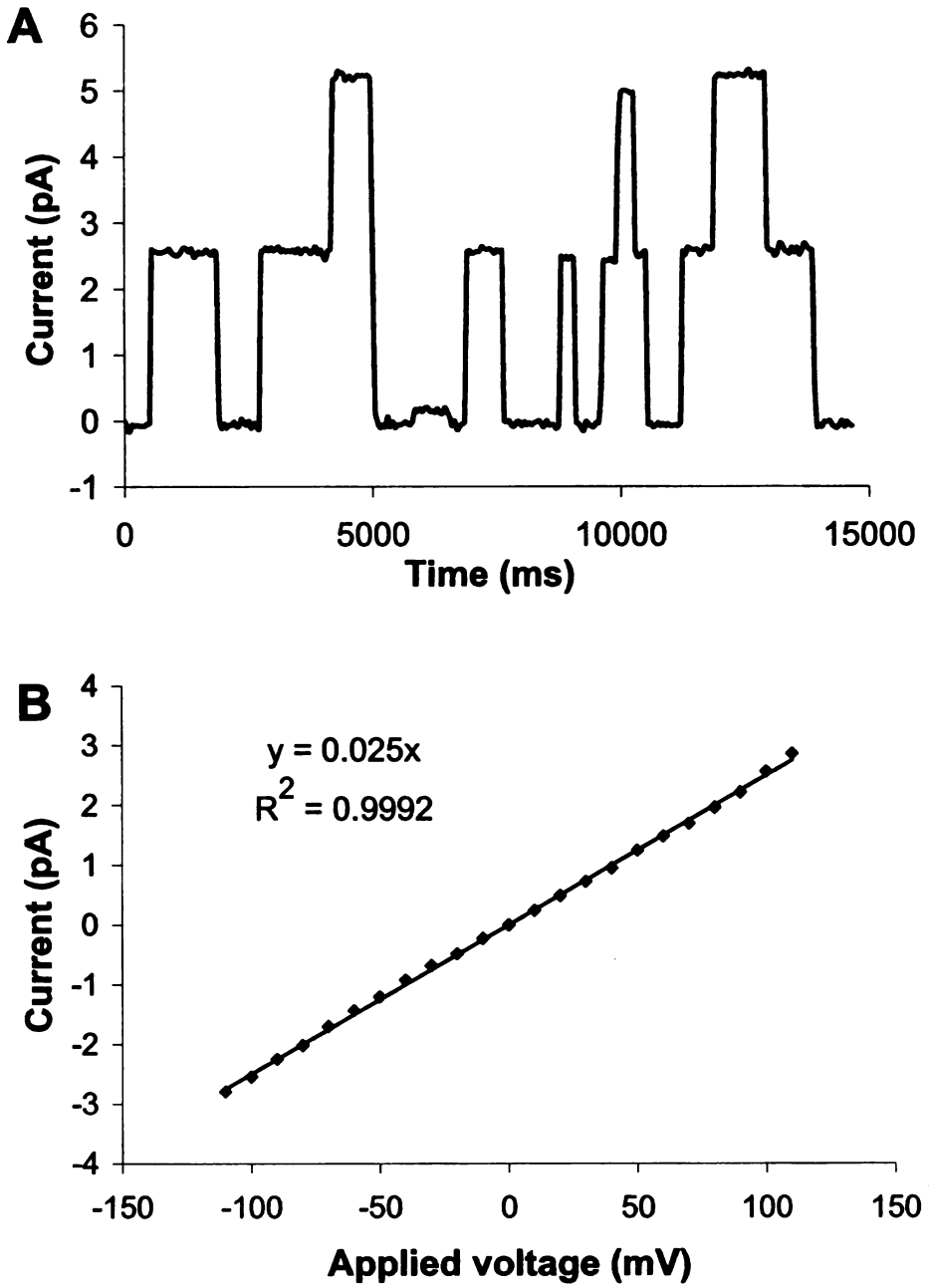

Figure 2.6: The ion transport activity of gramicidin peptides measured using a planar BLM interface. DPhytPC lipids were painted across 250 μm aperture. (A) Single channel currents corresponding to a conductance value of 25 pS were obtained. Incorporation of multiple channels proportionally increased the current response. (B) Single channel study was conducted to obtain the current-potential (I-V) relationship for gramicidin peptides. I-V curve was linear in the range of +110 mV to -110 mV. Experimental conditions: Both bilayer compartments had 1 mL of 20 mM HEPES buffer (pH 7.4) containing 1 M KCl; gramicidin concentration in *cis* chamber was 1 pg/mL.

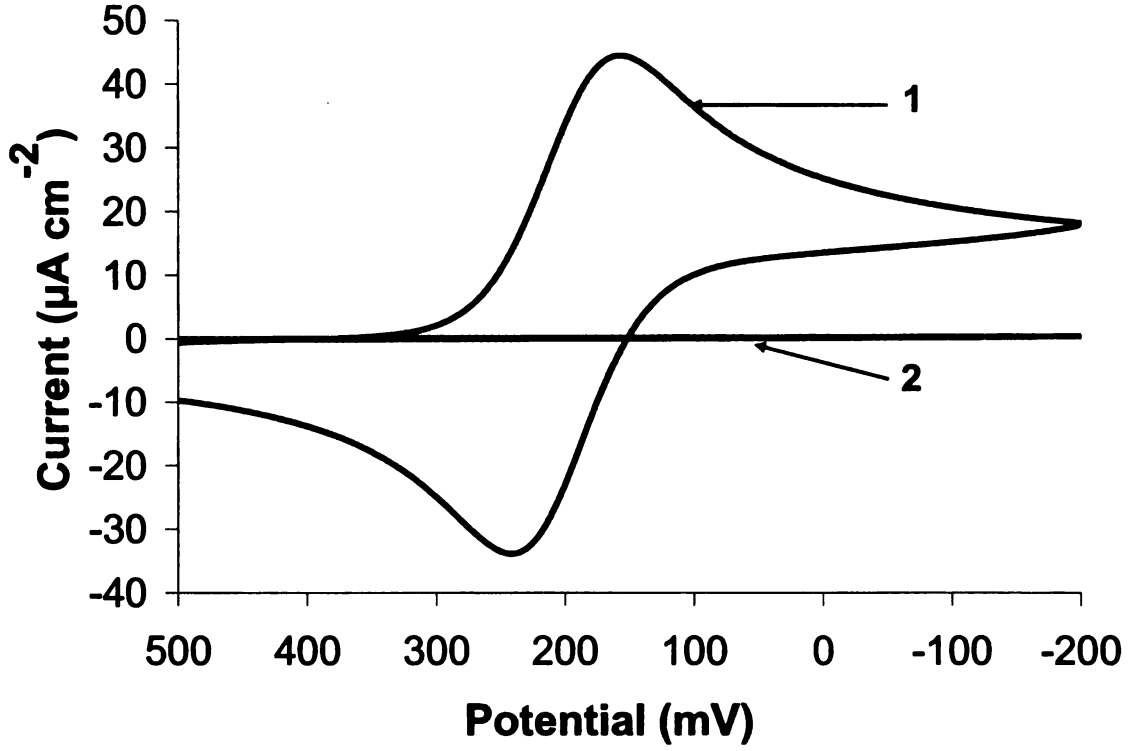

Figure 2.7: Cyclic voltammogram for bare GCE (curve 1) and for sBLM deposited on GCE (curve 2). Well defined oxidation and reduction peaks were obtained at bare GCE surface. The peak currents were completely diminished after sBLM formation suggesting that sBLM did not have large pinhole defects.

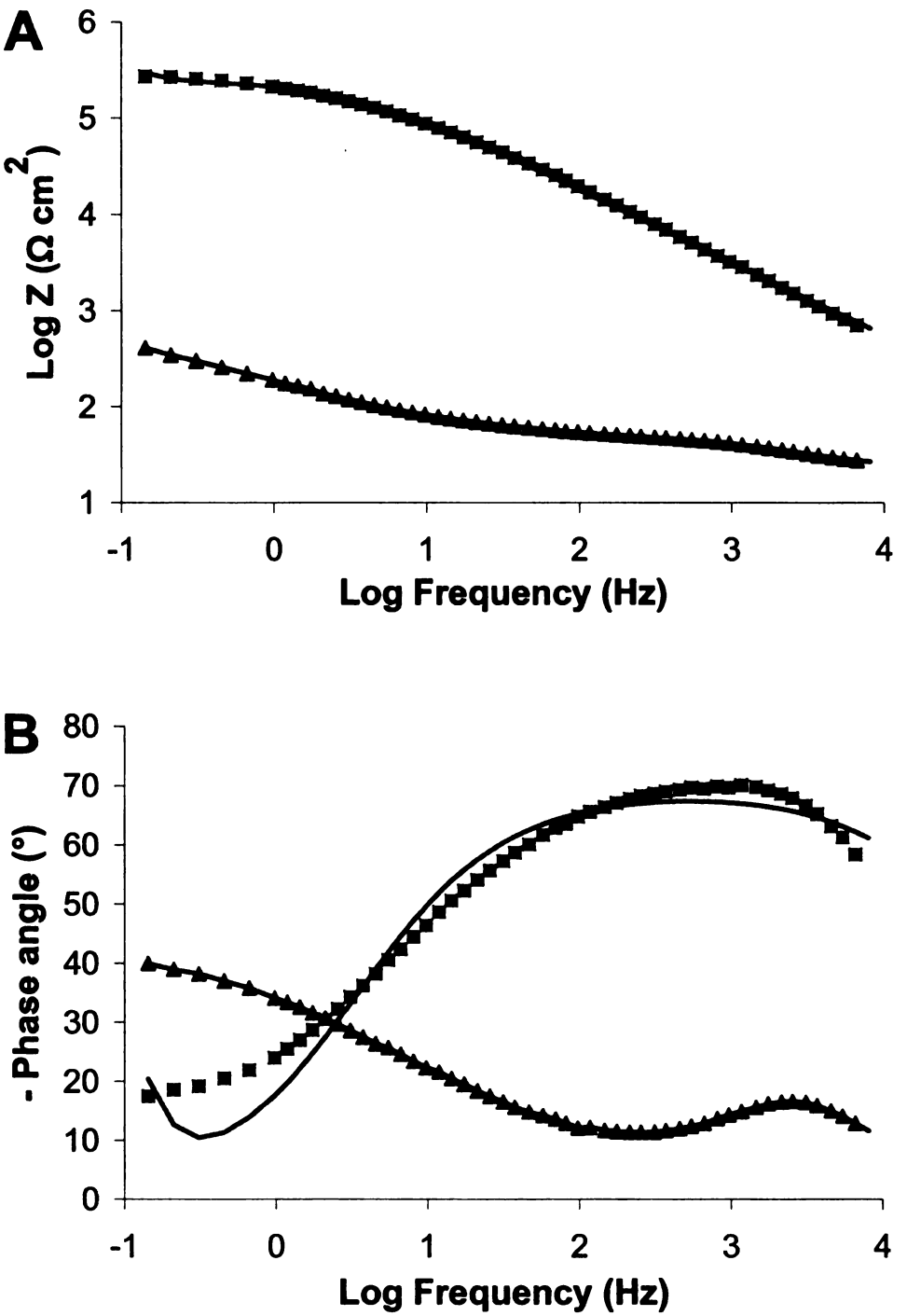

Figure 2.8: (A) Impedance (Log Z) data and (B) phase angle data were plotted as a function of Log frequency for bare GCE (triangles) and for sBLM deposited on GCE (squares). An equivalent circuit shown in Figure 2.9 was fitted to impedance data. The solid lines passing through the data points represent the model fit.

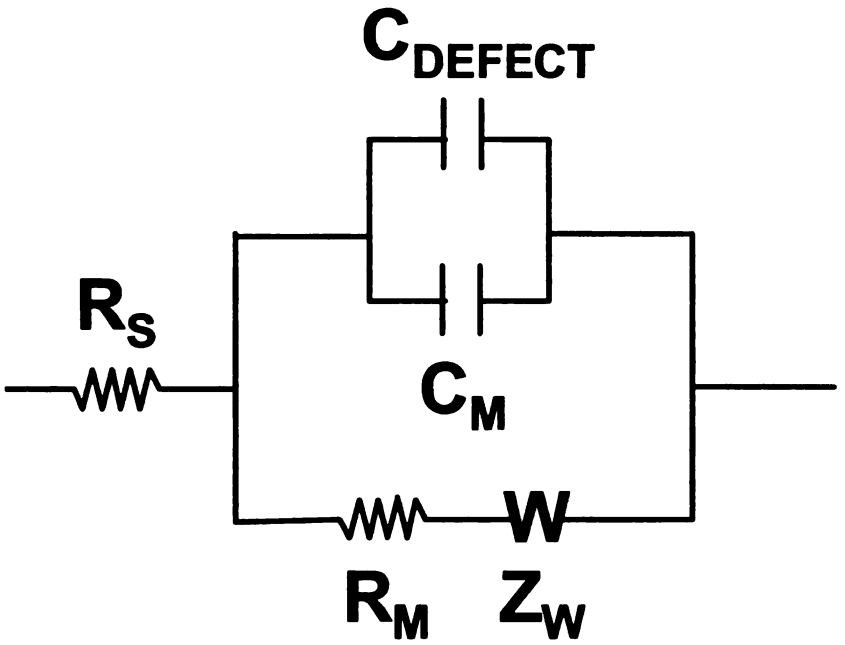

Figure 2.9: An equivalent circuit used to model impedance data obtained for bare GCE and sBLM on GCE. R_S represents the resistance of solution, C_{DEFECT} is the double layer capacitance of GCE at the defect sites in sBLM, C_M is the membrane capacitance, R_M represents membrane resistance, and Z_W is the Warburg impedance.

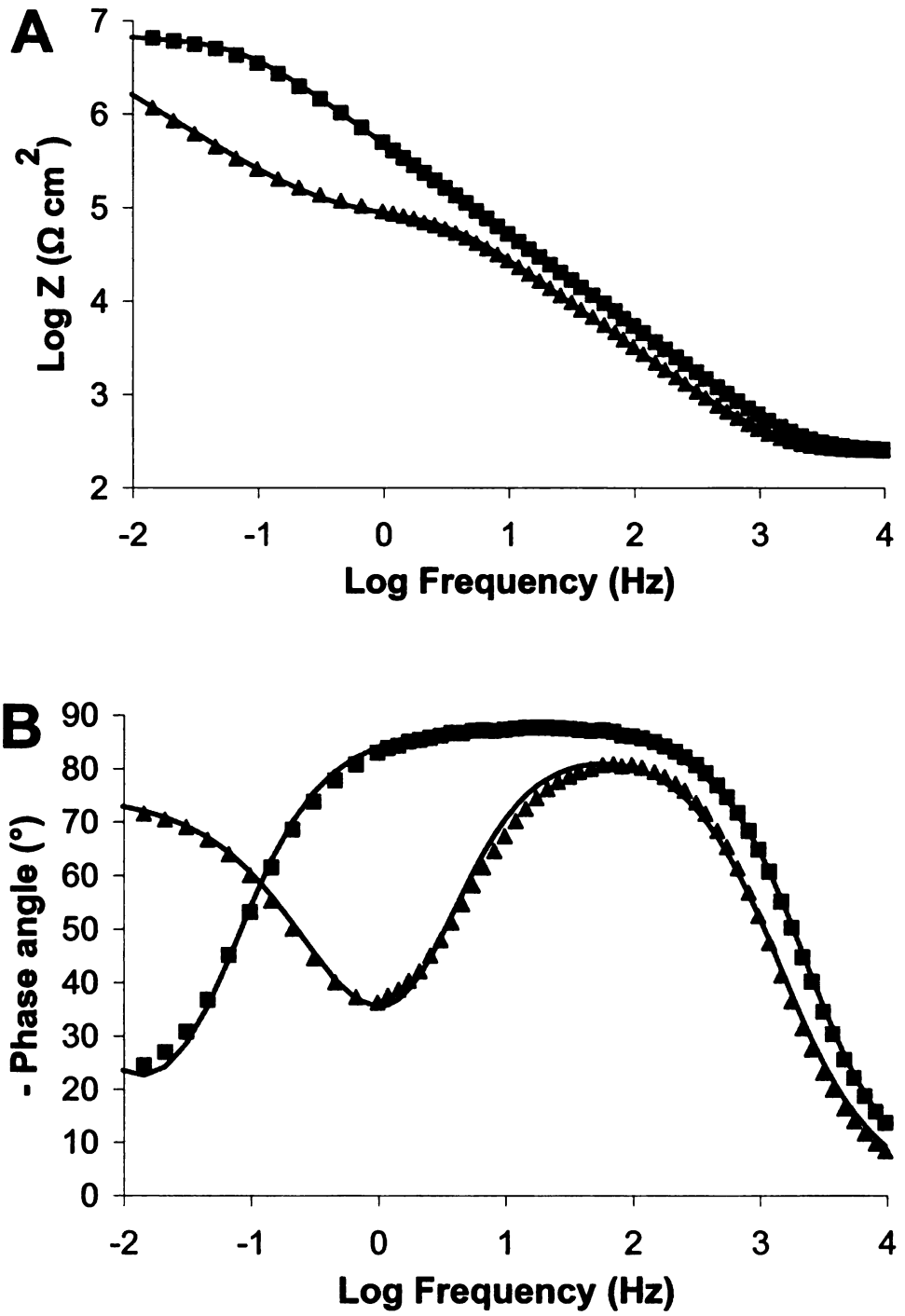

Figure 2.10: (A) Impedance (Log Z) data, and (B) phase angle data were plotted as a function of Log frequency for DPPTE tethering lipid monolayer (triangles) and tBLM (squares) formed with DOPC liposomes in 100 mM NaCl solution. An equivalent circuit shown in Figure 2.5 was fitted to the impedance data. The solid lines passing through the data points represent the model fit.

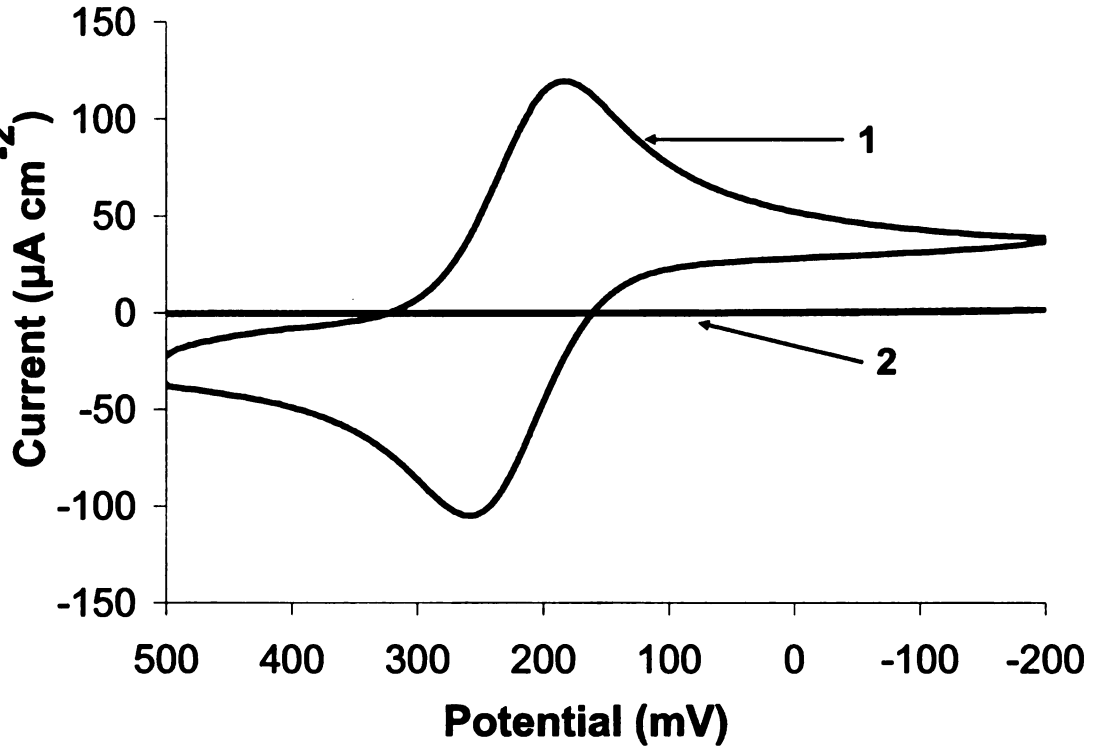

Figure 2.11: Cyclic voltammogram for bare gold electrode (curve 1) and for DPPTE-DOPC tBLM deposited on gold surface (curve 2). Well defined oxidation and reduction peaks were obtained at bare gold surface. The peak currents were completely diminished after tBLM formation suggesting that sBLM did not have large pinhole defects.

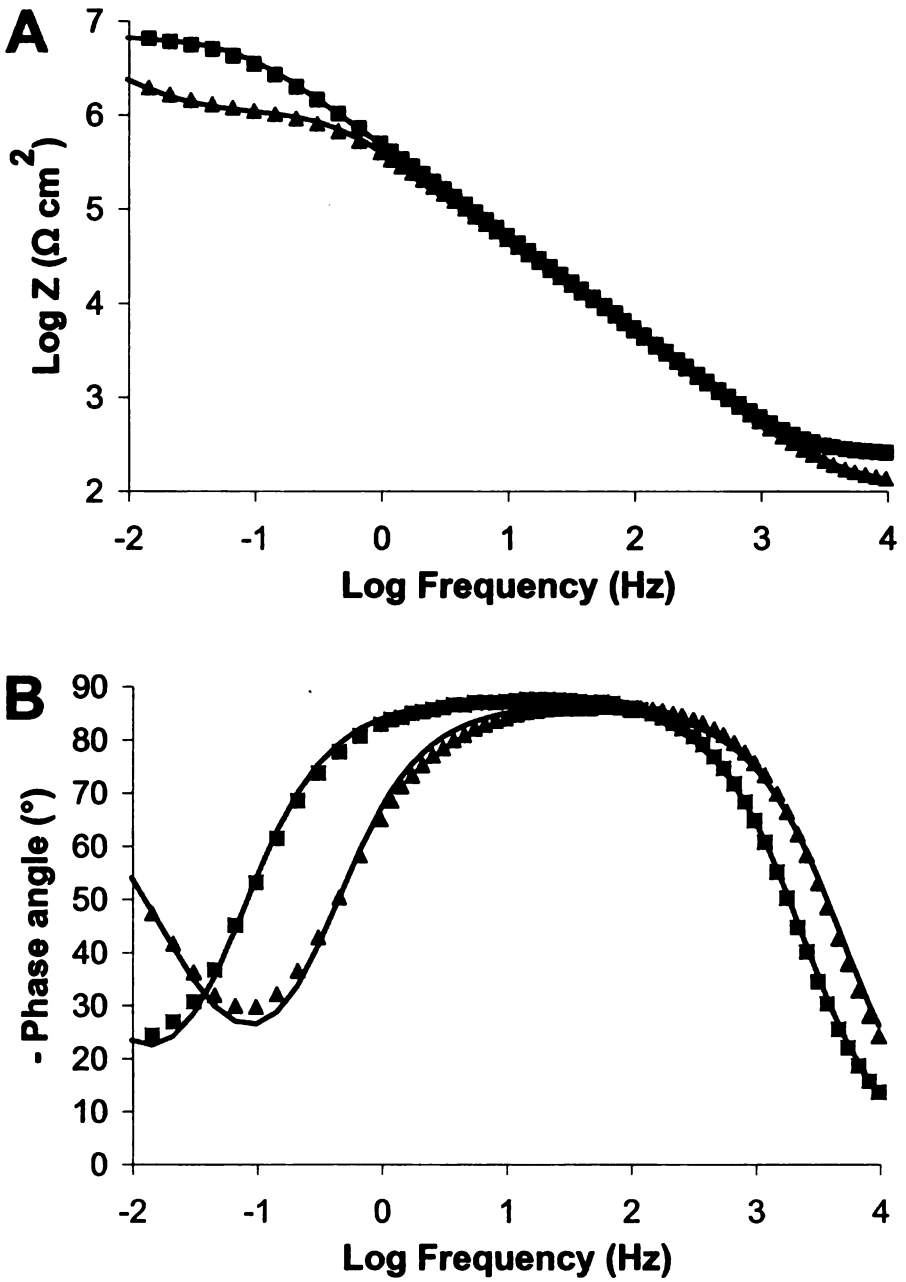

Figure 2.12: (A) Impedance (Log Z) data and (B) phase angle data were plotted as a function of Log frequency for DPPTE-DOPC tBLM (squares) and for DPPTE-DOPC tBLM after valinomycin incorporation (triangles). tBLM impedance was taken in 100 mM NaCl. Valinomycin was added to give a final concentration of 5 μM in an electrolyte solution. After valinomycin incorporation, 100 mM KCl was added. An equivalent circuit shown in Figure 2.5 was fitted to impedance data. The solid lines passing through the data points represent the model fit. Membrane resistance decreased significantly due to the ion transport through the tBLM, whereas there was no significant change in membrane capacitance. The solution resistance decreased due to increase in the ionic strength of an electrolyte solution after 100 mM KCl addition.

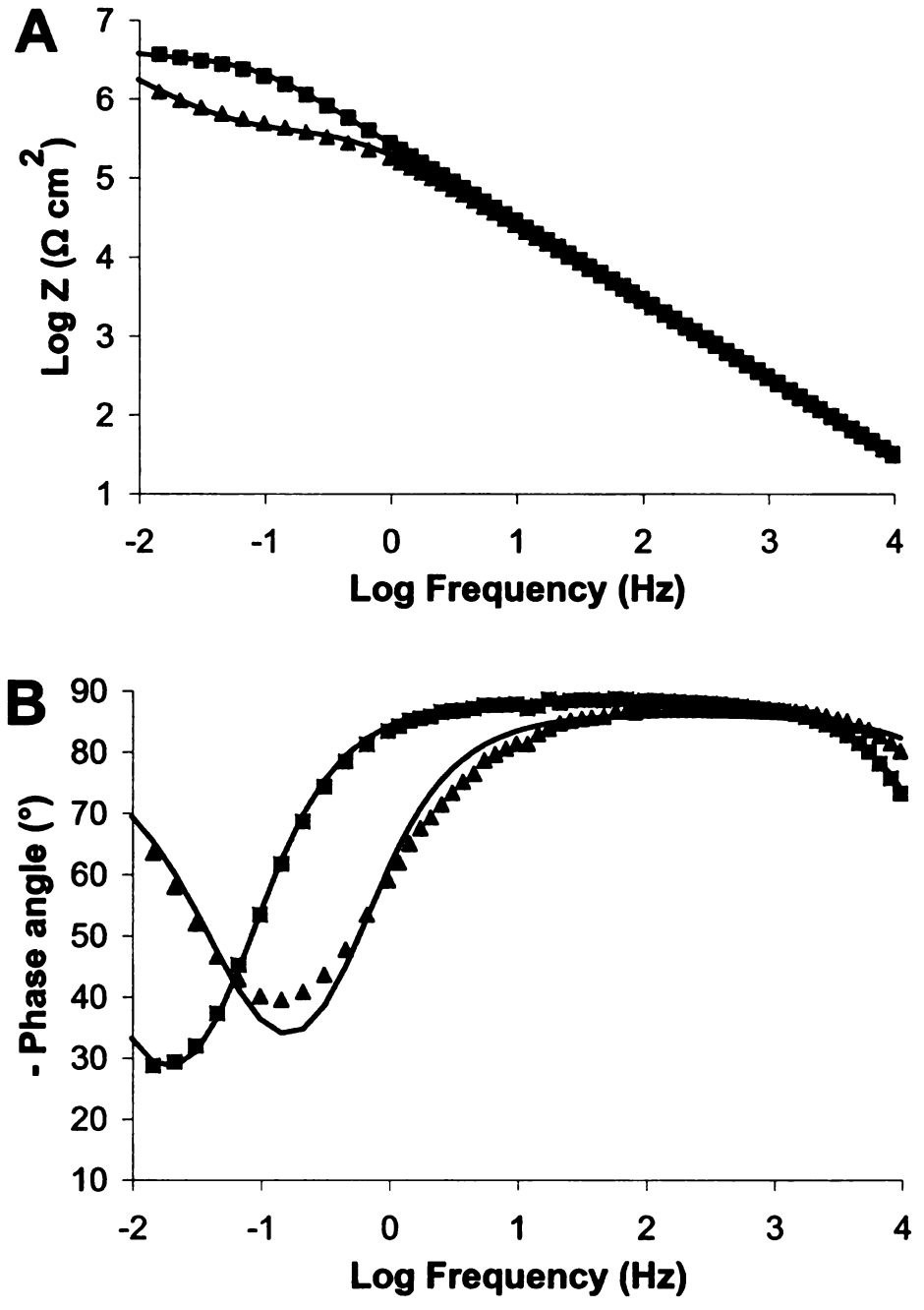

Figure 2.13: (A) Impedance (Log Z) data and (B) phase angle data were plotted as a function of Log frequency for DPPTE-DOPC tBLM (squares) and for DPPTE-DOPC tBLM after gramicidin incorporation (triangles) in 100 mM NaCl. An equivalent circuit shown in Figure 2.5 was fitted to impedance data. The solid lines passing through the data points represent the model fit. Gramicidin was added to give a final concentration of 1 μM protein (monomer) in an electrolyte solution. Membrane resistance decreased significantly due to the ion transport through the tBLM, whereas there was no significant change in membrane capacitance.

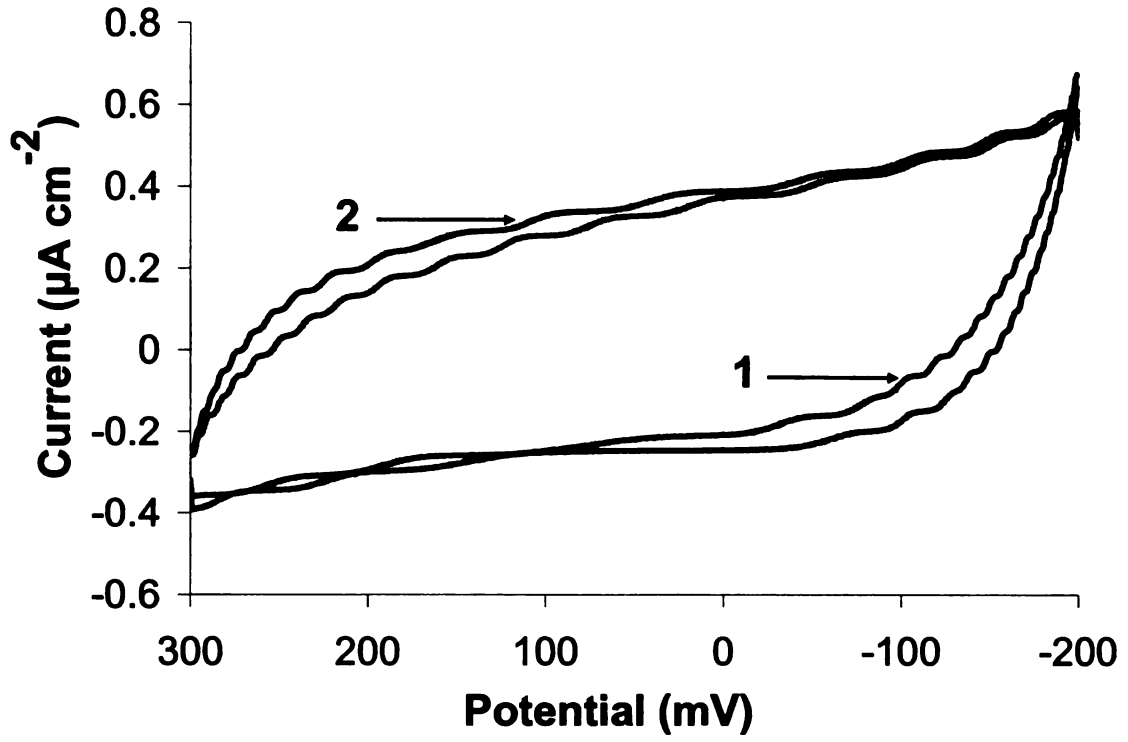

Figure 2.14: Cyclic voltammogram for tBLM (curve 1) and for DPPTE-DOPC tBLM after gramicidin incorporation (curve 2). The redox peaks were absent in both voltammograms whereas there was an increase in charging current after the addition of gramicidin suggesting the passage of ions through tBLM by gramicidin while excluding the passage of ferricyanide ions through tBLM.

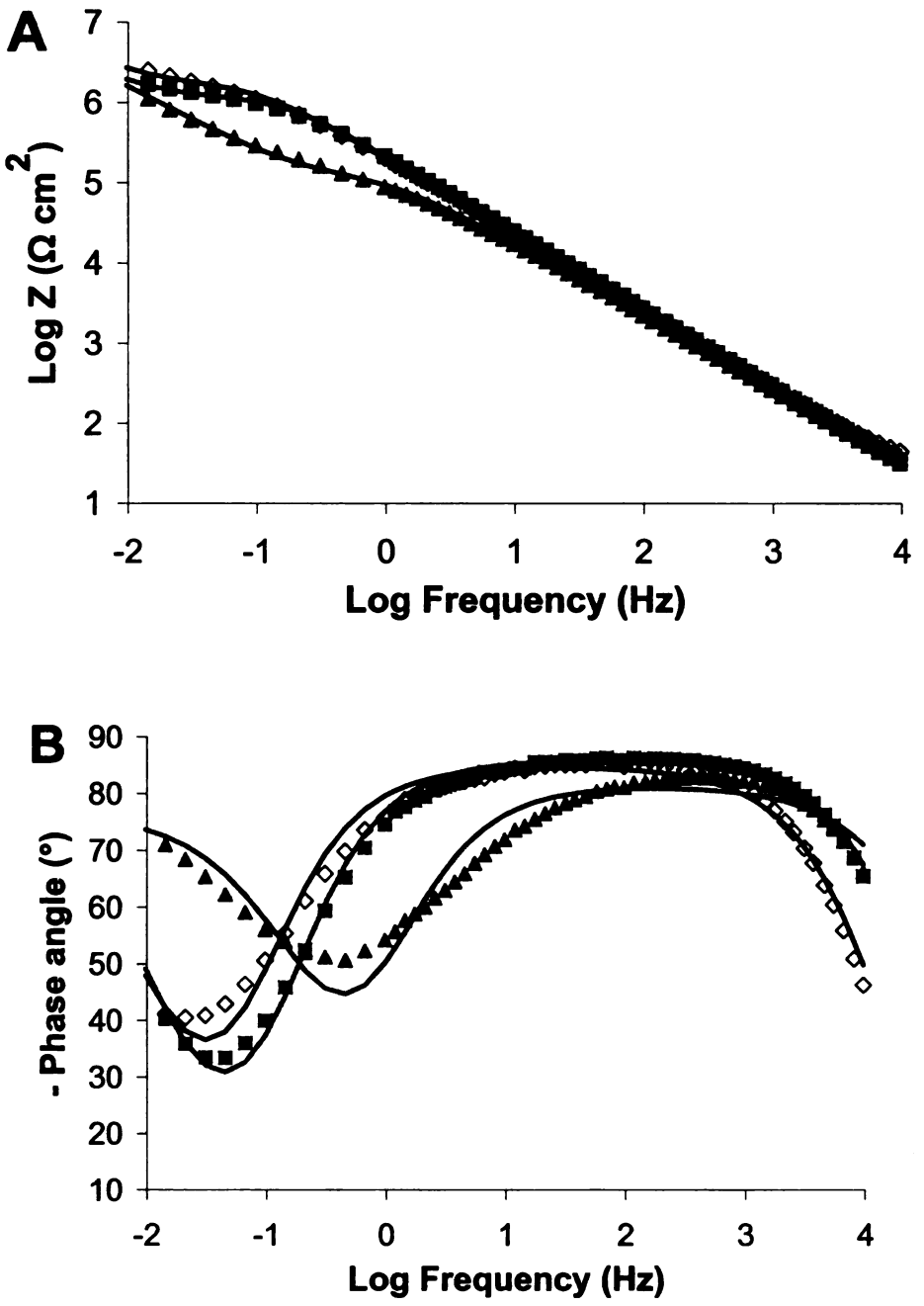

Figure 2.15: (A) Impedance (Log Z) data and (B) phase angle data were plotted as a function of Log frequency for DPPTE-DOPC tBLM in 100mM NaCl (squares), for DPPTE-DOPC tBLM after gramicidin incorporation (triangles) in 100 mM NaCl, and for gramicidin-incorporated tBLM after replacing the electrolyte solution to 100 mM tetramethylammonium chloride (open diamonds). An equivalent circuit shown in Figure 2.5 was fitted to the impedance data. The solid lines passing through the data points represent the model fit. Gramicidin was added to give a final concentration of 1 μM protein (monomer) in an electrolyte solution.

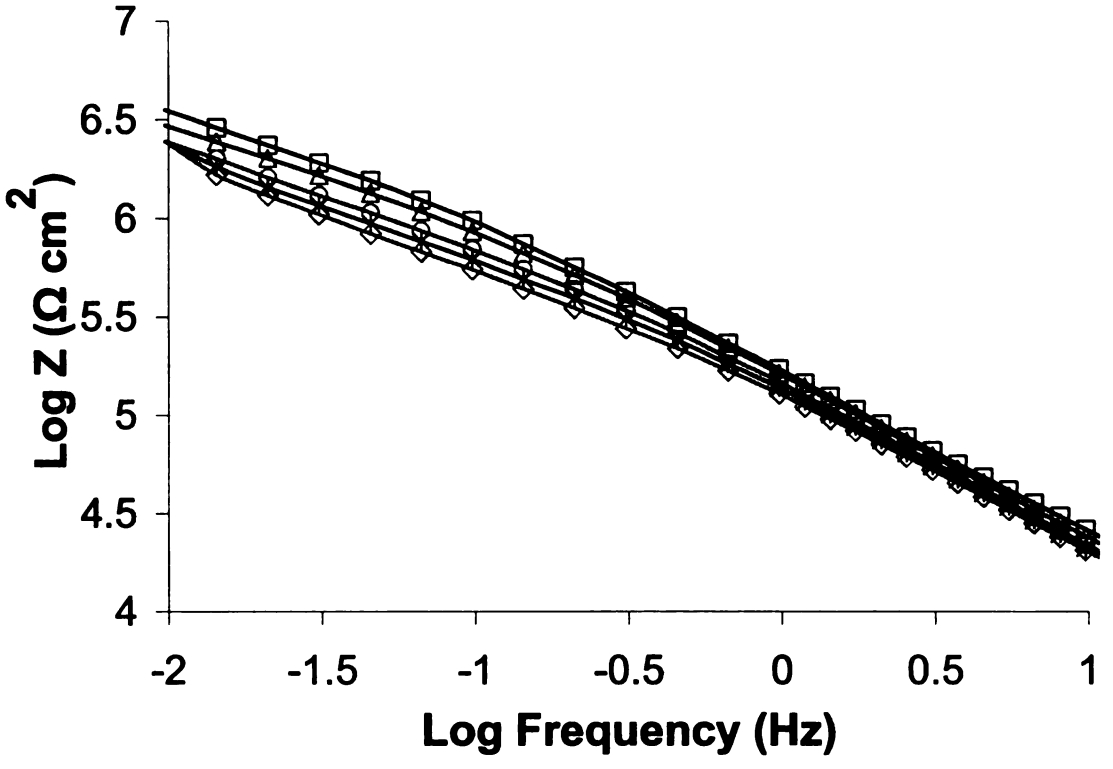

Figure 2.16: Impedance (Log Z) data were plotted as a function of Log frequency for DPPTE-DOPC tBLM and for DPPTE-DOPC tBLM after gramicidin incorporation at different protein concentration and ionic strength of NaCl solution. Squares: tBLM; triangles: tBLM containing 10 nM gramicidin in 10 mM NaCl solution; circles: tBLM containing 10 nM gramicidin in 100 mM NaCl solution; stars: tBLM containing 50 nM gramicidin in 100 mM NaCl solution; diamonds: tBLM containing 100 nM gramicidin in 100 mM NaCl solution. The membrane resistance decreased with increase in the ionic strength of solution and the protein concentration.

3. FUNCTIONAL CHARACTERIZATION OF PORB CLASS II PORIN FROM *NEISSERIA MENINGITIDIS* USING A TETHERED BILAYER LIPID MEMBRANE

3.1. Abstract

PorB class II (PorBII) from *Neisseria meningitidis* is a pore-forming, outer-membrane protein that can translocate to the host-cell membrane during *Neisserial* infections. This study describes development of tethered bilayer lipid membrane (tBLM) system to measure PorBII's conductance properties. tBLM was fabricated by depositing a self assembled monolayer (SAM) of 1,2-dipalmitoyl-*sn*-glycero-3-phosphothioethanol (DPPTE) tethering lipid on a gold electrode and then using 1,2-dioleoyl-*sn*-glycero-3-phosphocholine (DOPC) liposomes to deposit the upper tBLM leaflet. Electrochemical impedance spectroscopy (EIS) and cyclic voltammetry (CV) were used to monitor tBLM formation and subsequent PorBII incorporation. The highly insulating tBLM exhibited a membrane resistance and capacitance of 2.5 $M\Omega cm^2$ and 0.7 $\mu F/cm^2$, respectively. PorBII was incorporated into the tBLM in an active conformation, as evidenced by its mediation of ion passage and the decrease in membrane impedance. After PorBII incorporation, the membrane resistance decreased to 0.6 $M\Omega cm^2$. As expected, the PorBII channel was found to be non-selective, allowing the transport of both cations and anions. CV results indicated that ferricyanide ions can also pass through the pores. The PorBII-containing biomimetic interface developed in this study could potentially be used to screen for compounds that modulate PorBII activity.

3.2. Introduction

Porins are pore-forming, transmembrane proteins that allow the passage of water, ions, and nutrients through cell membranes. PorB class II (PorBII) outer membrane porin from *Neisseria meningitidis* functions similarly to other gram-negative bacterial porins (Murakami, K. *et al.*, 1989; Qi, H. L. *et al.*, 1994; Rudel, T. *et al.*, 1996; Minetti, C. *et al.*, 1997b). It forms a β-barrel structure in the *Neisserial* membrane (Weiss, M. S. *et al.*, 1991; Weiss, M. S. and Schulz, G. E., 1992) and has been implicated in the infection process (Weel, J. F. L. *et al.*, 1991; Weel, J. F. L. and Vanputten, J. P. M., 1991). PorBII can also translocate vectorially from the *Neisserial* membrane to host-cell membranes (Lynch, E. C. *et al.*, 1984). There, it interferes with the phagosome maturation and causes a rapid influx of calcium into the cell, which can trigger apoptotic cell death (Naumann, M. *et al.*, 1999). Thus, chemical agents that interfere with PorBII activity might be possible therapeutic agents to counteract *Neisserial* infections.

Artificial bilayer lipid membranes (BLM) have been extensively used to mimic biological cell membranes for studying membrane processes, such as signal transduction, ligand-receptor interactions and ion transport through cell membranes (Ottovaleitmannova, A. and Tien, H. T., 1992; Tien, H. T., 1995; Sackmann, E., 1996; Janshoff, A. and Steinem, C., 2006). The conventional planar bilayer approach involves forming a BLM across a small aperture in a partition between two aqueous solutions (Tien, H. T. and Ottova, A. L., 2001). Such free-standing BLMs are well suited to study protein-mediated ion transport, but they are very fragile and are typically stable for only about an hour. Tethered bilayer lipid membrane (tBLM) architecture (Lang, H. *et al.*, 1992; Lang, H. *et al.*, 1994; Cornell, B. A. *et al.*, 1997; Raguse, B. *et al.*, 1998; Krishna,

G. *et al.*, 2003) provides a stable BLM platform for studying ion channel proteins on an electrode's surface. In the tBLM approach, tethering molecules are used to establish a hydrophilic layer between the surface and the bilayer. These molecules bind to the electrode on one end, bind to the lipids that compose the lower bilayer leaflet on the other end, and have a hydrophilic central domain (Bunjes, N. *et al.*, 1997; Sinner, E. K. and Knoll, W., 2001; Schiller, S. M. *et al.*, 2003; Terrettaz, S. *et al.*, 2003; Jadhav, S. R. *et al.*, 2008a). This domain establishes a water-containing ion reservoir that facilitates ion transfer across the tBLM and also provides space to accommodate extra-membraneous protein domains. Electrochemical methods have been used to characterize tBLM containing a variety of proteins or ionophores, including valinomycin (Naumann, R. *et al.*, 2003a; Naumann, R. *et al.*, 2003b), gramicidin (Atanasov, V. *et al.*, 2005), mellitin (Becucci, L. and Guidelli, R., 2007), alamethicin (Yin, P. *et al.*, 2003), OmpF porin (Stora, T. *et al.*, 1999), M2 peptide (Vockenroth, I. K. *et al.*, 2007) and cytochrome c oxidase (Giess, F. *et al.*, 2004; Jeuken, L. J. C. *et al.*, 2006). Several electrode materials have been used for tBLM studies, such as gold (Schiller, S. M. *et al.*, 2003; Terrettaz, S. *et al.*, 2003; Kohli, N. *et al.*, 2006a) and mercury (Moncelli, M. R. *et al.*, 2004; Becucci, L. *et al.*, 2005a; Becucci, L. *et al.*, 2005b). The present study describes the functional incorporation of PorBII porin into a planar BLM interface, and a tBLM interface on a gold electrode. A highly insulating tBLM was deposited on a gold electrode in a two-step process, and solubilized PorBII porin was incorporated. Changes in tBLM impedance due PorBII incorporation were measured using electrical impedance spectroscopy (EIS) and cyclic voltammetry (CV).

3.3. Materials and methods

3.3.1. Expression and purification of PorBII porin

The PCR product of *Neisseria meningitidis* PorBII gene delta 1 to 62 was cloned into pGEM-Teasy (Promega), digested with *Nde*I and *Bam*HI, and ligated into pET17b (Novagen), which was engineered with an insert of an N-terminal hexa histidine tag and an rTev protease cleavage site, yielding pET17bNT-PorBII [Figure 3.1]. *E. coli* BL21-DE3 cells transformed with in plasmid pET17bNT-PorBII were inoculated into Luria-Bertani (LB) broth containing ampicillin (100 μg/mL) and grown at 37 °C. When the optical density at 600 nm (OD 600) of the cell culture reaches 1.0, a final concentration of 0.5 mM isopropyl-*β-D*-thiogalactopyranoside (IPTG) was added to induce the protein expression and the cell culture was incubated for an additional 3 h before harvested by centrifugation and stored at -70°C.

PorBII was purified using a modified procedure (Y. Zheng, D. Sui, and R. M. Garavito, manuscript in preparation) derived from protocols described elsewhere (Young, J. D. E. *et al.*, 1983; Qi, H. L. *et al.*, 1994; Minetti, C. *et al.*, 1997a; Minetti, C. *et al.*, 1998; Song, J. M. *et al.*, 1999). Brifly, for every gram of cell culture paste thawed, it was resuspended with 3 mL TEN buffer (50 mM Tris-HCl, 1 mM EDTA, 100 mM NaCl pH = 8.0). The cell suspension was pressurized up to 20,000 psi through Emulsiflex-C3 twice to thoroughly disrupt the cell membranes. Subsequently, phenylmethylsulfonyl fluoride (PMSF), $MgCl_2$, and DNase I, were added to the cell lysate at the final concentration of 1 mM, 20 mM, and 0.5 μg/mL, respectively. After 20 min of incubation on ice, the mixture was centrifuged at 10,000 rpm in an SS-34 rotor for 20 min at 4 °C.

The cell pellet was retained and homogenized with 0.5% (w/v) deoxycholic acid in the TEN buffer to wash off contaminant proteins. The second wash with TEN buffer alone was carried out to remove the deoxycholic acid. The washed cell pellet was unfolded with 10 mL TEN-urea buffer (8 M urea, one tablet of protease inhibitor cocktail obtained from Roche, Indianapolis, IN), resuspended, and sonicated for 3 min. The denatured protein solution was centrifuged at 12,000 rpm in SS-34 rotor for 20 min to remove any insoluble debris. The supernatant was mixed with an equal volume of 10% Zwittergent® 3-14 in TEN buffer. The PorBII protein mixture was then refolded by slowly (1 mL/min) diluting into 2X TEN buffer with 20 mM $CaCl_2$ and 0.05% Zwittergent® 3-14 to a final protein concentration of 3 mg/mL. The refolding PorBII solution was also centrifuged to remove any insoluble matter. The supernatant was loaded onto 20 mL Q-sepharose ion exchange column equilibtrated with buffer B (20 mM Tris-HCl, 200 mM NaCl, 0.05% Zwittergent® 3-14, pH 8.0). After 3 column volume wash of buffer B, the refolded PorBII protein was eluted by buffer B with a salt gradient from 200 mM to 1 M NaCl. PorBII fractions were pooled and loaded to metal chelating Ni-NTA column. The column was washed extensively with wash buffer (20 mM Tris-HCl, 200 mM NaCl, pH 8.0, 25 mM imidazole) containing 0.05% Zwittergent® 3-14. The PorBII protein was then eluted from the column by increasing imidazole concentration to 200 mM. The eluted protein is concentrated to about 1 mg/mL using ultrafiltration.

For cleaving hexa histidine tag from protein, the buffer was exchanged into rTev protease cleavage buffer (50 mM Tris-HCl, 0.1mM EDTA, 1 mM dithiothreitol) containing 0.2% *n*-decyl-β-D-maltoside or 0.02% *n*-dodecyl-β-D-maltoside. A higher

protein to rTev protease ratio was used to cleave off the hexa histidine tag from PorBII (for every 5 A.U. PorBII, 1 A.U. of rTev at OD 280 nm). The cleavage reaction was incubated at room temperature for 16 h. Cleaved PorBII was centrifuged to remove any insoluble matter. The supernatant was loaded to freshly equilibrated metal chelating Ni-NTA column to remove the rTev protease and the flow through was collected and concentrated to 5~10 mg/mL, using amicon ultra concentrators with molecular mass cutoff of 50 kDa (Millipore, Billerica, MA). Size exclusion chromatography (Superose 6 10/300 GL) was carried out to access the apparent molecular weight and the oligomeric state of the PorBII. The final purified protein, at >95% purity, was solubilized in 20 mM Tris-HCl buffer pH 8.0 containing 200 mM NaCl and 0.05% Zwittergent® 3-14.

3.3.2. Planar bilayer lipid membrane measurements

Planar BLM were painted across a 250 μm diameter aperture in a delrin cup (Warner Instruments, Hamden, CT) using a solution of DPhytPC lipids in *n*-decane (20 mg/mL). 10 mM HEPES buffer, pH 7.4 containing 1 M potassium chloride was used as electrolyte solution in both sides of BLM chamber (1 mL each). After painting the BLM, the BLM stability was tested by holding the potential at +100 mV and -100 mV for 5 min each. Detergent solubilized stock solution of PorBII was diluted in 20mM aqueous solution of tetraoxyethylene mono-*n*-octylether (C8E4). The diluted PorBII solution was added to *cis* side to achieve the required concentration of protein.

3.3.3. Fabrication and characterization of tBLM

SAM of DPPTE was assembled on cleaned gold substrates for 24 h. After SAM formation, the electrode was transferred to an electrochemical cell and small, unilamellar

of DOPC were added to deposit the upper tBLM leaflet. Bilayer formation was allowed to proceed for 24 h, after which the liposome solution was replaced with fresh 100 mM NaCl solution. The same procedure was used to create tBLM in $CaCl_2$ solution, except a 50 mM $CaCl_2$ solution was used instead of 100 mM NaCl. Purified PorBII solution was added to the pre-formed tBLM to give a final PorBII concentration of 1.0 μM protein (monomer) in electrolyte solution. Porin incorporation was allowed for an hour, and then the porin-containing solution was replaced with fresh electrolyte solution. Electrochemical measurements were performed using a CHI660B electrochemical workstation (CH Instruments Inc., Austin, TX). EIS was carried out in 100 mM NaCl solution using a 0 mV DC potential and a 5 mV sinusoidal potential across the frequency range of 0.001 to 10,000 Hz. Electrochemical parameters were calculated by fitting a Randles equivalent circuit to the impedance data [Figure 2.5], using Z-view software (Scribner Associates, Southern Pines, NC). CV was performed in 100 mM NaCl solution containing 1 mM potassium ferricyanide as a redox species. The potential was cycled in a range of 500 mV to -200 mV relative to an Ag/AgCl reference electrode at a scan rate of 50 mV/s.

3.4. Results and discussion

3.4.1. Measurement of PorBII activity using planar BLM

Planar BLMs were formed by painting either DOPC or DPhytPC lipids across a 250 μm aperture in delrin cup. PorBII was added to the *cis* side of the chamber to give a final concentration of 10 ng/mL in buffer solution. After PorBII addition, step increases in current were observed indicating incorporation of PorBII channels in BLM. Similar

conductance values were obtained using DPhytPC, and DOPC phospholipids. However, DPhytPC formed more stable BLMs than DOPC and hence, was used for further experiments. Using single channel experiments, it was observed that the channel remains fully open at +10 mV and the conductance remains constant for the duration of experiment (20 min). Around 1000 incorporations were examined to obtain the conductance distribution of PorBII in DPhytPC BLMs [Figure 3.2A]. It was found that the channel has varied conductance states (studied at +10 mV) with the most probable conductance state (60%) of 4.2 nS [Figure 3.2B]. It has been reported that porins from *Neisseria Sp.* exhibits multiple conductance states (Mauro, A. *et al.*, 1988; Song, J. M. *et al.*, 1998). The conductance state value was higher than the one obtained by other groups (Mauro, A. *et al.*, 1988; Rudel, T. *et al.*, 1996; Song, J. M. *et al.*, 1998) for PorBII from *N. gonorrhoeae* and for PorBIII from *N. meningitidis*. Factors such as type of lipids used to form BLM, method of forming BLM, and the presence of solvent in BLM might be responsible for the higher conductance value obtained with our system.

3.4.2. tBLM characterization and measurement of PorB II activity

3.4.2.1. Electrochemical impedance spectroscopy

tBLM was deposited and characterized as described earlier in Section 2.3.5. DOPC liposomes were used to deposit the upper leaflet of tBLM and EIS was used to monitor tBLM formation. EIS results indicated that the membrane resistance value (R_M) increased rapidly during the first few hours after adding vesicles to the SAM and then approached an asymptotic value after about 24 h. This trend is consistent with the mechanism of sBLM formation on planar glass surfaces, in which vesicles initially fuse onto the surface at random locations, forming bilayer patches, and then gaps are

gradually filled over time (Cremer, P. S. and Boxer, S. G., 1999). A Bode plot showing EIS results for the tBLM 24 h after vesicle addition is shown in Figure 3.3 (squares). Fitting the Randles equivalent circuit shown in Figure 2.5 to impedance data gave a total membrane capacitance (C_M) value of 0.709 $\mu F/cm^2$, which is in agreement with the reported tBLM capacitance value of 0.5 – 0.8 $\mu F/cm^2$ (Schiller, S. M. *et al.*, 2003). The R_M value of 2.50 $M\Omega cm^2$ for a tBLM indicated the formation of highly insulating tBLM that is impermeable to sodium and chloride ions. Addition of 1 μM PorBII (monomer) to the electrolyte solution after tBLM fabrication decreased R_M from 2.50 $M\Omega cm^2$ to 604 $k\Omega cm^2$ for the tBLM produced and characterized in 100 mM NaCl solution [Figure 3.3]. These results are consistent with a conceptual model in which PorBII monomers self-assemble in the bilayer membrane to form a trimeric pore that allows ion passage across the BLM (See planar BLM results in Chapter 4) thereby decreasing the membrane resistance. EIS data for a tBLM formed in 50 mM $CaCl_2$ solution gave C_M and R_M values of 0.81 $\mu F/cm^2$ and 24 $M\Omega cm^2$, respectively [Figure 3.4]. The tBLMs prepared in $CaCl_2$ solution consistently provided higher membrane resistance values than those prepared in NaCl, possibly because of tighter lipid packing in the presence of calcium salts. PorBII addition resulted in a membrane resistance decrease from 24 $M\Omega cm^2$ to 1.93 $M\Omega cm^2$. The large drops in R_M following PorBII addition suggested that PorBII significantly increases ion transport across the tBLM. A large ΔR_M obtained with tBLM interface is in agreement with the large conductance obtained with the planar BLM

studies. However, the PorBII-mediated ion influx inside host cell is reported to be regulated by the nucleotides (ATP and GTP) that may prevent toxic effects to the target cell (Rudel, T. *et al.*, 1996).

In contrast to the large change in resistance values, addition of PorBII to the tBLM had little effect on membrane capacitance, because the area occupied by the porin inside tBLM is negligibly small. A control experiment was conducted to determine whether the Zwittergent® 3-14 detergent used to solubilize PorBII affected the tBLM's impedance properties. Detergent was added to obtain the same total detergent concentration as was present after addition of detergent-solubilized protein. The impedance spectra of the pre-formed tBLM was unaffected by detergent addition.

We used the conductance data obtained from planar BLMs to estimate the number of channels in tBLM interface. The bulk (multiple) channel conductance in tBLM can be obtained using following relationship-

$$\frac{1}{R_{MTOTAL}} = G_{MTOTAL} = \frac{1}{R_{MBLM}} + \frac{1}{R_{PORE}} = G_{MBLM} + G_{PORE} \quad \ldots \text{ Eq (3.1)}$$

where, R_{MTOTAL} stands for the R_M value measured in the presence of PorBII in tBLM, R_{MBLM} represents the R_M obtained in absence of PorBII and R_{PORE} represents the pore resistance (G_{MTOTAL}, G_{MBLM} and G_{PORE} represent the corresponding conductance values). G_{PORE} obtained from Equation 3.1 was divided by the average single-channel conductance obtained from planar BLM study to calculate a PorBII channel density of about 354 channels per cm^2 of tBLM.

3.4.2.2. Cyclic voltammetry

Cyclic voltammograms of the tBLM in the presence of ferricyanide [Figure 3.5] lacked redox peaks, confirming formation of a high-impedance tBLM that is impermeable to ferricyanide anions. However, PorBII addition resulted in a well defined peak for ferricyanide reduction, presumably due to PorBII-mediated ferricyanide-ion transport across the bilayer. Minetti et al. studied permeation of oligosaccharides through proteoliposomes containing PorBII (Minetti, C. *et al.*, 1997b) and estimated a channel pore diameter of 1.6 nm, which is greater than the ionic radii of most of common ions.

These results indicate that detergent-solubilized PorBII readily incorporates itself into pre-formed tBLM in an active conformation. This finding is consistent with PorBII's previously reported ability to spontaneously incorporate itself into cell membranes, thereby facilitating the infection process (Lynch, E. C. *et al.*, 1984; Naumann, M. *et al.*, 1999). The relative ease with which PorBII can be inserted into a pre-formed tBLM provides a facile method for electrochemical characterization of the channel's activity. In this method, the tBLM's resistance is measured before and after PorBII addition, and the resulting change in resistance is taken to be a measure of the protein's channel-forming activity. The tBLM interface was easily fabricated using commercially available DPPTE lipids and provided a large drop in membrane resistance following PorBII addition. This approach obviates the need for custom-synthesized tethering lipids that are used in tBLM based interfaces for studying ion transport across BLM (Raguse, B. *et al.*, 1998; Stora, T. *et al.*, 1999; Schiller, S. M. *et al.*, 2003). In contrast to PorBII, many ion-transporting membrane proteins cannot be easily transferred from aqueous solution into a preformed tBLM. An alternative method for such proteins is to first embed the proteins into

liposomes, and then to use the resulting proteoliposomes to simultaneously deposit both the top leaflet of the tBLM and the protein (Vockenroth, I. K. *et al.*, 2007). However, this approach precludes direct measurement of the tBLM's resistance before and after protein addition.

This study describes for the first time the functional characterization of a *Neisserial* PorBII porin using EIS. The facile method, which is based on molecular self-assembly, is suitable for miniaturization and automation, and thus may be adapted to biosensor arrays. PorBII was shown to be an excellent model ion channel for tBLM studies, because it is easily incorporated into pre-formed tBLM in concentrations that give substantial ΔR_M values. The PorBII-containing biomimetic interfaces were found to be stable and are suitable for applications including high-throughput screening for lead compounds that modulate PorBII activity, and optimization of methods to form biomimetic interfaces that express membrane-protein activities.

3.5. Conclusions

A novel biomimetic interface was developed by incorporating the *Neisserial* PorBII porin into a tBLM formed on gold using DPPTE tethering lipid and DOPC mobile lipids. Simultaneously, PorBII activity and its conductance distribution were characterized using conventional planar BLM technique. Detergent-solubilized PorBII spontaneously incorporated into highly-insulating tBLM in a functional conformation, allowing its ion-transport properties to be characterized using EIS and CV. EIS studies showed that contacting a tBLM with 1 μM PorBII solution resulted in roughly one order of magnitude decrease in R_M in both NaCl and $CaCl_2$ solutions, although both the R_M

and ΔR_M values were higher in $CaCl_2$ than in NaCl. CV studies indicated that PorBII also passes ferricyanide ions. The PorBII-containing biomimetic interface has potential utility for high-throughput screening of compounds that modulate PorBII activity and as a model interface for developing tBLM-based technologies.

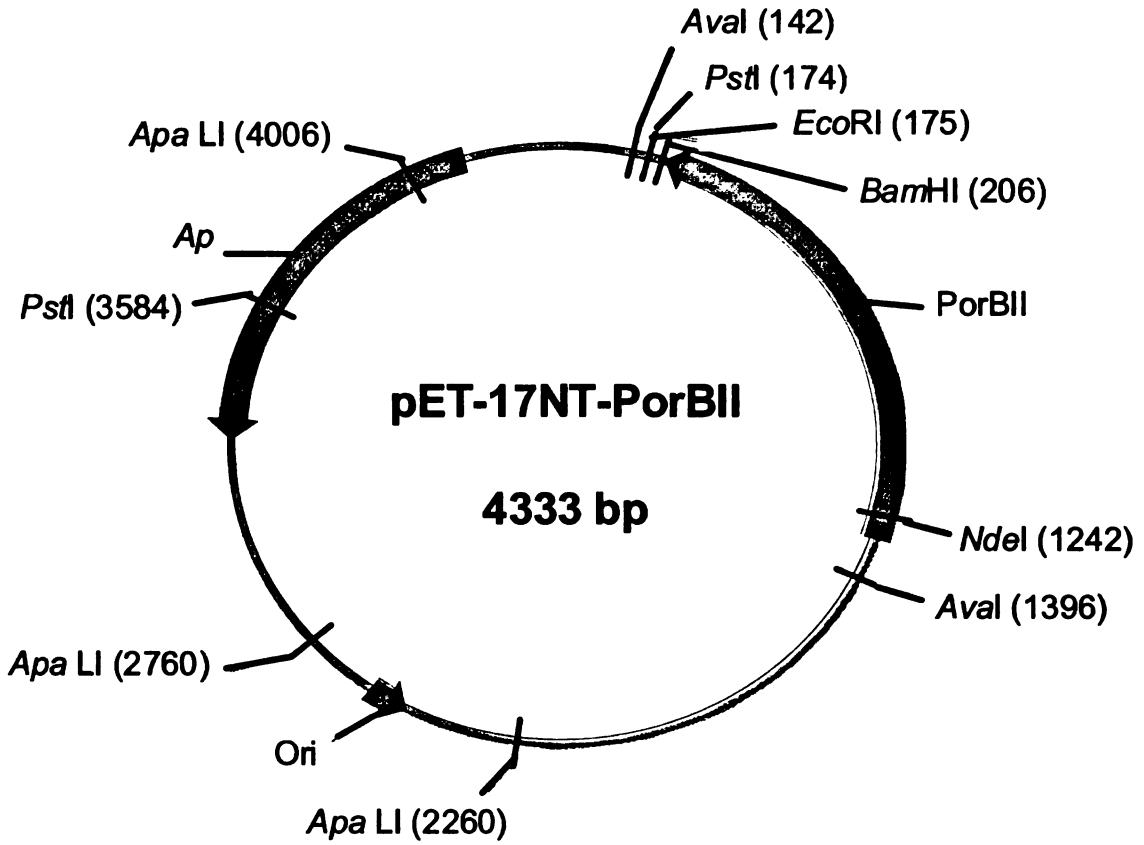

Figure 3.1: pET17bNT-PorBII construct used to transform *E.coli*BL21 cells for expressing PorBII. The PCR product of *Neisseria meningitidis* PorBII gene delta 1 to 62 was cloned into pGEM-Teasy, digested with *Nde*I and *Bam*HI, and ligated into pET17b (Novagen), which was engineered with an insert of an N-terminal hexa histidine tag and an rTev protease cleavage site, yielding pET17bNT-PorBII.

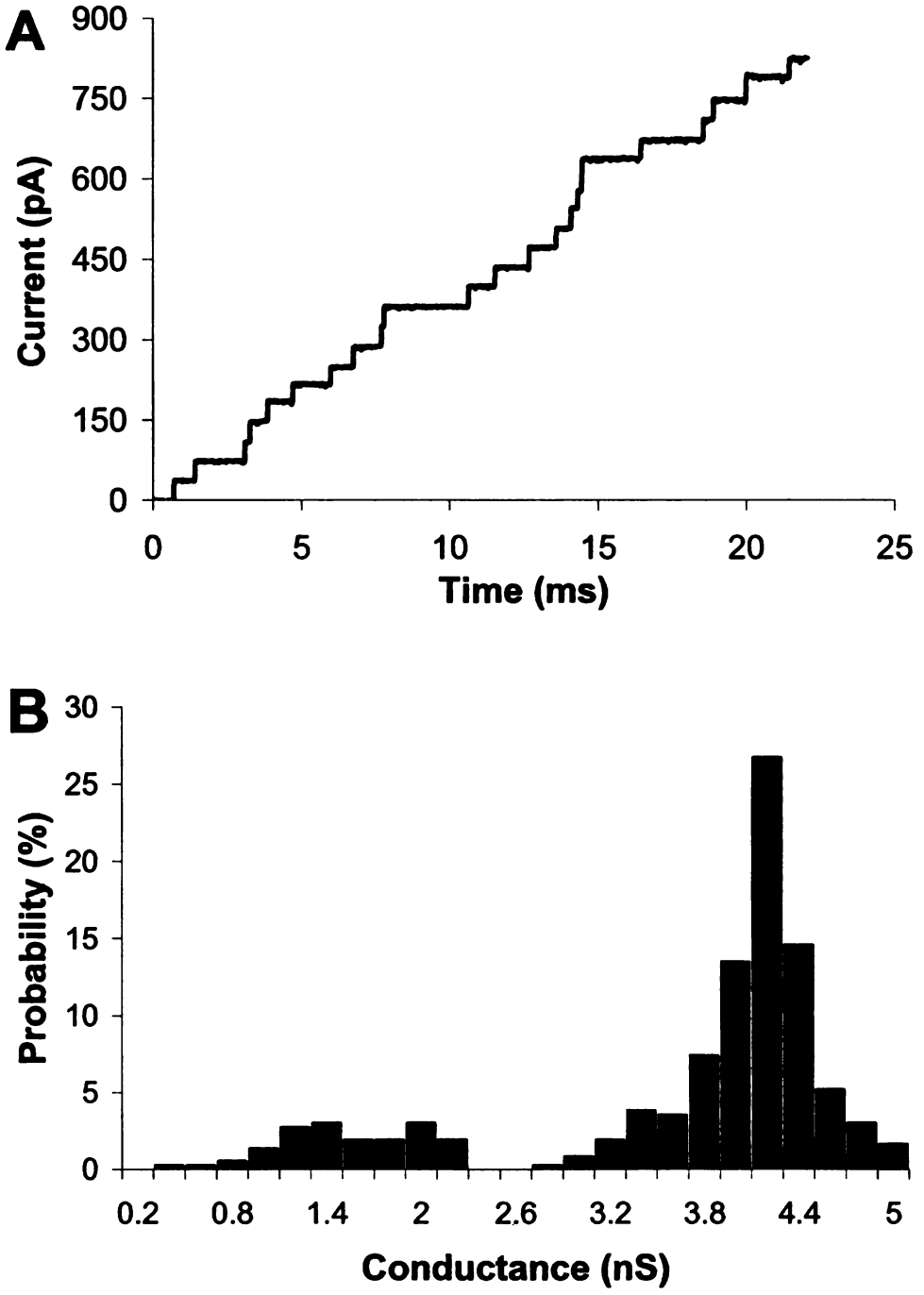

Figure 3.2: (A) Recordings of DPhytPC/*n*-decane BLM showing PorBII channel insertions. (B) Histogram of channel conductance of PorBII in DPhytPC BLM, obtained from 1000 channel insertion recordings, showing the probability of occurrence of particular conductance unit. The conductance values were pooled in bins of 0.2 nS. Experimental conditions: Both bilayer compartments had 1 mL of 20 mM HEPES buffer (pH 7.4) containing 1 M KCl; PorBII concentration in *cis* chamber was 100 pg/mL; Applied potential was +10 mV.

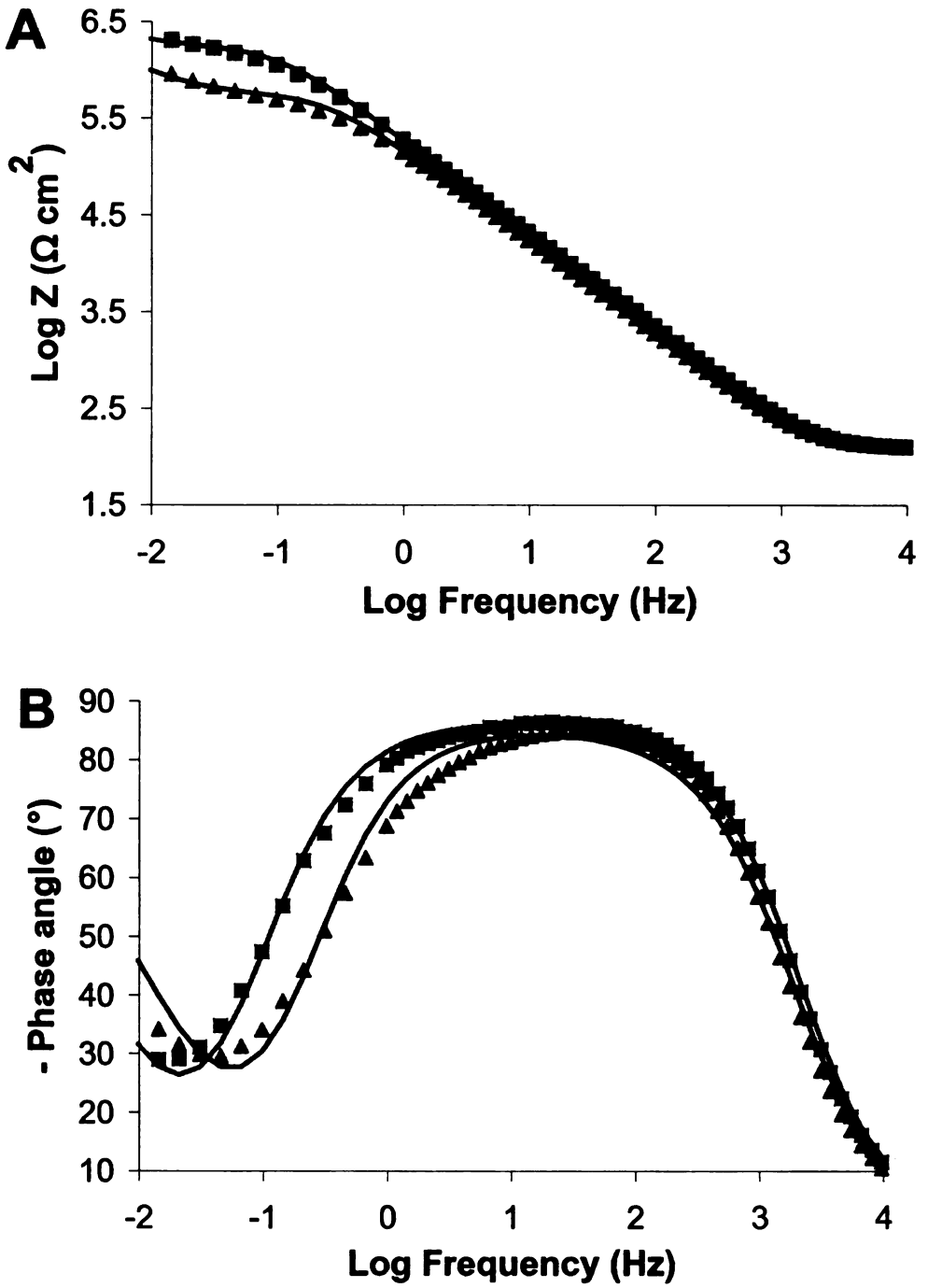

Figure 3.3: (A) Impedance (Log Z) data and (B) phase angle data were plotted as a function of Log frequency for DPPTE-DOPC tBLM (squares) and for DPPTE-DOPC tBLM after PorBII incorporation (triangles) in 100 mM NaCl. An equivalent circuit shown in Figure 2.5 was fitted to the impedance data. The solid lines passing through the data points represent the model fit. PorBII was added to give a final concentration of 1 μM protein (monomer) in an electrolyte solution. Membrane resistance decreased significantly due to the ion transport through the tBLM, whereas there was no significant change in membrane capacitance.

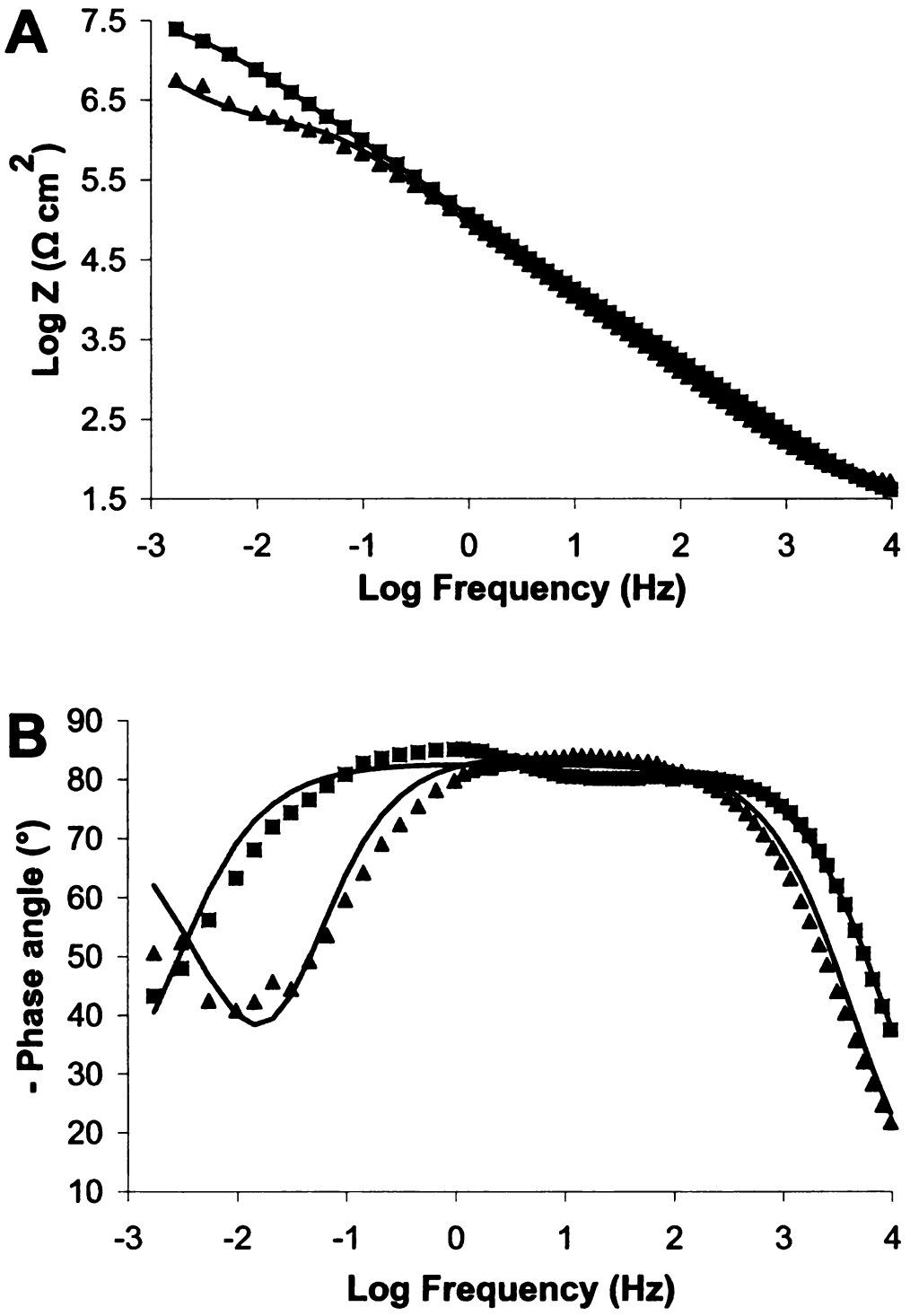

Figure 3.4: (A) Impedance (Log Z) data and (B) phase angle data were plotted as a function of Log frequency for DPPTE-DOPC tBLM (squares) and for DPPTE-DOPC tBLM after PorBII incorporation (triangles) in 50 mM calcium chloride. An equivalent circuit shown in Figure 2.5 was fitted to the impedance data. The solid lines passing through the data points represent the model fit. PorBII was added to give a final concentration of 1 μM protein (monomer) in an electrolyte solution.

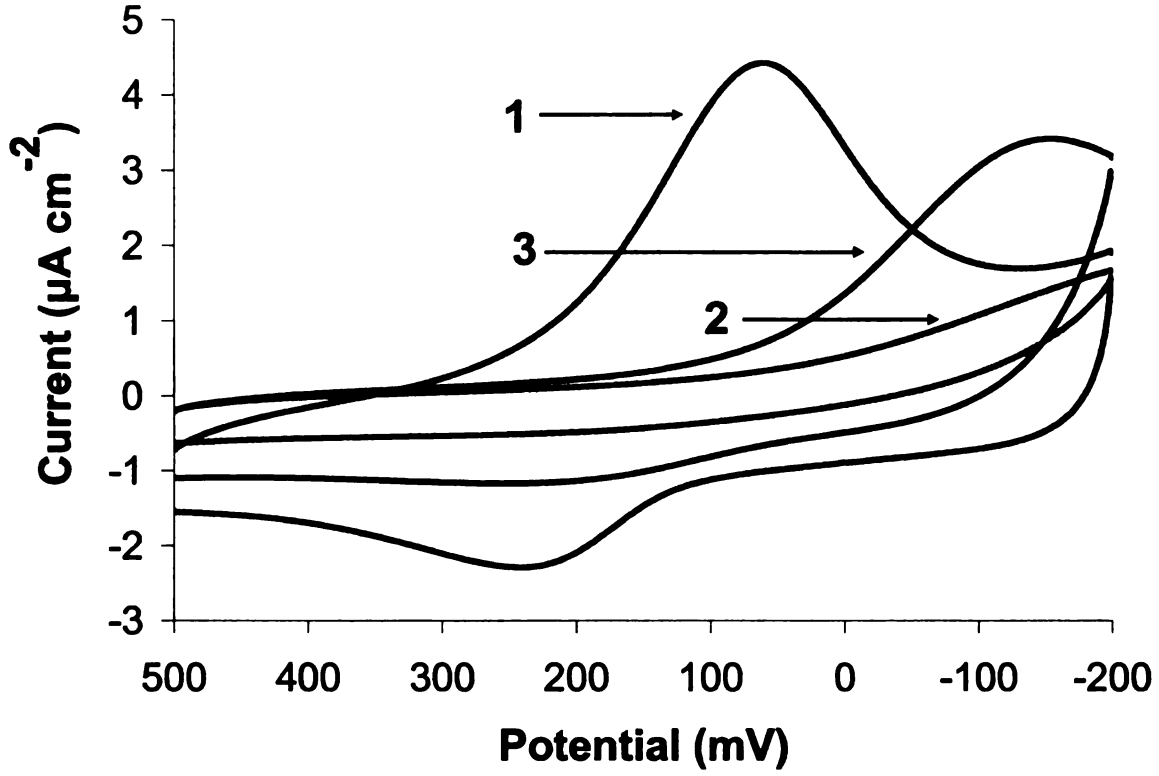

Figure 3.5: CV curves for a bare gold electrode coated with a tethering lipid monolayer (curve 1), a tBLM formed by deposition and rupture of DOPC liposomes on top of the DPPTE tethering lipid monolayer (curve 2), and the DPPTE-DOPC tBLM after PorBII incorporation (curve 3). The redox peaks were absent after bilayer formation but were observed after PorBII incorporation, suggesting PorBII-mediated transport of ferricyanide ions through tBLM.

4. VOLTAGE DEPENDENT CLOSURE OF PORB CLASS II PORIN FROM *NEISSERIA MENINGITIDIS* INVESTIGATED USING ELECTROCHEMICAL IMPEDANCE SPECTROSCOPY IN A TETHERED BLM INTERFACE

4.1. Abstract

Electrochemical impedance spectroscopy (EIS) was used to show a reversible, voltage dependent closure of PorB class II (PorBII) porin from *Neisseria meningitidis* incorporated in a tethered bilayer lipid membrane (tBLM) interface. The voltage dependent conductance properties of recombinant PorBII porin were characterized using two bilayer lipid membrane (BLM) interfaces: the conventional planar bilayer membrane and a tBLM interface. A stable tBLM interface was fabricated by depositing a self assembled monolayer (SAM) of 1,2-dipalmitoyl-*sn*-glycero-3-phosphothioethanol (DPPTE) tethering lipids on gold surface and then liposomes made of 1,2-dioleoyl-*sn*-glycero-3-phoshocholine (DOPC) lipids were used to deposit the upper leaflet of BLM. At 0 mV bias DC potential, incorporation of PorBII mediated transport of ions across tBLM decreasing the membrane resistance (R_M) from 2.5 $M\Omega cm^2$ to 0.6 $M\Omega cm^2$ (ΔR_M = 1.9 $M\Omega cm^2$). As DC potential was increased, the values for normalized R_M (ΔR_M normalized to the R_M of tBLM at respective potential) decreased, indicating a lower conductance of PorBII. At 200 mV bias DC potential, the normalized R_M value was 20% of the value observed at 0 mV DC. The decrease in conductance of PorBII porin at higher DC potentials suggested a voltage dependent closure of PorBII. Further, it was observed that changing the DC potential from 200 mV back to 0 mV reproduced the

ΔR_M value observed previously at 0 mV, indicating that the voltage dependent closure of PorBII was reversible. Single channel studies, conducted using planar DPhytPC BLM, confirmed the reversible, voltage dependent closure of PorBII porin at high transmembrane potentials. The trimeric porin closes in three discrete steps, each step corresponding to closure of one conducting monomer unit. The approach involving the use of tBLM interface and impedance spectroscopy provides a simple, high-throughput method for preliminary characterization of voltage-gated proteins.

4.2. Introduction

The conductance of *Neisserial* porins is modulated by transmembrane potential, thereby allowing regulation of ion and nutrient transport across *Neisserial* cell membranes (Blake, M. S., Gotschlich, E.C., 1987; Mauro, A. *et al.*, 1988; Bainbridge, G. *et al.*, 1998). Using planar bilayer lipid membrane (BLM) technique, a voltage dependent closure of porin has been reported for *Neisserial* porins such as protein I from *Neisseria gonorrhoeae* (Young, J. D. E. *et al.*, 1983), PorB class II (PorBII) porin from *N. gonorrhoeae* (Rudel, T. *et al.*, 1996), and PorB class III porin from *N. meningitidis* (Song, J. M. *et al.*, 1998). Blake and co-workers have done extensive structural and functional characterization of porins from *Neisseria sp.* (Blake, M. S. and Gotschlich, E. C., 1982; Lynch, E. C. *et al.*, 1984; Blake, M. S., Gotschlich, E.C., 1987; Mauro, A. *et al.*, 1988; Qi, H. L. *et al.*, 1994; Song, J. M. *et al.*, 1998; Song, J. M. *et al.*, 1999). They have reported that recombinant PorBII porin from *N. meningitidis* exhibits similar functional properties as wild type PorBII protein. They found that the recombinant PorBII assembles as a trimer in the membrane, forming pores that are ~1.6 nm in diameter (liposome swelling assay) (Minetti, C. *et al.*, 1997b).

In the present study, we have used two BLM interfaces to characterize the voltage dependent conductance properties of PorBII porin, namely a planar BLM, and a tethered bilayer lipid membrane (tBLM) interface. Using planar BLM technique, ion transfer through a single channel can be measured electrochemically to characterize the channel's conductance states, open probability, and gating properties (Miller, C., 1986). The voltage across the BLM can be tightly controlled to study the voltage dependence of the channel conductance, as well as the channel closure. However, the major limitation of the planar BLMs is that its very fragile lasting only a couple of hours before breaking. tBLM combines the stability of a supported BLM with an ion reservoir between the BLM and electrode. Electrochemical impedance spectroscopy (EIS) has been used to study ion-transporting membrane proteins embedded in tBLM interfaces (Naumann, R. *et al.*, 2003a; Naumann, R. *et al.*, 2003b; Schiller, S. M. *et al.*, 2003; Giess, F. *et al.*, 2004; Moncelli, M. R. *et al.*, 2004; Atanasov, V. *et al.*, 2005; Kohli, N. *et al.*, 2006a; Becucci, L. and Guidelli, R., 2007; Becucci, L. *et al.*, 2008; Jadhav, S. R. *et al.*, 2008a; Jadhav, S. R. *et al.*, 2008b; Knoll, W. *et al.*, 2008). Although tBLMs have been used to study membrane-insertion rate of voltage-dependent alamethicin peptides (Yin, P. *et al.*, 2003), and used with patch-clamp techniques to study ion channel gating by voltage-induced stress (Andersson, M. *et al.*, 2008), use of IS to study the voltage dependent change in a transmembrane protein's conductance properties due to channel closure has not been explored. In this study, we report, for the first time, use of IS to study the voltage-dependent closure of a transmembrane protein embedded in a tBLM interface. Changes in PorBII conductance were measured at different DC potentials in tBLM interface using

EIS, while single channel measurements were carried out in planar BLMs to confirm voltage-dependent closure of PorBII.

4.3. Materials and methods

Please refer to the Section 3.3 for the material and methods used. The voltage depedent properties were studied in a potential range of +110 mV to -110 mV in planar BLM experiments. In tBLM experiments, DC potential used in EIS studies was changed from +200 mV to -200 mV while the sinusoidal potential was 5 mV.

4.4. Results and discussion

4.4.1. Voltage dependence of PorBII conductance in planar BLM

At higher transmembrane potentials, PorBII conductance was found to decrease in three discrete steps suggesting that the pore has a trimeric structure [Figure 4.1]. Each step decrease in the conductance corresponded to closure of one conducting monomer unit. The closure pattern was not constant, with one, two or even three monomers closure events occuring at same time. Figure 4.1 indicates that the fully closed form of the porin still exhibits a low level of conductance. PorBII's closed-state conductance at a membrane potential of 100 mV was 26% that of the fully open trimeric pore. When the applied potentials were returned to lower potentials (between +50 mV to -50 mV), the fully open channel conductance was restored indicating that the voltage dependent channel closure was reversible. The plot of normalized conductance (ratio of conductance at respective applied potential to the conductance value at +10 mV) as a function of applied potential [Figure 4.2] showed that the pore closure starts after ± 50 mV. Rudel *et al.* observed similar channel closure behavior for PorBII porin from *N. gonorrhoeae*

(Rudel, T. *et al.*, 1996). The conductance study was limited to potentials between +120 mV to -120 mV range because BLM was found to be unstable at potentials above + 120 mV and below -120 mV. At positive potentials, it appeared that the closed conductance state of the porin approaches asymptotic steady state value. The following version of Boltzmann distribution used by Song *et al* (Song, J. M. *et al.*, 1998) was fitted to the voltage dependent conductance data to obtain the voltage dependent parameters of porin-

$$\ln\left[\frac{G_{MAX}-G}{G-G_{MIN}}\right]=\frac{nF}{RT}\left(V-V_0\right) \quad \text{..... Eq. (4.1)}$$

where, G_{MAX} is the maximum open channel conductance, G is the channel conductance observed at respective applied potential V, G_{MIN} is a voltage independent conductance, F is Faraday's constant, R is gas constant, T is temperature, n is the number of charges transferred across BLM, and V_0 is the voltage at which the channel has equal probability of being in open or closed state. The right hand side of Equation 4.1 was plotted as a function of applied potential V for positive and negative potentials and the values for n and V_0 were obtained from the slope and intercept of the plot, respectively. The voltage dependent free energy ($\Delta G = nFV_0$) can be calculated using experimentally obtained voltage-dependent parameters. At positive potentials, the ΔG value of 13.4 kJmol^{-1} was obtained whereas at negative potentials, ΔG value of 12.7 kJmol^{-1} was obtained. ΔG represents the voltage dependent energy that must be overcome for a channel to undergo

conformational change from open to closed state. Further, experimentally obtained n and V_0 values were used to obtain the open probability (P_{open}) using following equation

$$P_{open} = \frac{1}{\left[1 + \exp\left(\frac{n_+F\left(V - V_{0+}\right)}{RT}\right) + \exp\left(\frac{n\_F\left(V - V_{0-}\right)}{RT}\right)\right]} \quad \text{Eq (4.2)}$$

where n_+, V_{0+} and n_-, V_{0-} are the n and V_0 values obtained for the positive and negative potentials, respectively. The fitting of open probability to the voltage dependent porin conductance data is shown in Figure 4.3.

The planar BLM results indicated that PorBII porin self-assembles as a trimeric pore in BLM, the channel is fully open at low transmembrane potentials, and that the porin undergoes a reversible voltage dependent closure at higher transmembrane potentials. These results are in agreement with the reports that *Neisserial* porins show a large decrease in the single channel conductance at higher transmembrane potentials (Young, J. D. E. *et al.*, 1983; Mauro, A. *et al.*, 1988; Rudel, T. *et al.*, 1996). Planar BLM studies conducted by Rudel *et al.* on PorBII porin from *N. gonorrhoeae* showed a decrease in PorBII conductance at transmembrane potentials above +50 mV and below -50 mV (Rudel, T. *et al.*, 1996). Studies conducted by Song *et al* using PorB class III porin from *N. meningitidis* showed that the wild type and the recombinant porin have similar voltage dependent conductance properties (Song, J. M. *et al.*, 1998). They observed that PorBIII porin undergoes voltage dependent closure even at low applied potentials (V_0 = 14.8 mV). However, in our studies, we did not observe porin closure

upto ±50 mV. The exact mechanism of voltage dependent closure of porins is still not clear. Nonetheless, the voltage gating property of porins is crucial for regulating the conduction of ions and molecules across the cell membranes of bacteria.

4.4.2. EIS study of a voltage dependent channel closure in a tBLM interface

Unlike planar BLM, tBLM provides a mechanically robust BLM system that is addressable using various analytical techniques and adaptable to the automated high-throughput platforms. However, measurements using tBLM interface are less sensitive than planar BLMs. tBLMs are more suitable for measuring bulk channel behavior as opposed to single channel activity measurable by planar BLMs. tBLM's impedance was measured at different DC potentials ranging from +200 mV to -200 mV; a representative curve obtained at 200 mV is shown in Figure 4.4. The R_M and C_{DL} values changed with applied potential. The electrical double layer is believed to undergo rearrangement in response to a change in applied DC potential, resulting in altered ion distribution inside and around tBLM (Cevc, G. *et al.*, 1981), and, consequently, altered R_M and C_{DL} values. As the membrane capacitance is largely dominated by the dielectric constant of the BLM's hydrophobic core, there was negligible change observed in the C_M value. The difference in R_M value of tBLM before and after PorBII incorporation (ΔR_M) is a measure of ion conduction by porin across tBLM. From the impedance data at different DC potentials, the normalized R_M value, defined as the ratio of ΔR_M to the tBLM's R_M at that potential before protein addition, was calculated and was used to plot the

fractional NR_M (ratio of NR_M at respective potential to NR_M at 0 mV DC) as a function of applied DC potential [Figure 4.5]. As shown in Figure 4.5 (diamonds), the fractional NR_M value decreased continuously from 0 mV to 200 mV. These results indicated that the conductance of PorBII containing tBLM decreased at higher DC potentials, possibly due to a voltage dependent closure of PorBII. Toggling the DC potential back and forth between 0 mV and ±200 mV gave consistent and reproducible NR_M values, indicating that the pore closure is completely reversible. These observations were consistent with planar BLM results. Comparison of Figures 4.2 and Figure 4.5 (diamonds) indicates that the effect of transmembrane potential on PorBII conductance in tBLMs follow different trend than the one observed in planar BLMs. This result is not surprising considering the significant differences between the two experimental systems. Unlike the planar bilayer, the tBLM has the working electrode in close proximity to the bilayer and tethering linkages that bind the lower leaflet of the bilayer to the electrode. This difference would be expected to result in differences in the charge distribution across the tBLM, the ion concentration in the vicinity of the bilayer, and the electrical double layer structure, all factors that could influence the transmembrane potential.

To establish that the voltage dependence of ΔR_M was a porin-related phenomenon, the tBLM experiments were repeated using the cation-selective peptide gramicidin in place of PorBII. There was a <10% change in NR_M values when the DC potential was varied from -200 mV to +200 mV [Figure 4.5 (squares)]. Small changes in NR_M observed at high positive potentials for tBLMs containing gramicidin have been

attributed to cation repulsion by the positively charged electrode (Yin, P. *et al.*, 2003). This study clearly demonstrates the ability of EIS and tBLM interface to differentiate between the voltage dependent and voltage independent protein activities.

4.4.3. Voltage dependent closure of PorB II in symmetric tBLM

To address the effect of membrane asymmetry on the PorBII conductance behavior, the upper leaflet of tBLM was deposited using liposomes made of DPPTE. The DPPTE liposomes were prepared by hydrating the dry lipid film in 10 mM HEPES buffer, pH 7.4 at 60°C. Small unilamellar vesicles were obtained by sonicating the lipid suspension (using bath sonicator) above the phase transition temperature of DPPTE (~ 40°C). DPPTE liposomes were incubated with DPPTE SAM for 24 h to complete tBLM formation. The tBLM experiments were conducted at 22°C, a temperature at which the tBLM exists in a gel state. As a result, a very high impedance tBLM with the membrane resistance of 41.2 $M\Omega cm^2$ was obtained. After addition of 1 μM PorBII (monomer), the R_M value decreased to 4.75 $M\Omega cm^2$ at 0 mV DC potential (Figure 4.6A). However, at 200 mV DC potential, the R_M value decreased from 42.5 $M\Omega cm^2$ to 37.3 $M\Omega cm^2$ (Figure 4.6B), corresponding to a normalized R_M of 0.12. These results indicated that PorBII shows a voltage dependent behavior in both symmetric and asymmetric tBLMs.

4.5. Conclusions

The study demonstrates, for the first time, the use of tBLM along with EIS to measure voltage-dependent closure of a channel protein. A strong dependence of ΔR_M on applied voltage was observed for PorBII but not gramicidin, indicating voltage-

induced closure of PorBII. Single channel measurements conducted using the traditional planar BLM technique clearly demonstrated a three step closure of the porin at higher transmembrane potentials decreasing porin conductance, supporting the EIS results. The finding that voltage-dependent closure of channel proteins can be measured in tBLM using EIS is significant, because this approach can be readily miniaturized and adapted to robotic systems for high-throughput applications including functional proteomics, biosensors, and drug screening.

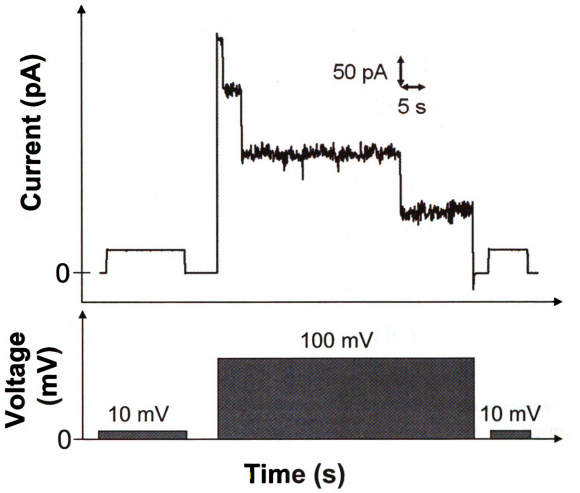

Figure 4.1: Unitary response of recombinant PorBII porin incorporated in DPhytPC lipid bilayer. The magnitude and length of applied potential is indicated below the current recording. Single channel insertion of 4.2 nS was observed at +10 mV. Increasing the potential to +100 mV closes the porin in three discrete steps, indicative of closure of each conducting monomer. The porin channel was reopened by reducing the potential to +10 mV, indicating that the porin closure is completely reversible.

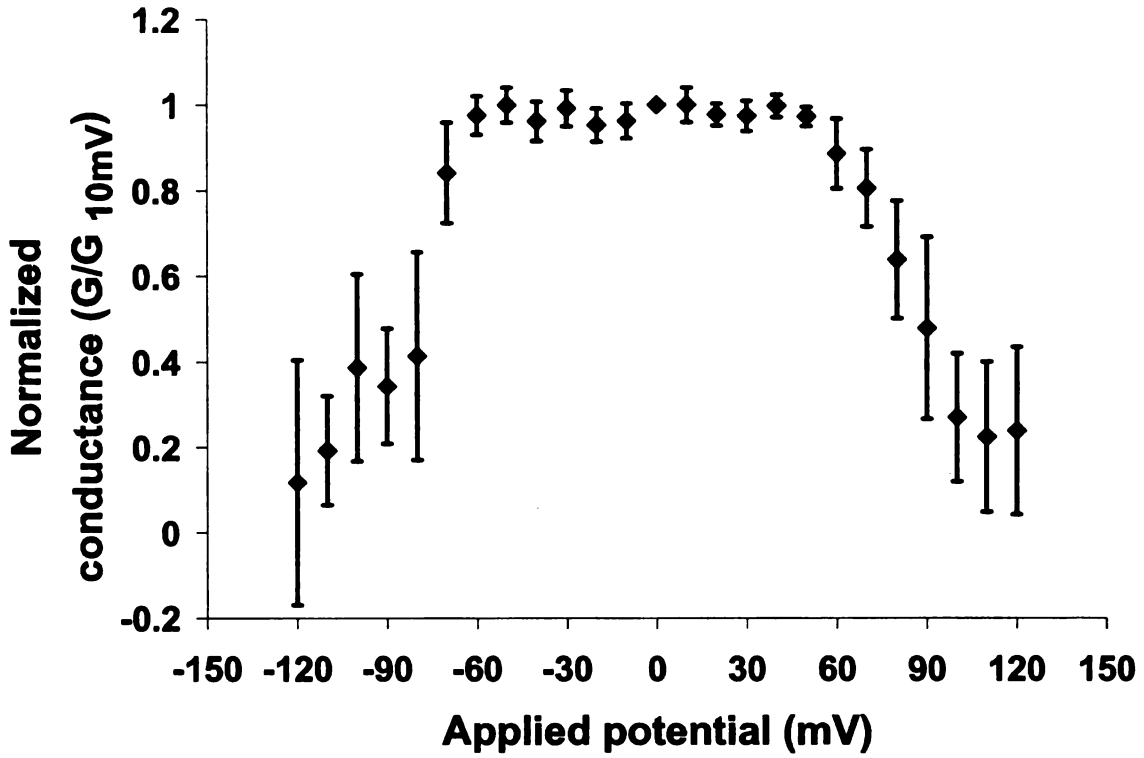

Figure 4.2: Normalized single channel conductance (Ratio of conductance at respective potential [G] to the conductance at +10 mV [G_{10mV}] plotted as a function of applied potential. Five separate experiments were conducted at each potential. Lipids used- DPhytPC, PorBII concentration- 1 pg/mL, other experimental conditions were same as described in Figure 3.2.

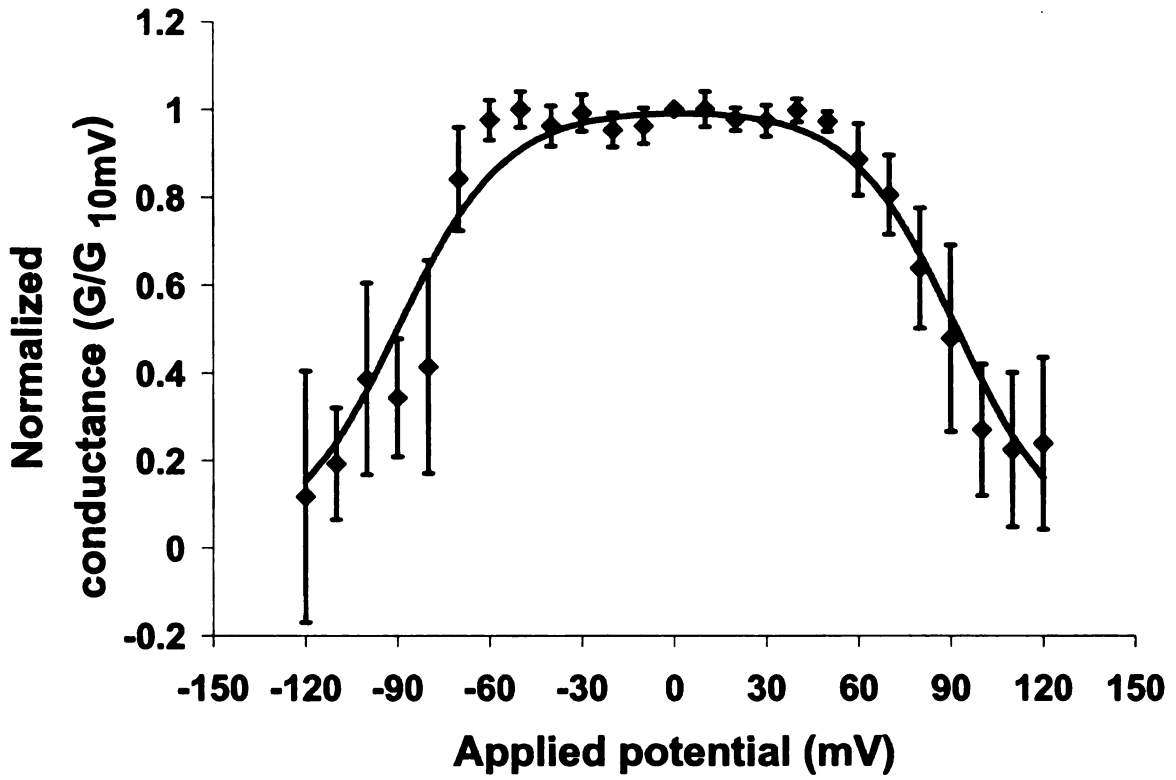

Figure 4.3: Open probability calculated from Equation 4.2 using experimentally obtained n and V_0 values. Open probability, shown using solid line, is overlaid on the voltage dependent porin conductance data.

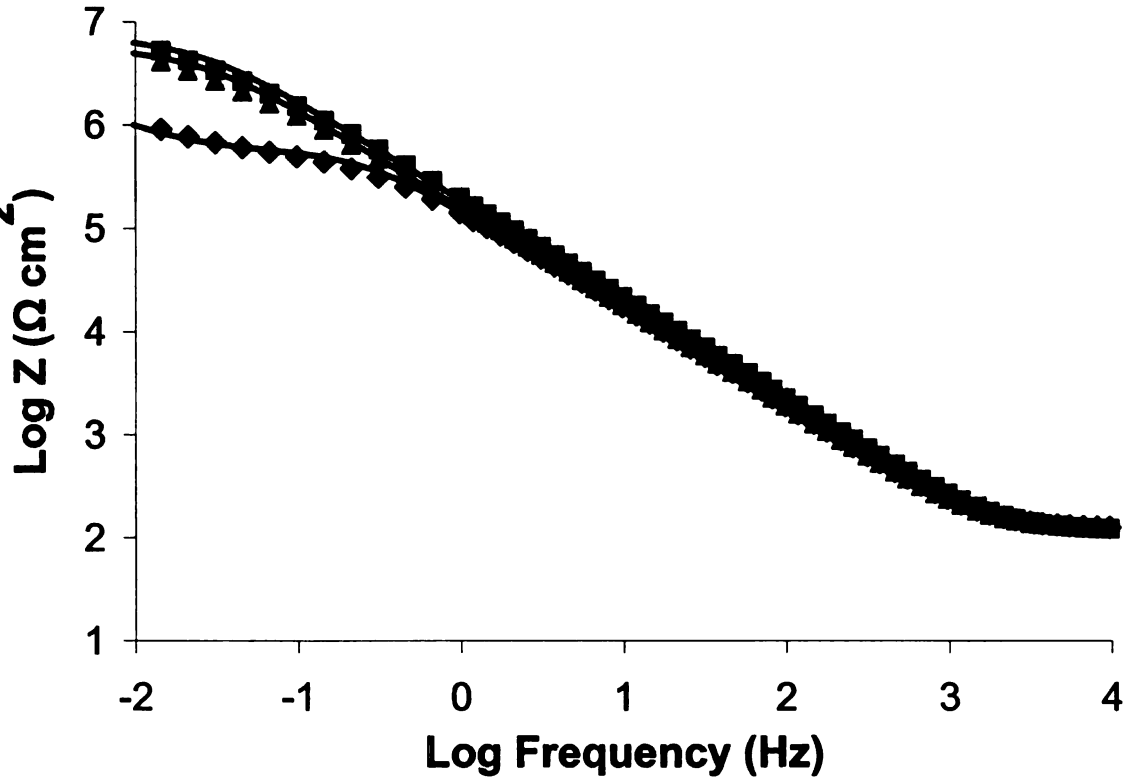

Figure 4.4: Impedance (Log Z) data were plotted as a function of Log frequency for DPPTE-DOPC tBLM at 200 mV DC potential (squares), for DPPTE-DOPC tBLM after PorBII incorporation at 200 mV DC potential (triangles), and for DPPTE-DOPC tBLM containing PorBII after toggling the DC potential to 0 mV (diamonds) in 100 mM NaCl. An equivalent circuit shown in Figure 2.5 was fitted to the impedance data. The solid lines passing through the data points represent the model fit. PorBII was added to give a final concentration of 1 μM protein (monomer) in an electrolyte solution.

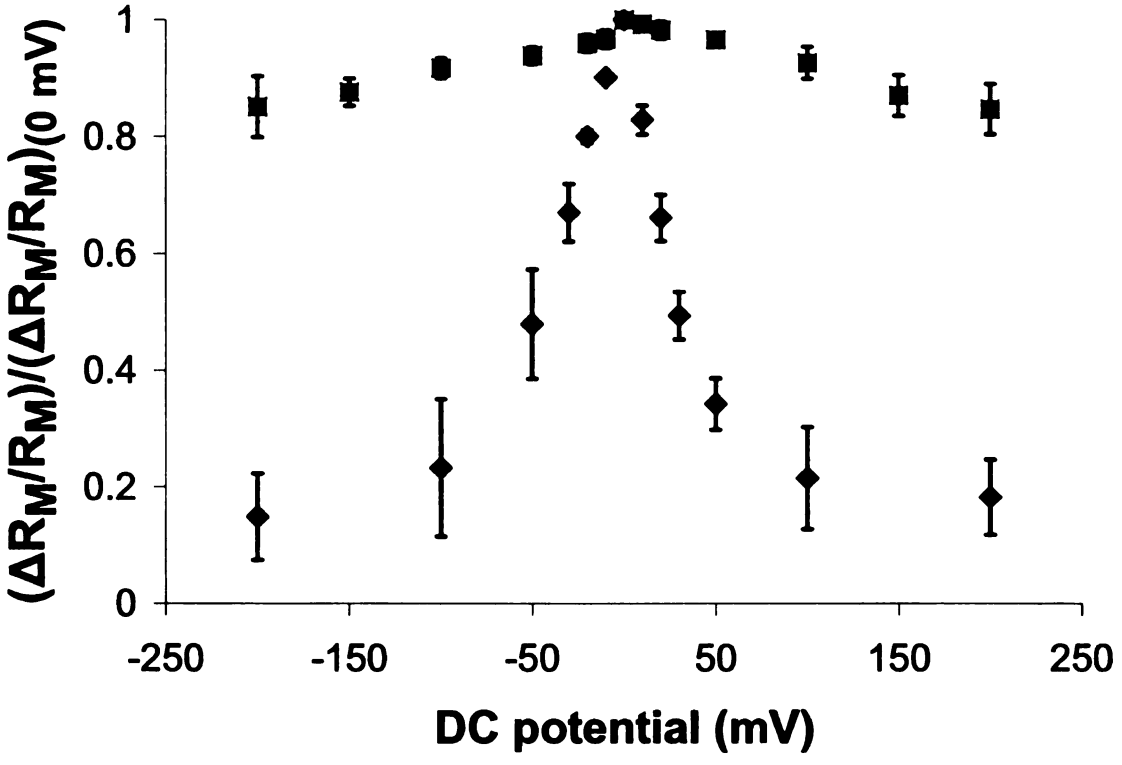

Figure 4.5: Fractional NR_M plotted as a function of applied DC potential used in EIS for a PorBII incorporated DPPTE-DOPC tBLM (diamonds) and gramicidin incorporated DPPTE-DOPC tBLM (squares).

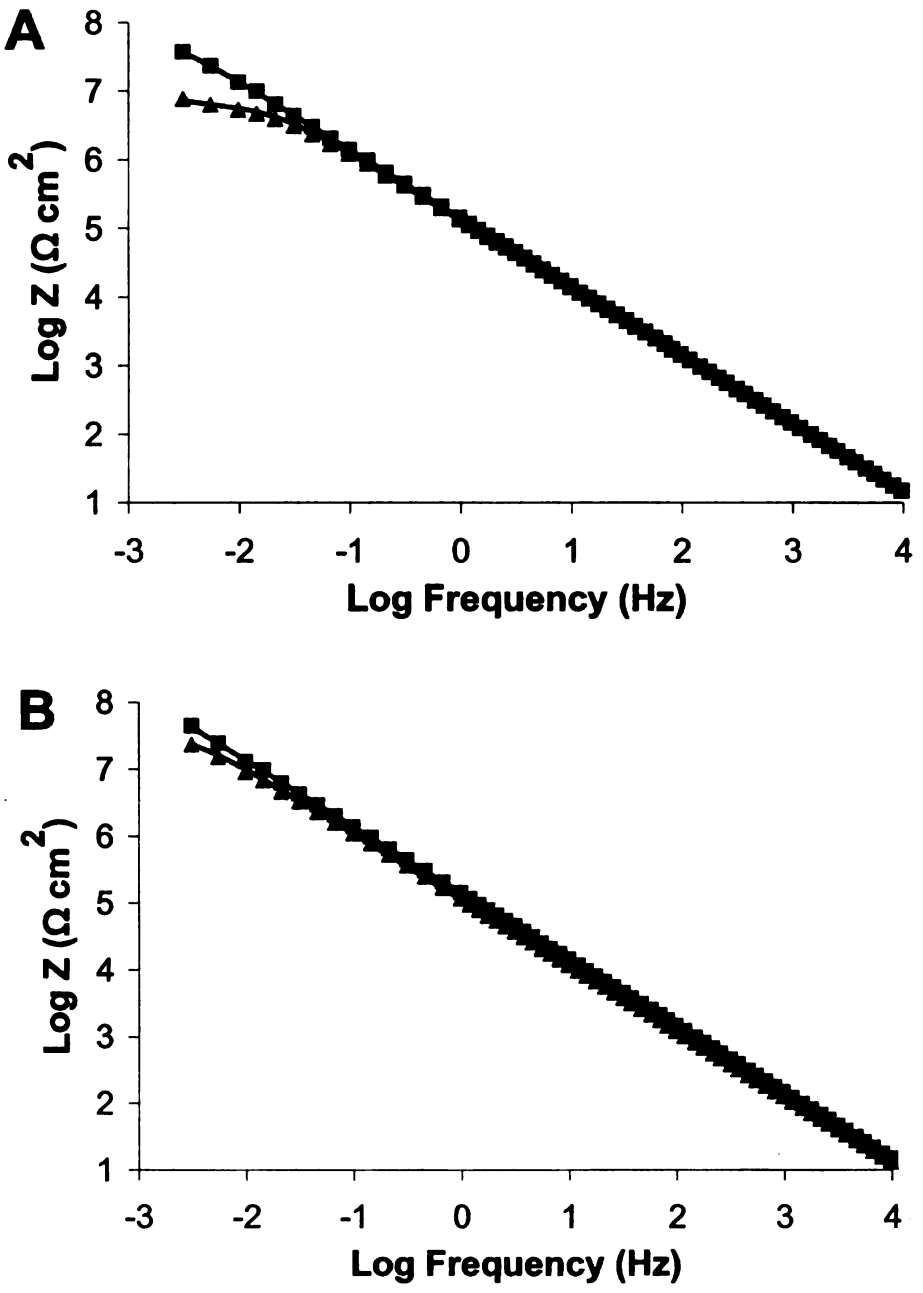

Figure 4.6: (A) Impedance (Log Z) data were plotted as a function of Log frequency for DPPTE-DPPTE tBLM at 0 mV DC potential (squares) and for DPPTE-DPPTE tBLM after PorBII incorporation at 0 mV DC potential (triangles). (B) Impedance (Log Z) data were plotted as a function of Log frequency for DPPTE-DPPTE tBLM at 200 mV DC potential (squares) and for DPPTE-DPPTE tBLM after PorBII incorporation at 200 mV DC potential (triangles) in 100 mM NaCl. An equivalent circuit shown in Figure 2.5 was fitted to the impedance data. The solid lines passing through the data points represent the model fit. PorBII was added to give a final concentration of 1 μM protein (monomer) in an electrolyte solution.

5. FABRICATION OF HIGHLY INSULATING TETHERED BILAYER LIPID MEMBRANES USING YEAST CELL MEMBRANE FRACTIONS FOR MEASURING ION CHANNEL ACTIVITY

5.1. Abstract

A tethered bilayer lipid membrane (tBLM) was fabricated on a gold electrode using 1,2-dipalmitoyl-*sn*-glycero-3-phosphothioethanol as a tethering lipid and the membrane fractions of *Schizosaccharomyces pombe* yeast cells to deposit the upper leaflet. The membrane fractions were characterized using transmission electron microscopy (TEM) and dynamic light scattering (DLS) and found to be similar in size to small unilamellar vesicles of synthetic lipids. The dynamics of membrane fraction deposition and rupture on the tethering lipid layer were measured using quartz crystal microgravimetry (QCM). Fluorescence recovery after patterned photobleaching (FRAPP) was used to study the formation of microsomal sBLM on a glass substrate. The electrochemical properties of the tBLM were characterized using electrical impedance spectroscopy (EIS) and cyclic voltammetry (CV). The tBLM's electrical resistance was greater than 1 $M\Omega cm^2$, suggesting a defect-free membrane. The suitability of tBLM produced using membrane fractions for measuring ion-channel activities was shown by a decrease in membrane resistance from 1.6 $M\Omega cm^2$ to 0.43 $M\Omega cm^2$ following addition of gramicidin. The use of membrane fractions to form high-quality tBLM on gold electrodes suggests a new approach to characterize membrane proteins, in which the upper leaflet of the tBLM is deposited, and overexpressed membrane proteins are incorporated, in a single step. This approach would be especially useful for proteins

whose activity is lost or altered during extraction, purification, and reconstitution, or whose activities are strongly influenced by the lipid composition of the bilayer.

5.2. Introduction

Typically, tBLM are fabricated in a two-step process, in which a self-assembled monolayer of the tethering lipid is first bound to the electrode, and then the remainder of the BLM is added via liposome adsorption and rupture. Lipid-tethering chemistries have been established for a variety of electrode materials, including gold (Raguse, B. *et al.*, 1998), silica (Atanasov, V. *et al.*, 2005) and mercury (Becucci, L. *et al.*, 2005a). A variety of methods have been developed to deposit the upper BLM leaflet on the tethering layer and incorporate a variety of ionophores, peptides, and transmembrane proteins. In one commonly used approach, the purified protein is reconstituted into liposomes, and the resulting proteoliposomes simultaneously deposit the upper BLM leaflet and the protein (Graneli, A. *et al.*, 2003; Zebrowska, A. and Krysinski, P., 2004; Elie-Caille, C. *et al.*, 2005). In a second method, the liposomes are used to deposit the upper BLM leaflet. Then, proteins that are either naturally soluble or detergent solubilized are added to the surrounding aqueous phase and allowed to become embedded into the BLM, in some cases with the assistance of detergent removal. Both of these approaches require the target protein to be purified and then reconstituted into a BLM. These steps can be problematic for membrane proteins whose activity is lost or altered during extraction, purification, and reconstitution, or whose activities are strongly influenced by the lipid composition of the membrane. In such cases, it may be preferable to form the tBLM by direct deposition of semi-purified membrane fractions (microsomes) containing the target protein, thereby circumventing the abovementioned processing steps.

The goal of this study was to fabricate a high-quality tBLM using the membrane fractions of yeast cells that would be suitable for the studying ion transport across BLM. Previous attempts to form sBLM using microsomes containing membrane proteins did not yield an insulating bilayer membrane (Elie-Caille, C. *et al.*, 2005; Jeuken, L. J. C. *et al.*, 2006) and were not suitable to study the ion-channel proteins using electrochemical techniques. This study describes for the first time a method to produce high-impedance tBLM on a gold electrode using membrane fractions. *Schizosaccharomyces pombe* was selected as the source of microsomes because it has many desirable traits as an expression host for recombinant membrane proteins. It is robust, easy to grow, capable of expressing even bulky and high molecular weight eukaryotic proteins, and, unlike *E. coli*, can carry out many types of post-translational modification. The dynamics of membrane-fraction deposition and rupture on the tethering-lipid layer were measured using quartz crystal microbalance (QCM) gravimetry. The electrochemical properties of the resulting tBLM were characterized using electrical impedance spectroscopy (EIS) and cyclic voltammetry (CV). The suitability of the interface for ion channel assays was demonstrated by measuring the impedance drop following gramicidin addition.

5.3. Materials and methods

5.3.1. Preparation of membrane fractions

S. pombe cells were grown in YPD medium (20 g/L yeast peptone, 10 g/L yeast extract and 2% w/v glucose) at 30°C for 48 h. Cells were harvested by centrifugation at 5,500g for 15 min at 4°C and suspended in lysis buffer (25 mM Tris buffer, pH 8.0, containing 250 mM sucrose). The cells were then passed through an Emulsiflex-C3 homogenizer at 28 kpsi three times. The cell debris was separated using centrifugation at

46,300g for 20 min at 4°C. The supernatant was transferred to ultracentrifuge tubes and centrifuged at 245,000g for 110 min at 4°C. The membrane pellet was frozen at -80°C. To prepare membrane fractions, a portion of the membrane pellet was suspended in 20 mM Tris-HCl buffer, pH 8.0, containing 200 mM NaCl and 10% glycerol. The membrane fraction suspension was ultrasonicated for 5 min with 30 s pulses and cooling for 1 min after each pulse. Finally, the microsome suspension was passed through a 200 nm filter.

5.3.2. Fabrication of tethered bilayer lipid membrane on gold surface

Cleaned gold electrodes were placed in a chloroform solution containing 1 mM DPPTE tethering lipid and 0.5 mM DOPC mobile lipids for 24 h. After SAM formation, the electrodes were washed with chloroform to remove weakly attached lipids and dried using nitrogen. The electrodes were transferred to an electrochemical cell that maintained 0.2 cm^2 of electrode area in contact with electrolyte solution (100 mM sodium chloride). A liposome (7.86 mg/mL) or membrane-fraction solution (7.6 mg/mL) was added to electrolyte solution. After allowing 24 h for the bilayer to develop, the solution was replaced with fresh 100 mM sodium chloride solution. Gramicidin was added as an ethanolic solution to give a final concentration of 1 μM protein in the electrolyte solution [Figure 5.1]. At least one hour was allowed for gramicidin to partition into the bilayer, and then EIS was performed.

5.3.3. Instrumentation

Transmission electron microscopy (TEM) images were taken using a JEOL 100CX transmission electron microscope (JEOL USA Inc., Cranford, NJ) at an

acceleration voltage of 80 kV. A quartz crystal microbalance (QCM) analyzer (Research Quartz Crystal Microbalance, Maxtek Inc., Santa Fe Springs, CA) linked to a computer with Maxtek RQCM Data Log software was used for microgravimetric measurements. The Maxtek quartz crystals, which oscillated at 5 MHz, were sandwiched between two gold electrodes having a surface area of 1.26 cm^2. The procedure used to clean the QCM electrodes and establish a tethering-lipid SAM was identical to that previously described for the gold-coated silicon wafers. After SAM formation, the crystal was mounted on a crystal holder. Frequency changes were measured at 22°C after obtaining a baseline oscillation frequency in a 10 mM HEPES buffer (pH 7.4).

DLS, ellipsometry, and electrochemical measurements were carried out as described in Section 2.3.6.

Fluorescence recoveries after pattern photobleaching (FRAPP) measurements were carried out in collaboration with Aaron Greiner and Dr. R. Y. Ofoli from Department of Chemical Engineering and Materials Science. The following description of FRAPP set-up (shown in Figure 5.2) is contributed by Aaron Greiner. FRAPP was used to measure the translational diffusion and mobile fraction of sBLMs formed on silica surface (Starr, T. E. and Thompson, N. L., 2002). A double syringe pump system (Harvard Apparatus, Holliston, MA) was used to infuse and withdraw solutions simultaneously from a custom-made 1 mL flow cell. The 488 nm laser line from an argon ion laser (95, Lexel Laser, Fremont, CA) was directed through a 5x beam expander (Edmund Optics, Inc., Barrington, NJ), a filter cube (Ex: 450-490/DM: 510/Em: 515-565), and a pair of optical flats that toggle between a low intensity (20μW) monitoring beam for continuous fluorescence emission measurements, and a high intensity (500

mW) beam for photobleaching chromophores. Light passing through the sample was collected by an inverted microscope (Zeiss Axiovert 135M, Carl Zeiss, Thornwood, NY) with a Zeiss 32x objective lens. The light intensity was measured by a side-on photomultiplier tube (PMT, Hamamatsu R4632, Bridgewater, NJ) connected to a photon counter (SR400 Stanford Research Systems, Sunnyvale, CA) and a fast preamplifier (SR445 Stanford Research Systems, Sunnyvale, CA). A Ronchi ruling (50 lines per inch, Edmund Optics, Inc., Barrington, NJ) in the back image plane of the microscope created a fringe pattern on the sample. An aperture placed in the image plane in front of the PMT restricted the observation area, resulting in an illuminated area of approximately 200 μm in diameter and an observed area of 75 μm. This arrangement prevented unbleached fluorophores from diffusing from outside the bleached (patterned) area into the observation zone during fluorescence recovery measurements. A Ronchi ruling was placed in the rear image plane of the microscope, creating a striped pattern (periodicity of 25 μm in the sample plane) of alternating light and dark fringes on the sBLM. Chromophores in illuminated zones were photobleached by exposure to the high intensity laser beam. Unbleached chromophores in the dark zones diffused into the photobleached areas, leading to recovery of a spatially homogeneous fluorescence signal. The time constant and functional form of this recovery are given by (Starr, T. E. and Thompson, N. L., 2002),

$$f(t) = f(0) + \frac{m}{2}[1 - f(0)]\left\{1 - \left(\frac{8}{\pi^2}\right)\exp\left(-\frac{4\pi^2 Dt}{a^2}\right) + \frac{1}{9}\exp\left(-\frac{36\pi^2 Dt}{a^2}\right)\right\} \quad \text{Eq. (5.1)}$$

where, $f(t)$ is the post-bleach fluorescence intensity ($t > 0$) normalized with respect to the constant pre-bleach fluorescence intensity ($t < 0$), with $t = 0$ being the time of the

bleach pulse, D is the average translational diffusion coefficient of the chromophores within the bleached area, m is the mobile fraction, and a is the stripe periodicity of the Ronchi ruling in the sample plane. Equation 5.1 assumes a single diffusing species, corresponding to the chromophores in the fluid sBLM for our experiments, and an immobile species of chromophores that reside in intact unruptured vesicles attached to the surface.

5.4. Results and discussion

5.4.1. Characterization of membrane fraction of yeast cells

Transmission electron microscopy indicated that the membrane fractions had a spherical shape and size comparable to the small unilamellar vesicles produced using DOPC [Figure 5.3]. Dynamic light scattering showed a weight-averaged diameter of 20.5 ± 0.2 nm for the liposomes and 47.4 ± 1.4 nm for the membrane fraction, respectively. Both of these size distributions lie in the range (less than 200 nm) reported to facilitate liposome rupture to form sBLM (Cremer, P. S. and Boxer, S. G., 1999).

5.4.2. Characterization of tBLM formation using QCMD

Formation of an upper tBLM leaflet by fusion of *S. pombe* membrane fractions on the tethering-lipid SAM is analogous to the widely used approach in which liposomes of synthetic lipids are used to deposit the upper bilayer leaflet on an alkanethiol SAM (Peng, Z. Q. *et al.*, 2002). QCM gravimetry was used to explore the kinetics of microsome deposition and rupture during tBLM formation. The method involves measuring the change in oscillating frequency (Δf) due to adsorption of material onto the quartz

crystal's surface, and then using the Sauerbrey equation (Sauerbrey, G., 1959) to estimate the mass adsorbed from the Δf data. The tethering lipid SAM and the lipid bilayer are compact, rigid, structures that couple strongly to the crystal's motion, resulting in minimal viscoelastic energy loss and thus low $\Delta Dissipation$ values. In contrast, the adsorbed vesicles are loosely bound structures that undergo significant deformation, resulting in larger $\Delta Dissipation$ values. Adsorption of intact vesicles onto an oxidized gold surface has been shown to cause a large change in $\Delta Dissipation$ values (Keller, C. A. and Kasemo, B., 1998).

Figure 5.4A compares the Δf and $\Delta Dissipation$ curves for liposome and microsome deposition onto silica-coated QCM crystals. The liposome curve exhibits a rapid decrease to a minimum, followed by an increase to a steady-state value. Keller and Kasemo (Keller, C. A. and Kasemo, B., 1998) observed such a two-phase trend during liposome adsorption on silica. In the first phase, the intact vesicles adsorb on the surface, decreasing the oscillation frequency. In the second phase, the adsorbed vesicles rupture to form a bilayer, releasing entrapped water thereby increasing the frequency. The presence of some intact adsorbed vesicles on surface contributes to net $\Delta Dissipation$. In our experiments, there was a net change in $\Delta Dissipation$ values, suggesting that not all adsorbed vesicles rupture. The microsome curve showed a continuous decline, rather than a two-phase trend. The larger magnitude of the Δf and $\Delta Dissipation$ values obtained for microsomes than for liposomes suggests that the microsomes'

adsorption rate exceeded their rupture rate during the period of the experiment, resulting in both bilayer patches and intact microsomes on the surface.

Figure 5.4B compares the Δf and $\Delta Dissipation$ curves for liposome and microsome deposition on a tethered monolayer. Both curves exhibit a continuous decline in Δf. This trend was previously reported for liposome deposition on a gold surface with a chemisorbed alkanethiol SAM (Keller, C. A. and Kasemo, B., 1998). In that case, the steady-state Δf value obtained on the alkanethiol SAM was half that on the bare silica, indicating deposition of only one leaflet, rather than two. Also, Δf was shown to decrease with time as a decaying exponential, suggesting a first order kinetic model, in which adsorption and rupture steps occur simultaneously to form the upper sBLM leaflet (Keller, C. A. and Kasemo, B., 1998; Richter, R. *et al.*, 2003). Δf values for deposition of both liposomes and membrane fractions on a tethering lipid monolayer [Figure 5.3A], decayed continuously but did not follow first order kinetics. The change in Δf values obtained for liposome fusion over tethering lipid SAM was greater than the one reported for liposome rupture over alkanethiol SAM (Keller, C. A. and Kasemo, B., 1998), presumably because the tethering lipid SAM was not as tightly packed and ordered as the alkanethiol SAM, allowing mobile lipids from the liposomes to incorporate into the tethering lipid SAM. Rupture kinetics of liposomes and membrane fractions on the tethering lipid monolayer was slower than on silica. The higher $\Delta Dissipation$ values indicated that most of the vesicles remained adsorbed on surface during the period of experiment. In our experience, development of a high-impedance tBLM using liposomes

and microsomes on the tethering lipid monolayer takes several hours, compared to the 25 min duration of the QCM experiments. This observation is consistent with our impedance results, wherein the membrane resistance required about 10 h to reach the steady-state value.

The QCM studies also demonstrated that microsome rupture kinetics were slower than those of DOPC liposomes. Liposome rupture kinetics have been found to be strongly affected by the phospholipid composition (Richter, R. *et al.*, 2003). Bilayer formation for liposomes composed of single type of phospholipids occurs faster than liposomes composed of different phospholipids (Richter, R. P. and Brisson, A. R., 2005). Membrane fractions are a complex mixture of phospholipids and other membrane constituents that collectively determine the relative rates of microsome binding and rupture on a surface. Ohlsson *et al* (Ohlsson, P. A. *et al.*, 1995) found that the rupture of proteoliposomes of ganglioside GM1 receptor protein did not follow the same rupture behavior as liposomes. The proteoliposomes exhibited a continuous decrease in Δf magnitude over an hour without achieving a steady state value, similar to the trends we observed for microsomes. However, the adsorbed microsomes did ultimately undergo rupture to form upper leaflet of tBLM as shown by the electrochemical characterization results.

5.4.3. Fluorescence recovery after pattern photobleaching (FRAPP) study of microsomal sBLM on glass

After rupture, BLM should provide a fluid environment for lateral diffusion of lipid and protein molecules. This study, conducted in collaboration with Dr. R.Y. Ofoli's lab, used Fluorescence recovery after photo-bleaching (FRAP) to determine the

translational diffusion coefficient of lipids embedded in the BLM, as well as the BLM's mobile fraction (Starr, T. E. and Thompson, N. L., 2002; Kohli, N. *et al.*, 2006b; Lapinski, M. M. *et al.*, 2007). sBLM was deposited on a hydrophilic transparent surface (mostly, glass) using liposomes or microsomes containing around 2% of fluorescently labeled lipids. Then, a small region of BLM was bleached using intense laser radiation, and the rate of fluorescence recovery due to a lateral diffusion of fluorescent lipid molecules in the photo-bleached region was monitored. In FRAPP technique, the photo-bleaching is performed on a patterned region. A Ronchi ruling (50 lines per inch) was used to create well defined striped pattern resulting in photobleaching of half of the illuminated area. Since only 50% area is photo-bleached, a maximum of 50% fluorescent recovery is possible.

We performed three experiments to study the fluidity of microsomal BLM on glass surface. In the first experiment, modeled after that reported by Eli-calli *et al.* (Elie-Caille, C. *et al.*, 2005), liposomes were created containing 1-oleoyl-2-[6-[(7-nitro-2-1,3-benzoxadiazol-4-yl)amino]hexanoyl]-*sn*-glycero-3-phosphocholine (NBD-PC) and 1-palmitoyl-2-oleoyl-*sn*-glycero-3-phosphocholine (POPC) in a ratio of 2:98. These liposomes were then mixed with yeast microsomes in 1:1 ratio (dry weight basis). The mixture was sonicated for 15 min at 40°C using a bath sonicator. The microsome-liposome mixture was then used to deposit sBLM on glass surface for 3 h. FRAPP experiments were conducted in several locations across the sBLM, and the D and m values were calculated by fitting Equation 5.1 to the fluorescence recovery data. In the second experiment, microsomal suspension was mixed with 2% by weight NBD-PC and sonicated for 15 min at 40°C. The resulting fluorescently tagged microsomes were used

to deposit sBLM on a glass surface for 3 h, and then FRAPP analysis was performed. In the third experiment, a solvent mixture (chloroform:methanol:water in ratio 68:31:1) was used to extract lipids from the microsomes using reported procedure (Schneiter, R. and Daum, G., 2006). The extracted and dried microsomal lipids were then mixed with 2% by weight NBD-PC and sonicated in buffer at 40°C for 15 min. The resulting liposomes were used to form sBLMs, and FRAPP analysis was performed.

The model described in Equation 5.1 fitted well to data for POPC sBLM (R^2 = 0.98) [Figure 5.5], microsome-POPC sBLM (R^2 = 0.93), and microsome lipid sBLM (R^2 = 0.96) [Figure 5.6] whereas the model did not fit well to data for pure microsomal sBLM (R^2 = 0.78) [Figure 5.7]. The diffusion coefficient was similar for all four cases [Table 5.1]. The mobile fractions or the POPC liposome, microsome-POPC liposome mixture, and liposomes made from extracted microsomal lipids have relatively high mobile fractions (between 0.67 and 0.81). However, the mobile fraction for the microsomes was substantially lower (0.26). In addition, the standard deviation among replicate D and m values for the microsomes was considerably larger than for the other lipid mixtures [Figure 5.7]. It indicated that the model described in Equation 5.1 may not adequately describe the complexity of microsomal BLM. These findings are consistent with the hypothesis that the microsomes produce a heterogeneous interface that may contain a significant number of unruptured microsomes. Unbleached, labeled lipids would not be able to diffuse into or out of unruptured microsomes, resulting in a low m value. A higher m value obtained for the liposomes produced from extracted microsomal

lipids suggests that a non-extracted component of the microsomes, such as membrane proteins, may slow down the rupture kinetics. From the FRAPP data, it can be inferred that presence of proteins prolongs the rupture process resulting in lower mobile fraction that hiders the diffusion of fluorescent species.

5.4.4. Electrochemical characterization of tBLM

The thickness of tBLM deposited using DOPC liposome and yeast membrane fractions was determined using ellipsometry to be 5.7 ± 1.0 nm and 6.2 ± 0.9 nm, respectively. The slightly higher thickness for tBLM formed using membrane fractions may have been due to the presence of yeast membrane proteins in the resulting tBLM. The EIS data for a tBLM formed using DOPC liposomes [Figure 5.9A] and *S. pombe* microsomes [Figure 5.9B], were analyzed using to a Randles equivalent circuit model [Figure 5.10]. Z-view software was used to obtain membrane resistance (R_M) values of 1.59 $M\Omega cm^2$ and 1.62 $M\Omega cm^2$ for the liposomes and microsomes, respectively, and membrane capacitance (C_M) values were 0.78 $\mu F/cm^2$ and 0.68 $\mu F/cm^2$ for the liposomes and microsomes, respectively. In both cases, these data are consistent with production of a highly insulating tBLM. Figure 5.11 shows the impedance spectrum for tBLM taken at different times. The membrane's resistance increased and its capacitance decreased consistently, until steady-state was reached somewhere between the 8 h and 22 h time points. These data are consistent with our QCM results, which suggested that microsome rupture to form a tBLM requires longer than 30 min. The highly insulating nature of the tBLMs produced using microsomes was further confirmed by CV, wherein

the redox peaks for ferro/ferricyanide system were totally subdued, and only a curve representative of charging current was obtained [Figure 5.12A].

The suitability of the microsome-derived tBLM for characterizing ion channel activity was evaluated using gramicidin. Active gramicidin channels are dimers, in which one monomer exists in each leaflet of the bilayer, and alignment of the monomers creates a channel through the entire bilayer. Gramicidin selectively passes alkali metal ions, so the presence of these ions results in a decrease in membrane resistance (Naumann, R. *et al.*, 2003b). Incorporation of gramicidin in tBLM formed with membrane fractions decreased the membrane resistance from 1.62 $M\Omega cm^2$ to 0.43 $M\Omega cm^2$ [Figure 5.13B]. A similar resistance drop (from 1.61 $M\Omega cm^2$ to 0.10 $k\Omega cm^2$) was observed following incorporation of gramicidin into tBLM formed using DOPC liposomes [Figure 5.13A]. The gramicidin-containing tBLM produced using microsomes was further characterized using CV. As shown in Figure 5.12B, addition of gramicidin did not yield a significant redox peak characteristic of ferricyanide, despite the observed decrease in resistance measured using EIS. Because gramicidin selectively passes sodium but not ferricyanide, these results are also consistent with a defect-free tBLM in which ion channels can exhibit their characteristic activities.

The results presented above establish for the first time that a high-impedance tBLM can be formed using *S. pombe* microsomes. The QCM results showed that both microsomes and DOPC liposomes adsorb strongly onto both silica and a tethering lipid SAM, but that the rate of microsome rupture is slower for than for DOPC liposomes. The EIS and CV results showed that tBLM produced using microsomes have similar

membrane resistance and capacitance to those produced using DOPC liposomes, and allow the activity of ion channels to be measured.

This novel approach extends previously reported methods that used microsomal preparations to characterize the activities of membrane proteins that do not require an insulating membrane on interface, such as cytochrome c oxidase, Na-K ATPase and mitochondrial membrane proteins (Elie-Caille, C. *et al.*, 2005). The ability to fabricate a high impedance tBLM using membrane fractions suggests the possibility that recombinant membrane proteins overexpressed in *S. pombe* could be directly incorporated into tBLM on gold electrodes without the need to (1) separate the proteins from the membrane, (2) purify the proteins, and (3) reconstitute the proteins into liposomes. This approach would be particularly well suited to characterize membrane proteins that lose activity during one of these processing steps. It could also simplify the use of biomimetic interfaces to characterize membrane proteins advancing efforts to rapidly characterize novel proteins in a high-throughput mode for drug screening or functional proteomics research.

5.5. Conclusions

Membrane fractions recovered from homogenized *S. pombe* cells were characterized using transmission electron microscopy and dynamic light scattering and found to resemble small, unilamellar liposomes. QCM results indicated that the microsomes and DOPC liposomes exhibited similar adsorption kinetics on the tethering-lipid SAM, characterized by a continuous increase in adsorbed mass over the 25 minute experiment. On silica, a similar QCM profile was exhibited for the microsomes, but the liposomes exhibited distinct adsorption and rupture phases. EIS and CV confirmed that

both liposomes and microsomes formed highly insulating tBLM on gold that had high membrane resistance values. The high impedance tBLM formed using membrane fractions effectively mimics the properties of the biological cell membrane and is suitable model to study membrane protein activities. The subsequent addition of gramicidin resulted in a substantial drop in membrane resistance, indicating the flow of ions across the tBLM. These results demonstrate that tBLM derived from microsomes are suitable for ion channel studies. This novel method may provide a means to establish a biomimetic interface consisting of recombinant membrane proteins in a tBLM without the need to separate the target protein from the membrane, purify it, and then reconstitute it into proteoliposomes. This capability could streamline efforts to characterize novel proteins and screen drug candidates for activity against membrane proteins.

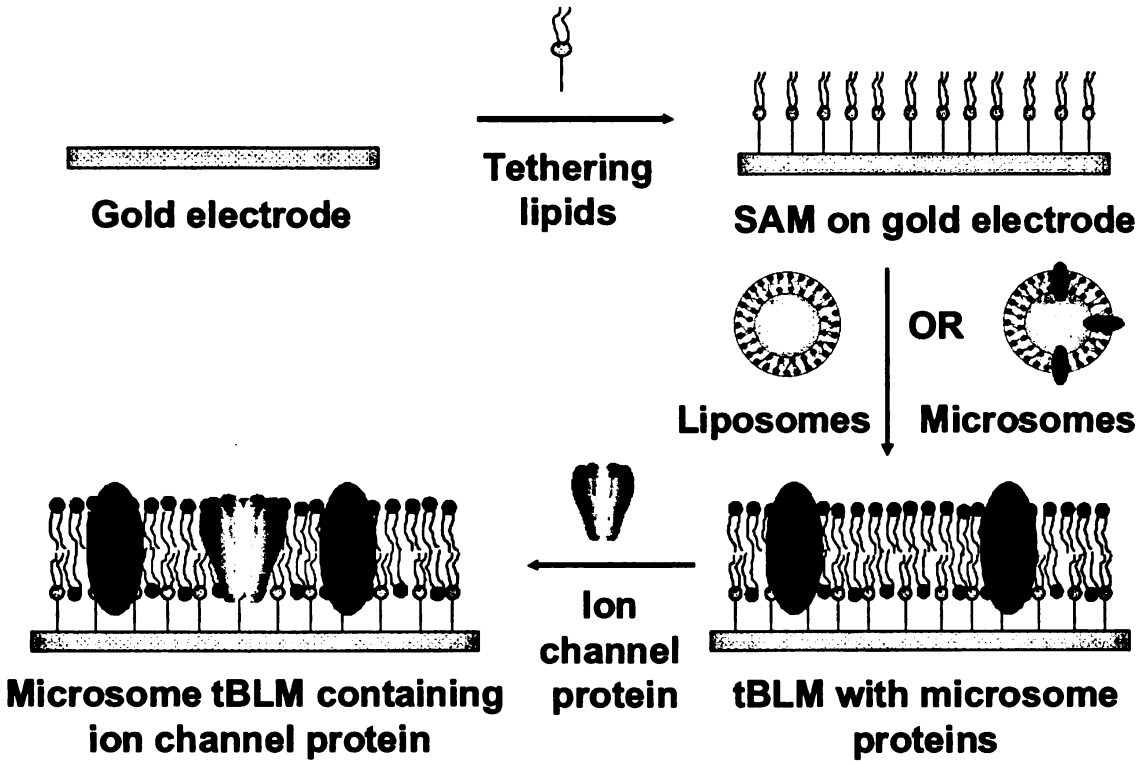

Figure 5.1: Fabrication of tBLM using liposome or yeast membrane fractions. A self assembled monolayer of tethering lipid was deposited on the gold substrate, and the liposomes or microsomes were added to deposit the upper tBLM leaflet. Gramicidin was incorporated into the tBLM, and gramicidin-mediated ion transport across the tBLM was monitored using EIS. [Figure not to scale]

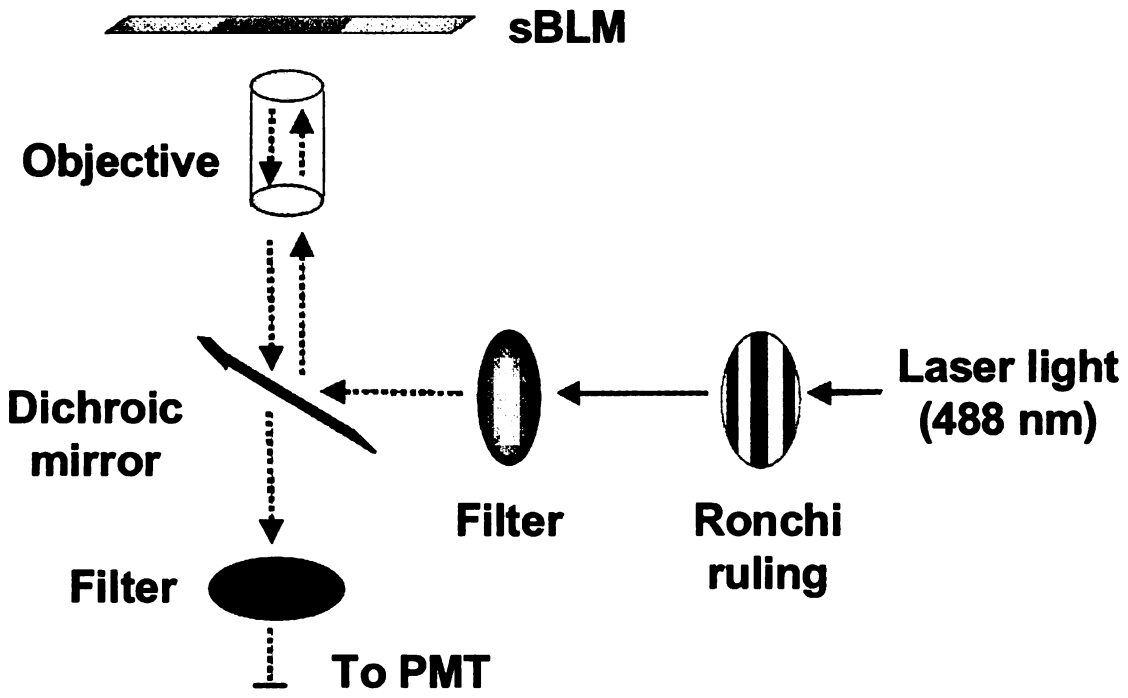

Figure 5.2: Schematic diagram of the FRAPP experimental setup. sBLM: supported bilayer lipid membrane; PMT: photomultiplier tube. [Figure not to scale]

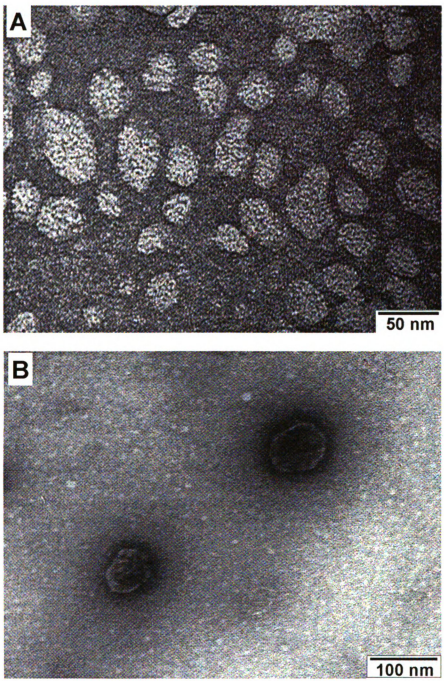

Figure 5.3: Transmission electron microscopy (TEM) image of (A) DOPC liposomes, and (B) membrane fractions of *S. pombe* yeast cells. Liposome and membrane fractions were stained using 1% uranyl acetate solution. The size of liposome and membrane fractions was well below 200 nm which would be necessary for facile rupture of these vesicles to yield planar bilayer membranes.

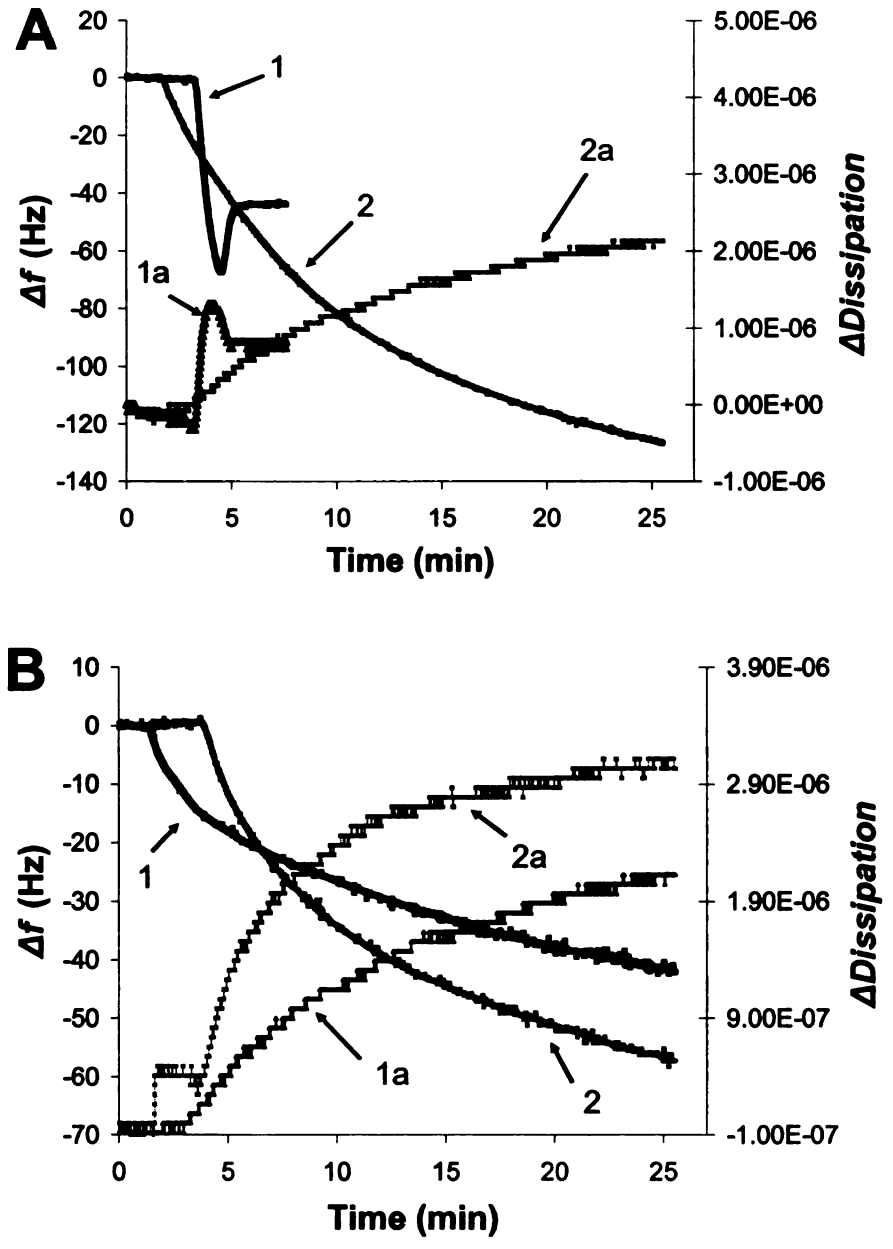

Figure 5.4: Quartz crystal microbalance study for formation of tBLM using liposome and tBLM using yeast microsomes. (A) Liposome deposition directly on the silica surface is shown in Curve 1 (Δf data) and Curve 1a ($\Delta Dissipation$ data). Liposome deposition on the tethering lipid SAM is shown in Curve 2 (Δf data) and Curve 2a ($\Delta Dissipation$ data). (B) Microsome deposition directly on the silica surface is shown in Curve 1 (Δf data) and Curve 1a ($\Delta Dissipation$ data). Microsome deposition on the tethering lipid SAM is shown in Curve 2 (Δf data) and Curve 2a ($\Delta Dissipation$ data).

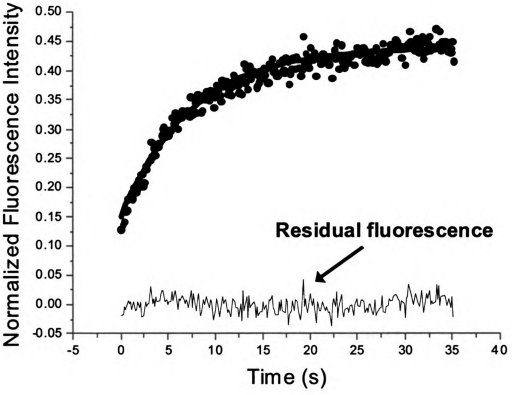

Figure 5.5: Fluorescence recovery curves for sBLM on glass formed using POPC liposomes incorporated with 2% NBD-PC obtained using FRAPP.

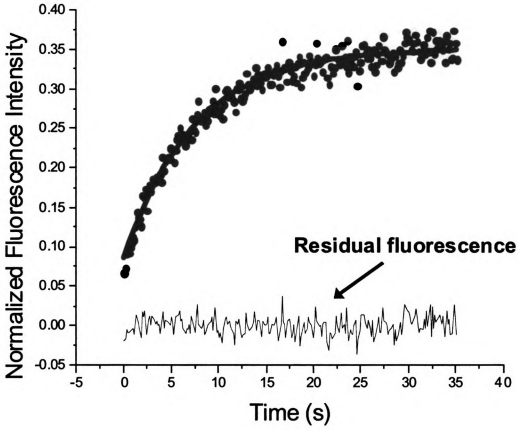

Figure 5.6: Fluorescence recovery curves for sBLM on glass formed using liposomes obtained using lipids extracted from microsomes and mixed with 2% NBD-PC.

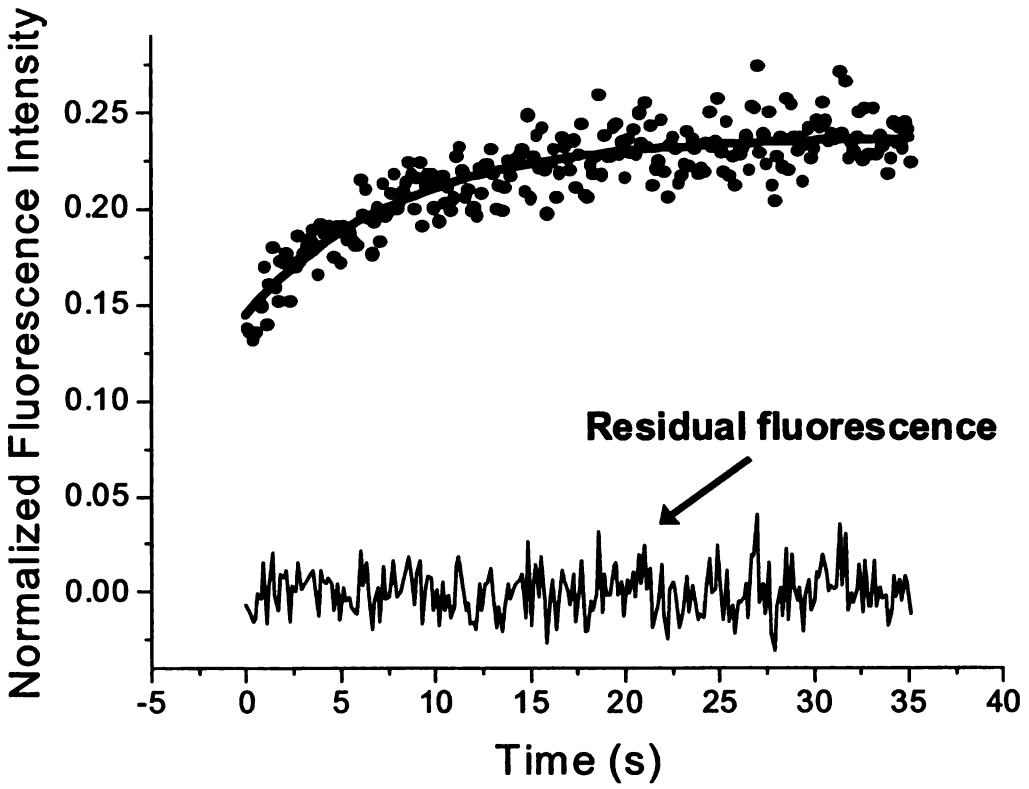

Figure 5.7: Fluorescence recovery curves for sBLM on glass formed using microsomes incorporated with 2% NBD-PC.

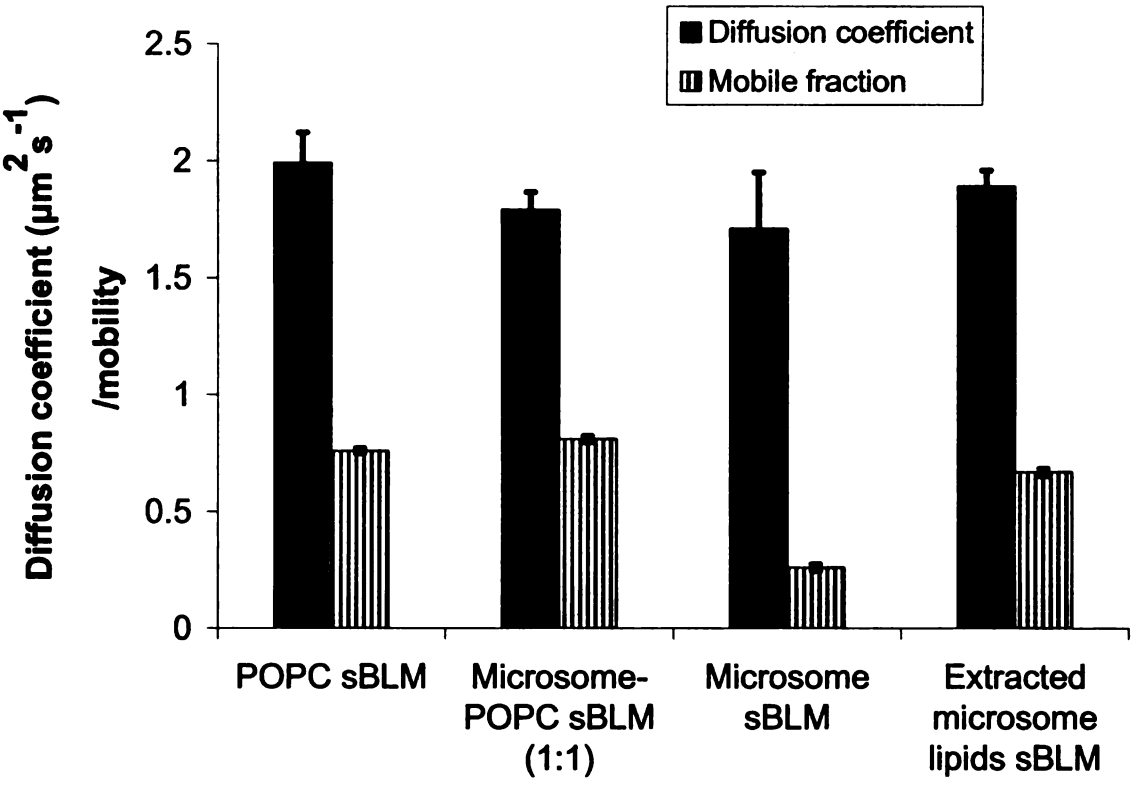

Figure 5.8: Diffusion coefficient and mobile fraction data obtained using FRAPP were plotted for different sBLMs deposited on glass substrate.

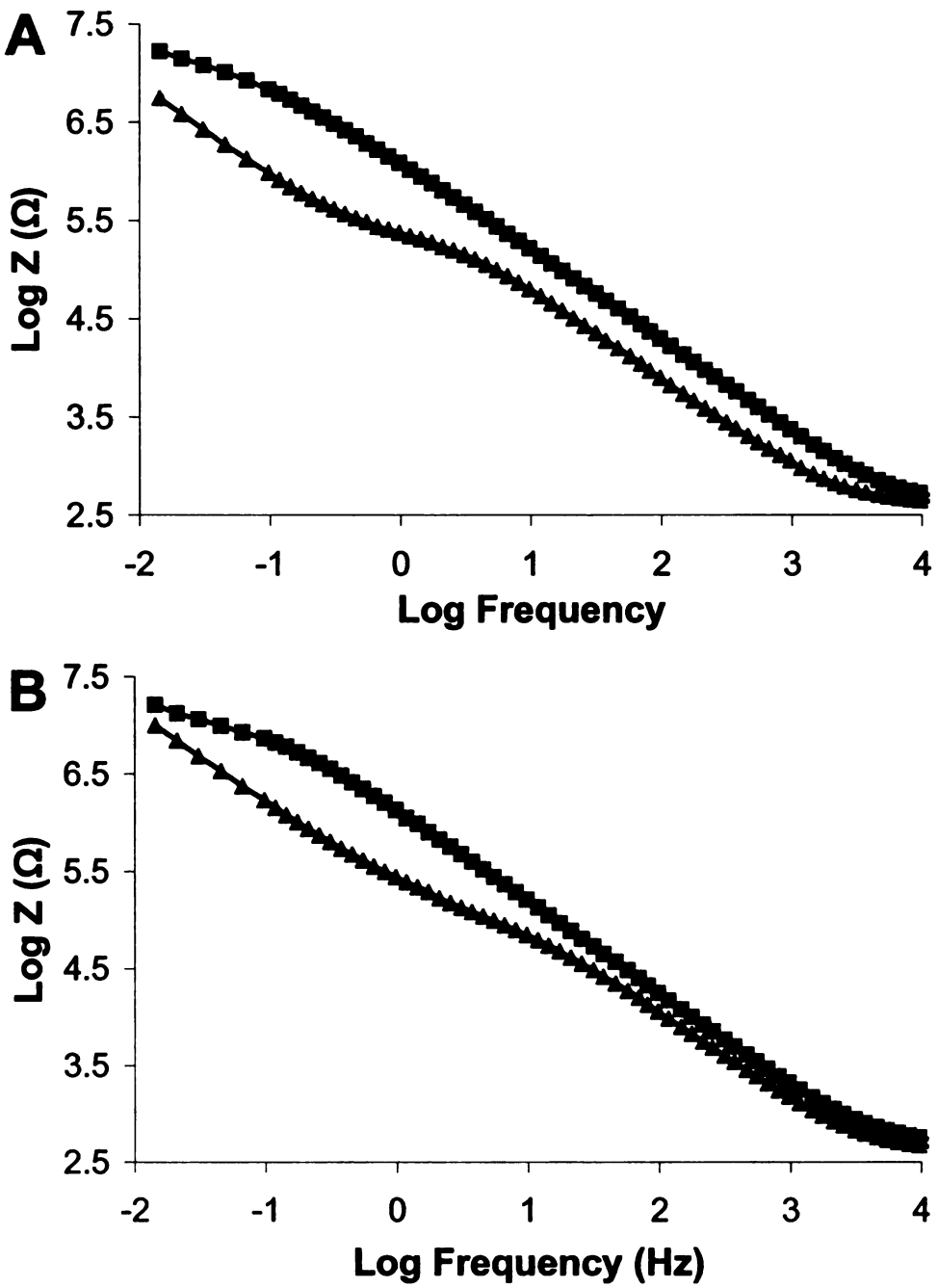

Figure 5.9: Comparison of tBLM formed with DOPC liposome (A), and with membrane fractions of yeast cells (B) over tethering lipid SAM using EIS. Impedance data (Log Z) were plotted as a function of Log frequency for tethering lipid monolayer (triangles) and tBLM (squares). An equivalent circuit shown in Figure 5.8 was used to fit impedance data. The solid lines passing through the data points represent model fit. The resistance of membrane increases whereas the capacitance of membrane decreases after the formation of bilayer membrane. [Electrode area is 0.2 cm^2]

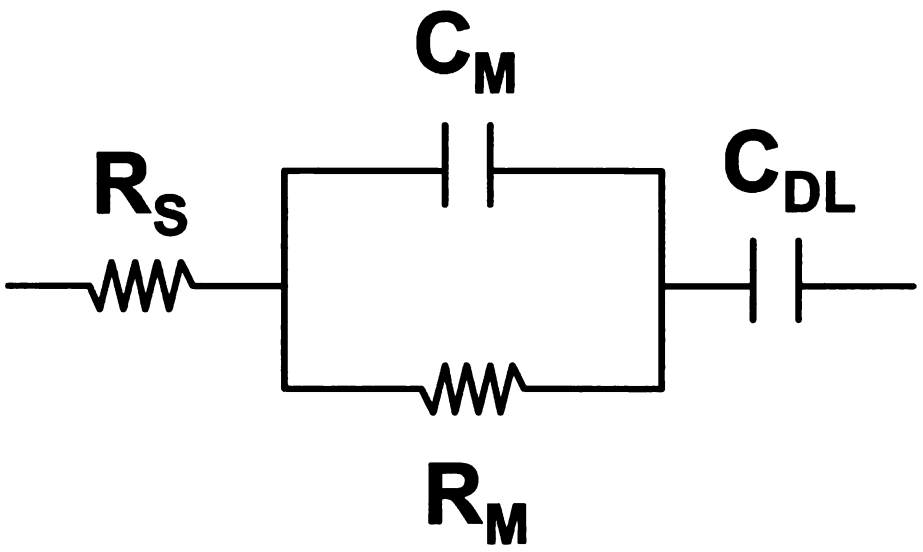

Figure 5.10: A Randles equivalent circuit was fitted to the impedance data to calculate the values of electrochemical characteristics. R_S represent the resistance of solution, C_M represents the capacitance of membrane, R_M represents the resistance of membrane and C_{DL} represents the capacitance of double layer that includes the Hemholtz capacitance.

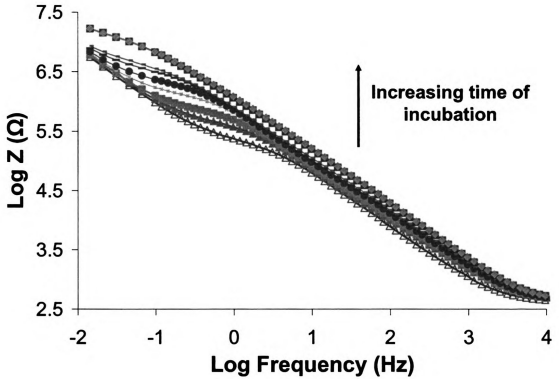

Figure 5.11: Impedance spectrum for tBLM recorded at different intervals after addition of microsomes. The order of curves from bottom to top is- tethering lipid monolayer, tBLM at 30 min, tBLM at 1 h, tBLM at 2 h, tBLM at 3 h, tBLM at 5 h, tBLM at 8 h, tBLM at 22 h and tBLM at 24 h. The membrane resistance increased whereas the membrane capacitance decreased with time of incubation. The initial rate of bilayer formation was higher, which decreases with time. The impedance spectrum for tBLM at 22 h, and 24 h were same indicating that the tBLM formation is complete. The electrolyte solution was replaced after the tBLM formation. The impedance spectrum of tBLM did not change after replacing the electrolyte solution with fresh 100 mM NaCl solution. [Electrode area is 0.2 cm^2]

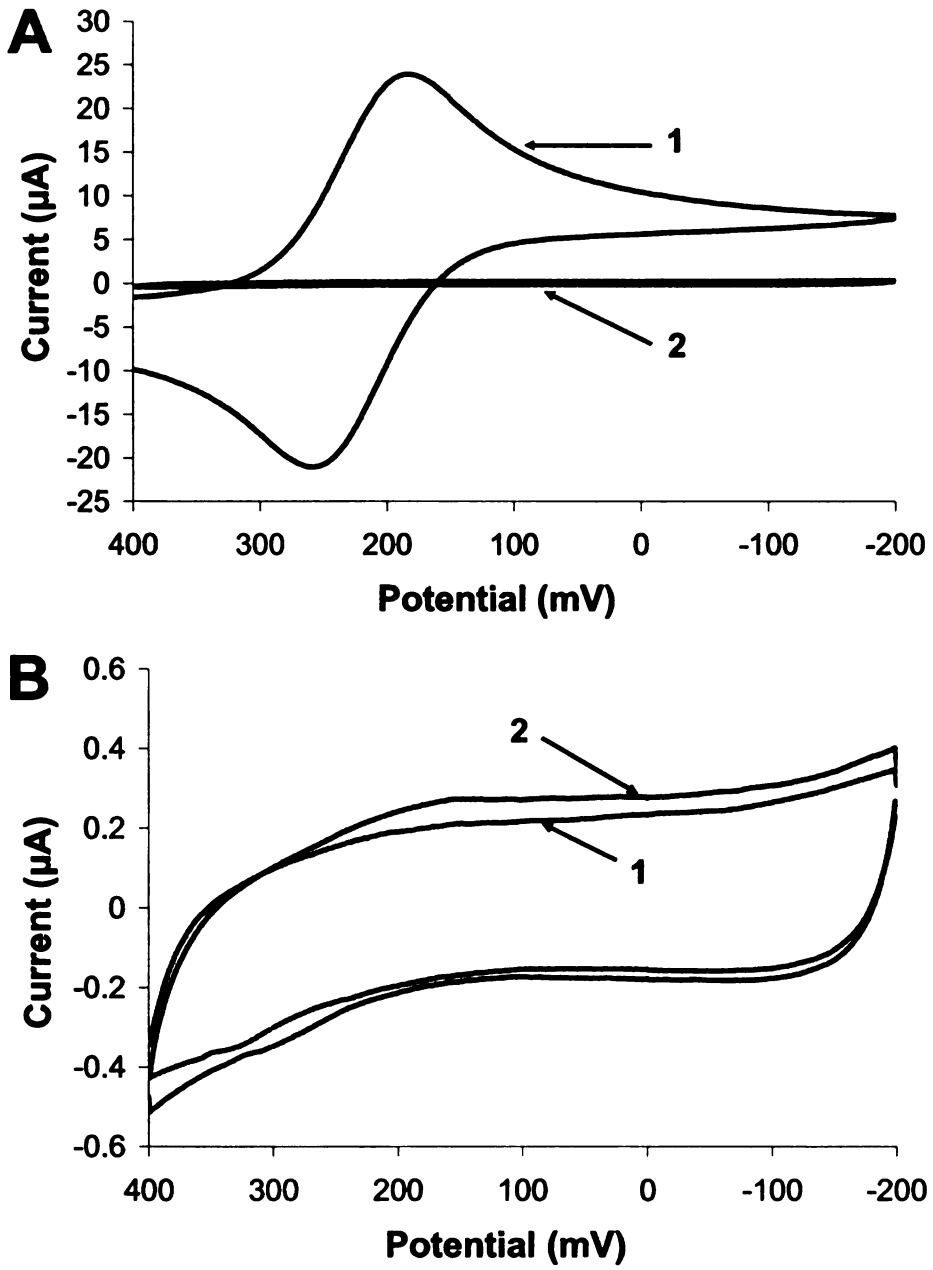

Figure 5.12: (A) Cyclic voltammogram of bare gold (curve 1) was plotted along with the voltammogram obtained after tBLM fabrication (curve 2). The redox peaks were subdued after the formation of tBLM. (B) Cyclic voltammogram for tBLM formed using membrane fractions of yeast cells (curve 1), and microsomal tBLM after gramicidin incorporation (curve 2). The redox peaks were absent in both tBLM voltammograms whereas there was an increase in charging current after the addition of gramicidin suggesting the passage of ions through tBLM by gramicidin while excluding the passage of ferricyanide ions through tBLM. [Electrode area is 0.2 cm^2]

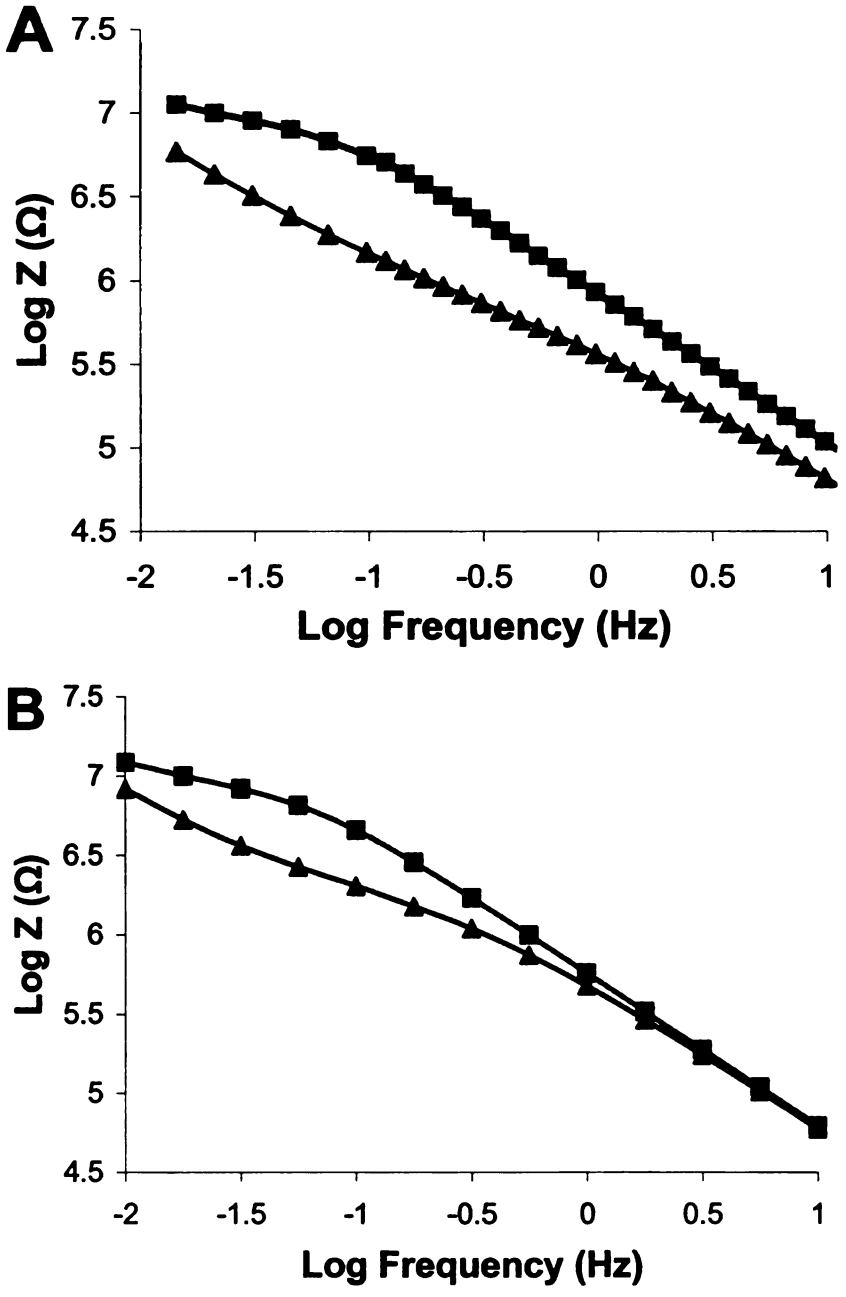

Figure 5.13: Measurement of gramicidin ion channel activity using EIS. (A) tBLM was fabricated by fusion of DOPC liposome over tethering lipid monolayer and (B) tBLM was fabricated by fusion of membrane fractions of yeast cell over tethering lipid monolayer. Impedance (Log Z) data for tBLM (squares) and tBLM after gramicidin incorporation (triangles) were plotted as function of Log frequency. Gramicidin was added as an ethanol solution to give a final concentration of 1 μM. Membrane resistance drops due to the passage of sodium ions through tBLM. [Electrode area is 0.2 cm^2]

6. ELECTROCHEMICAL CHARACTERIZATION OF INTERACTIONS BETWEEN NANOPARTICLES AND SUPPORTED BILAYER LIPID MEMBRANES

6.1. Abstract

Electrochemical techniques were used to investigate the interactions of polymeric nanoparticles (NPs) with 1,2-dioleoyl-*sn*-glycero-3-phosphocholine (DOPC) supported bilayer lipid membranes (sBLM) on a glassy carbon electrode. For the first part of the study, PAMAM dendrimers were used as model nanoparticles. PAMAM dendrimers are hyperbranched monodisperse polymeric nanoparticles whose molecular size, molecular weight, and number of functional groups can be controlled. Dendrimers of generation 2 through generation 4 (G2-G4) did not cause significant damage to the sBLM, whereas G5-G7 dendrimers created large defects in sBLM. In cyclic voltammetry (CV) studies, the peak current obtained after dendrimer addition was used to estimate the defect area. Electrochemical impedance spectroscopy (EIS) showed an increase in capacitance values after addition of G5-G7 dendrimers, consistent with a decrease in sBLM surface coverage. Nanoparticle mass, diameter, and surface charge density all increase significantly with generation number, suggesting that these variables may influence nanoparticles' ability to rupture sBLM. To further understand the effect of functional group and charge density of the NPs, custom nanoparticles were synthesized having a polyethylene glycol (PEG) backbone. Both positively and negatively charged NPs were able to disrupt sBLM having a zwitterionic head group. PEG NPs having a functional group with multiple charged groups created larger defects in sBLM suggesting that higher charge density increases the NP-BLM interaction. The method presented in this

study provides a convenient and sensitive way to detect interactions between nanoparticles and lipid bilayers, and may be useful in evaluating nanoparticles' safety profile or suitability as drug or gene delivery vehicles.

6.2. Introduction

Recently, nanoparticles (NPs) have been introduced in various commercial applications including cosmetics, paints, textiles and others. The small size of NPs provides them unique properties. Incorporation of NPs in biosensor interfaces increases the surface area for enzyme adsorption by several folds, thereby increasing enzyme loading and in turn, the sensitivity of biosensor. In medical applications, a low immunogenicity of NPs has been exploited by using NPs as gene and drug delivery vehicles. Charged polymeric NPs, in particular, are highly effective in disrupting lipid bilayers, mediating the internalization of molecular cargos into the host cell. This property raises a concern that NP-mediated defect formation in cell membranes might lead to cytotoxicity. Therefore, a detail understanding of NP-BLM interactions is required.

In this study, a supported BLM interface was developed for studying the interaction of NPs with bilayer lipid membranes. Monodisperse positively charged polyamidoamine (PAMAM) dendrimers of different size and generation number were used as model NPs to study the effect of nanoparticles' physical properties on their ability to disrupt BLMs. Polyamidoamine (PAMAM) dendrimers are hyperbranched polymeric NPs that are formed in concentric layers [Figure 6.1]. As each subsequent layer (generation) is added, the molecular size, molecular weight, and number of functional groups increases by a known amount [Table 6.1]. This property makes dendrimers well

suited for use as monodisperse NPs having a desired size, shape, and surface charge (Zeng, F. W. and Zimmerman, S. C., 1997). Recently, PAMAM dendrimers have also been investigated as non-viral vectors for the gene delivery (Dufes, C. *et al.*, 2005; Zhou, J. H. *et al.*, 2006) that offer the potential for low immunogenicity (Malik, N. *et al.*, 2000; Duncan, R. and Izzo, L., 2005) and may protect the gene from DNase activity. The mechanism of gene delivery involves internalization of the charged polymer by host cells, though a mechanism that may involve disruption of the host cell membrane (Domanski, D. M. *et al.*, 2004). Dendrimers' ability to cross cell membranes makes also makes them an alternative vehicle for drug delivery (Esfand, R. and Tomalia, D. A., 2001; Crampton, H. L. and Simanek, E. E., 2007). Atomic force microscopy studies have shown that PAMAM dendrimers form 15-40 nm holes in 1,2-dimyristoyl-*sn*-glycero-3-phosphocholine (DMPC) supported bilayer lipid membrane (sBLM) on mica (Diao, P. *et al.*, 1999; Mecke, A. *et al.*, 2004; Hong, S. P. *et al.*, 2006). These studies concluded that the high surface charge density of amino groups found in higher generation dendrimers was responsible for disruption of bilayer membranes.

sBLMs are more robust and stable than unsupported planar bilayer membranes and can be deposited on a variety of hydrophilic surfaces, such as oxidized glassy carbon, silica, and mica (Sackmann, E., 1996). Even though a sBLM is only about 5 nm thick, it is an excellent electrical insulator. Thus, disruption of the sBLM by NPs could, in principle, be measured electrochemically. The approach described in this study provides a rapid, sensitive, and convenient electrochemical method to detect disruption of sBLM by NPs. The approach involves fabricating a sBLM on a glassy carbon electrode (GCE), and then using electrochemical methods to monitor interactions between NPs and the

sBLM. Disruption of a 1,2-dioleoyl-sn-glycero-3-phosphocholine (DOPC) sBLM formed on a GCE was investigated using cyclic voltammetry (CV) and electrochemical impedance spectroscopy (EIS).

6.3. Methods and instrumentation

6.3.1. Method

Each GCE (Bioanalytical Systems, West Lafayette, IN) was sequentially polished with 1000, 300 and 50 nm alumina slurry, followed by washing with de-ionized (DI) water and methanol. The electrode was ultrasonicated for 2 min in DI water to remove physically adsorbed alumina, given final rinses with methanol and DI water, and then dried under a nitrogen stream. The GCE was placed in 100 mM NaCl solution and oxidized at a potential of 1500mV for 3 min(Du, L. W. *et al.*, 2006). It was then washed with DI water and dried under a nitrogen stream. Five μL of DOPC lipid solution (5 mg/mL in chloroform) was applied to the electrode surface, and the electrode was immediately immersed in an electrolyte solution (100 mM sodium phosphate buffer, pH 7.4, containing 1 mM of potassium ferrocyanide and 1 mM of potassium ferricyanide). After 20 min, PAMAM dendrimers (G2 - G7, provided by Dr. Steve Kaganove, Michigan Molecular Institute, Midland, MI) were added to obtain a final concentration of 20 μM (based on the surface amino groups). PEG NPs were added to a concentration 1 μM (based on the molecular weight). CV was then used to monitor changes in the sBLM's electrochemical properties until a steady-state situation was observed [Figure 6.1].

6.3.2. Instrumentation

Electrochemical measurements were performed using a CHI660B electrochemical workstation (CH Instruments Inc., Austin, TX). EIS was performed in 100 mM sodium phosphate buffer, pH 7.4, containing 1 mM potassium ferrocyanide and 1 mM potassium ferricyanide. The DC potential was E^o = 220 mV vs a Ag/AgCl reference electrode, and a 5 mV sinusoidal potential was applied across the frequency range of 0.1 to 10,000 Hz. A modified Randles equivalent circuit model (Bard, A. and Faulkner, L., 2001) was fitted to the impedance data using Z-view software (Scribner Associates, Southern Pines, NC). CV was performed in same electrolyte solution as used for EIS studies. The potential was cycled in a range of 500 mV to -200 mV at a scan rate of 50 mV/s.

6.4. Results and discussion

6.4.1. Interface formation

The CV and EIS characterization of sBLM have been discussed in Section 2.4.2.

6.4.2. Interaction of PAMAM dendrimers with sBLM

After sBLM formation, PAMAM dendrimers were added to the electrolyte solution, and their interaction with the sBLM was monitored electrochemically. The system typically reached steady state 15 min after the addition of dendrimer solution, but the electrochemical parameters were monitored for 30 min to ensure a constant value. The dendrimer concentration was calculated based on surface amino groups to ensure that the same number of charged groups was used in all experiments. The CV curves obtained after addition of G2 and G3 dendrimers are shown in Figure 6.2. No redox peaks were obtained for G2, and only a small peak current of 0.12 μA was obtained for G3. These

results indicate that lower generation dendrimers cause minimal defects in the sBLM, and are consistent with the AFM study by Mecke *et al* (Mecke, A. *et al.*, 2005b), which found that G2 and G3 primarily adsorbed on the sBLM, without creating obvious holes. The CV curves obtained after addition of G4-G7 dendrimers are shown in Figure 6.3. The peak current increased roughly linearly with generation number for G5 – G7, suggesting that larger dendrimers more effectively create defects in the bilayer, through which the redox species can reach the electrode surface. The peak current values for G2-G7 dendrimers are summarized in Table 6.1. These values were used with the Randles-Sevick equation [Equation 2.2] to calculate the approximate sBLM defect area value for each generation (Bard, A. and Faulkner, L., 2001)

$$i_P = (2.69 \times 10^5)\, n^{3/2} A\, C_{BULK}\, (Dv)^{1/2} \quad \text{.....(Eq. 2.2)}$$

where, i_P is the peak current (μA), n is the number of electrons transferred (1), A is electrode area exposed (for bare GCE = 0.0706 cm^2), C_{BULK} is the bulk concentration of redox species (1×10^{-6} $molcm^{-3}$), D is the diffusion coefficient ((8.4×10^{-6} cm^2/s) and v is the scan rate (0.05 V/s). The diffusion coefficient of the redox species was calculated from the slope of the plot of peak current vs scan rate for a bare GCE surface.

EIS results indicated that the overall capacitance increased significantly with generation number, presumably due to a larger fraction of electrode area being exposed to the electrolyte solution [Figure 6.4], and hence a significant C_{DEFECT} value. Large peak current and higher capacitance values obtained for high generation dendrimers were a direct measure of the ability of dendrimer to pull out lipids from the sBLM. Based on the

data provided in Table 6.1, G7 dendrimers have a 36 times greater mass, 2.6 times greater diameter, and a 4.6 times greater surface charge density than G2 dendrimers.

We noted that the molecular mass, diameter, and surface charge density of PAMAM dendrimers all increase with generation number. Therefore, the relative role of nanoparticle properties in determining their ability to disrupt BLMs was not fully understood from these studies. Mecke *et al* (Mecke, A. *et al.*, 2004) and Hong *et al* (Diao, P. *et al.*, 1999; Hong, S. P. *et al.*, 2006) have studied defect formation by PAMAM dendrimers in DMPC sBLM on mica using AFM. A mechanism in which the dendrimer molecules take off the lipids from the sBLM forming so called 'dendrimer filled vesicles' was proposed (Mecke, A. *et al.*, 2005a; Mecke, A. *et al.*, 2005b). They reported that the size and the surface charge density are both important properties of a dendrimer that would act together in determining its efficacy to interact with BLM. Our results indicated that a nanoparticle may have to have sufficient size for enough interactions between the charged functional groups of NP and the head group of phospholipids. A nanoparticle with a particle size equal to or greater than thickness of BLM (5 nm) might be required for enough NP-BLM interaction that results in disruption of BLM. Recently, Ginzburg and Balijepalli (Ginzburg, V. V. and Balijepailli, S., 2007) developed a thermodynamic model for interaction of NPs with sBLM. Their simulations show that the NPs need to have sufficient size to have interaction with large number of phospholipids molecules and create a defect in BLM. They concluded that the diameter of a nanoparticle should be comparable or greater than the thickness of bilayer membrane. Our results are in agreement with their simulation results.

6.4.3. Interaction of PEG NPs with sBLM

Three main parameters associated with a nanoparticle can be deduced as critical ones for its interaction with lipid bilayer membranes, namely the size of a nanoparticle, the surface functional group (and thereby surface charge), and the surface charge density of a nanoparticle. The issue of nanoparticle size has been well addressed with the study on PAMAM dendrimers. Different polycationic polymers have been reported in literature for their interaction with sBLM, such as polyethyleneimine (PEI), polylysine and diethylaminoethyl-dextran (Mecke, A. *et al.*, 2005a; Hong, S. P. *et al.*, 2006; Leroueil, P. R. *et al.*, 2008). All of these polycationic polymers were found to be effective in disrupting sBLM. A recent report by Leroueil *et al* (Leroueil, P. R. *et al.*, 2008) has shown that inorganic NPs such as amine coated gold and silica NPs are effective in disrupting supported BLMs. These reports further support the hypothesis that NPs with a particle size equal to or greater than thickness of BLM are effective in disrupting BLMs.

Further studies wee required to investigate how a presence of charge on a NP, type of surface charge, and the surface charge density affects the NP-BLM interaction. We proposed a hypothesis that a charged surface is essential for BLM-NP interaction. Further, for a sBLM formed using zwitterionic lipids, the NP-BLM interaction should be independent of type of charge on NP. Finally, increase in the charge density of nanoparticle shall increase the BLM disrupting efficiency of the NP. To test these hypotheses, novel polyethylene glycol (PEG) NPs synthesized by Dr. Baker's group in Department of Chemistry at MSU were used. These nanoparticles were synthetically tailored to provide desired size, functionality and charge density to the NP. The structures of these NPs have been shown in Figure 6.5. The basic backbone was composed of

hydrophobic as well as hydrophilic groups, providing similar chemical environment as that of PAMAM backbone (Diao, P. *et al.*, 1999; Baker, G. L. *et al.*, 2008). These novel NPs were not monodisperse but they have a very narrow particle size distribution. The particle size for all of these NPs varied from 15-30 nm. The diameter of PEG NPs was greater than 5 nm and hence, they satisfy the criteria suggested by the thermodynamic model. PEG NPs have been custom designed to give particular functionality and charge on the surface. The monomers of these polymeric NPs have been linked via polyethylene glycol chain. These NPs were functionalized to provide cationic groups such as amine (PEG amine) and guanidine (PEG guanidine) groups on surface. PEG guanidine NPs would provide higher cation density per functional group compared to PEG amine NPs. One of the NPs has anionic carboxylic acid groups (PEG acid) on the side chain which will be exposed on surface. The basic uncharged PEG NPs did not have any functionalized side chain and hence did not have a surface charge. These NPs provided range of functional groups that can be assessed for their role in determining the efficiency of the interaction of NPs with sBLMs.

Similar to the PAMAM study, sBLM interface was assembled on GCE. CV and EIS were used to characterize the PEG NPs' interactions with sBLM. The nanoparticle-membrane interaction was quantitated using the peak current data obtained from CV and the capacitance values obtained from impedance data. The peak current data is shown in Table 6.2. Uncharged PEG NPs had negligible effect on sBLM [Figure 6.6] whereas all other three NPs namely PEG amine [Figure 6.7], PEG acid [Figure 6.8] and PEG guanidine [Figure 6.9] caused significant defect formation in sBLM. PEG amine and PEG acid were found to be almost equally effective in disrupting sBLM. PEG guanidine

was 55% more effective in disrupting sBLM than PEG amine. EIS results indicated that following the addition of PEG guanidine NPs, the membrane capacitance of sBLM increased from 0.75 $\mu F/cm^2$ to 15 $\mu F/cm^2$ [Figure 6.10] corresponding to a surface coverage of only 0.44 (56% of sBLM was removed). These results suggested that surface charge is essential for a NP to interact with BLMs. NPs should have suitable functional group that can interact with the head group of the phospholipids. The charged groups of polymers interact strongly with head group of phospholipids making membrane lose its planar morphology and reduce its free energy by creating a hole (Ginzburg, V. V. and Balijepailli, S., 2007). In our studies, both positively and negatively charged NPs disrupted sBLM formed using phospholipids with zwitterionic head group. The higher efficiency of PEG guanidine NPs in disrupting sBLM compared to PEG amine suggested that increasing the charge density of a NP leads to greater NP-BLM interaction. This study establishes that the molecules used in this study can be potential gene or drug delivery agents and provides a basis for designing new drug and gene delivery agents. The approach will also facilitate development of new methods to assess the toxicity of the NPs to be used in products intended for human or animal use.

6.5. Conclusions

A biomimetic interface consisting of a sBLM deposited on a GCE was used to study the interaction of various NPs with lipid bilayers. CV and EIS studies showed that dendrimer addition dramatically decreased impedance and increased ferricyanide peak currents, presumably by creating defects in the sBLM. Higher generation dendrimers had a much stronger effect on the sBLM than did lower generation dendrimers. CV data were used to estimate the defect area as a function of generation. EIS results showed an

increase in overall capacitance values following dendrimer addition, consistent with a decrease in sBLM surface coverage. PEG NPs were used to assess the effect of different surface charge and charge density on the BLM disrupting ability of NPs. The study showed that suitable surface charge is essential for NPs to interact with BLMs. Higher charge density provided better efficiency. The sBLM interface provides a rapid and convenient way to screen NPs for strong interactions with lipid bilayers and may have utility in assessing nanoparticles' toxicity or suitability for intracellular genes or drug delivery.

Sample	Molecular weight	Surface amino groups per molecule	Particle diameter (nm)	Area of electrode exposed after NP-BLM interaction (mm^2)
Bilayer	N/A	N/A	2.2	0.044 ± 0.008
PAMAM G2	3256	16	2.9	0.082 ± 0.015
PAMAM G3	6909	32	3.6	0.088 ± 0.010
PAMAM G4	14215	64	4.5	0.430 ± 0.023
PAMAM G5	28826	128	5.3	1.761 ± 0.164
PAMAM G6	58048	256	6.7	2.902 ± 0.190
PAMAM G7	116493	512	7.6	4.077 ± 0.156
Bare GCE	N/A	N/A	N/A	7.065 ± 0.324

Table 6.1: Characteristics of PAMAM dendrimers, along with the parameters showing their effect on sBLM.

Nanoparticle	Molecular weight	Peak current (μA)	Area of electrode exposed after NP-BLM interaction (mm^2)
Uncharged PEG NP	98000	0.126 ± 0.021	0.057 ± 0.012
PEG-amine NP	87000	3.767 ± 0.227	2.251 ± 0.131
PEG-guanidine NP	68800	5.30 ± 0.604	3.503 ± 0.062
PEG-acid NP	82100	3.433 ± 0.108	2.119 ± 0.347

Table 6.2: Characterization of PEG NPs' interaction with sBLM studied using CV. [Electrode area of GCE is 7.064 mm^2]

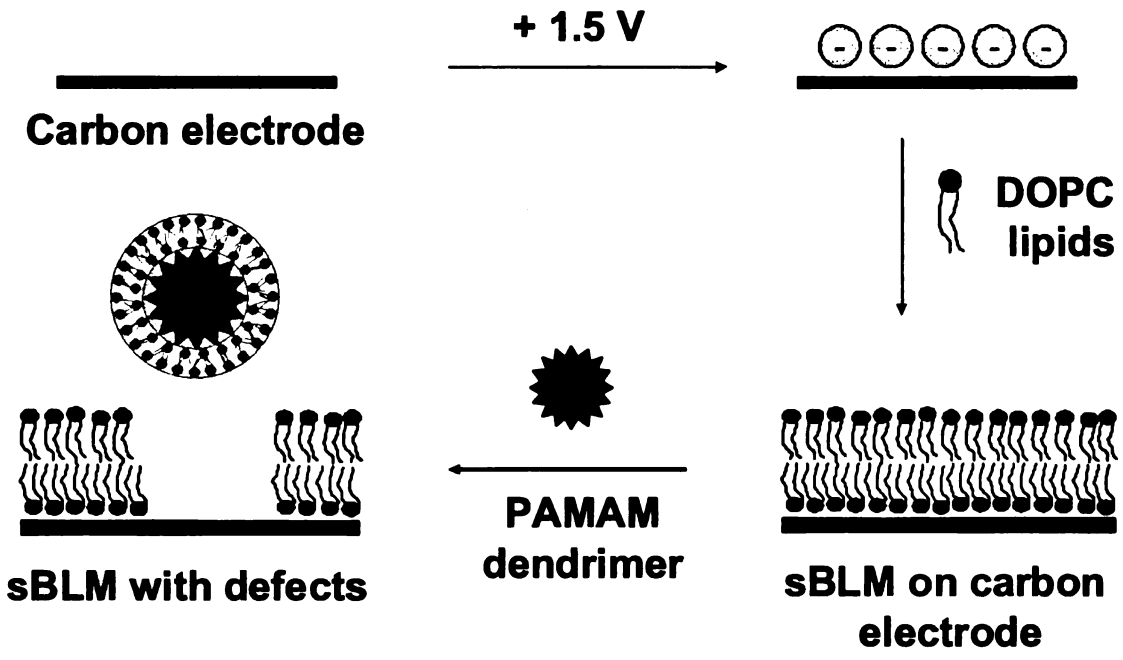

Figure 6.1: sBLM formation on GCE. GCE was first oxidized at +1.5 V to impart negative charge. DOPC sBLM was self assembled on oxidized GCE by depositing DOPC lipids, solubilized in chloroform, on GCE and immediately transferring the interface in an aqueous electrolyte solution. sBLM stability was tested using EIS and CV. Nanoparticles, when added in required concentration, disrupted sBLM and exposed electrode area which can be calculated from the redox peaks obtained using CV. In one of the proposed mechanisms, dendrimers form so called 'dendrimer filled vesicles' after their interaction with sBLM (Mecke, A. *et al.*, 2005b).

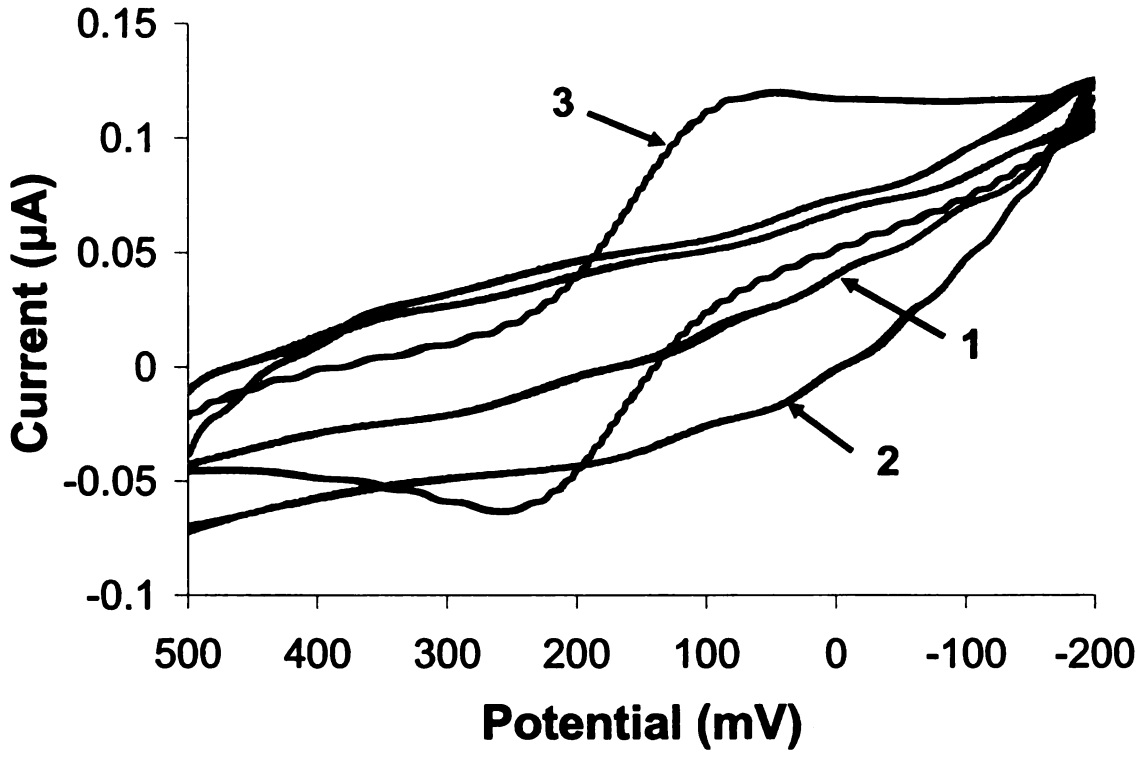

Figure 6.2: Cyclic voltammograms showing the effect of lower generation PAMAM dendrimers on sBLM: PAMAM G2 (curve 2) and PAMAM G3 (curve 3). [Electrode area: 7.064 mm^2]

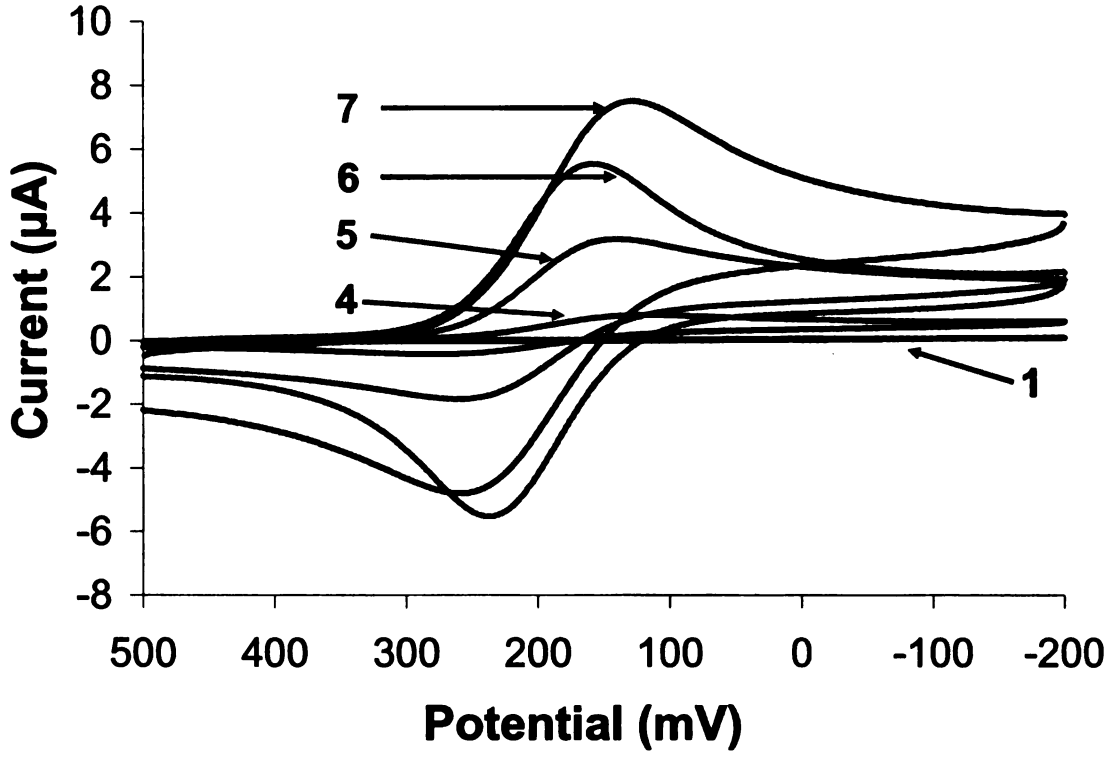

Figure 6.3: Cyclic voltammograms showing the effect of higher generation PAMAM dendrimers on sBLM: PAMAM G4 (curve 4), PAMAM G5 (curve 5), PAMAM G6 (curve 6), and PAMAM G7 (curve 7). Curve 1 represents the sBLM before dendrimer addition. [Electrode area: 7.064 mm^2]

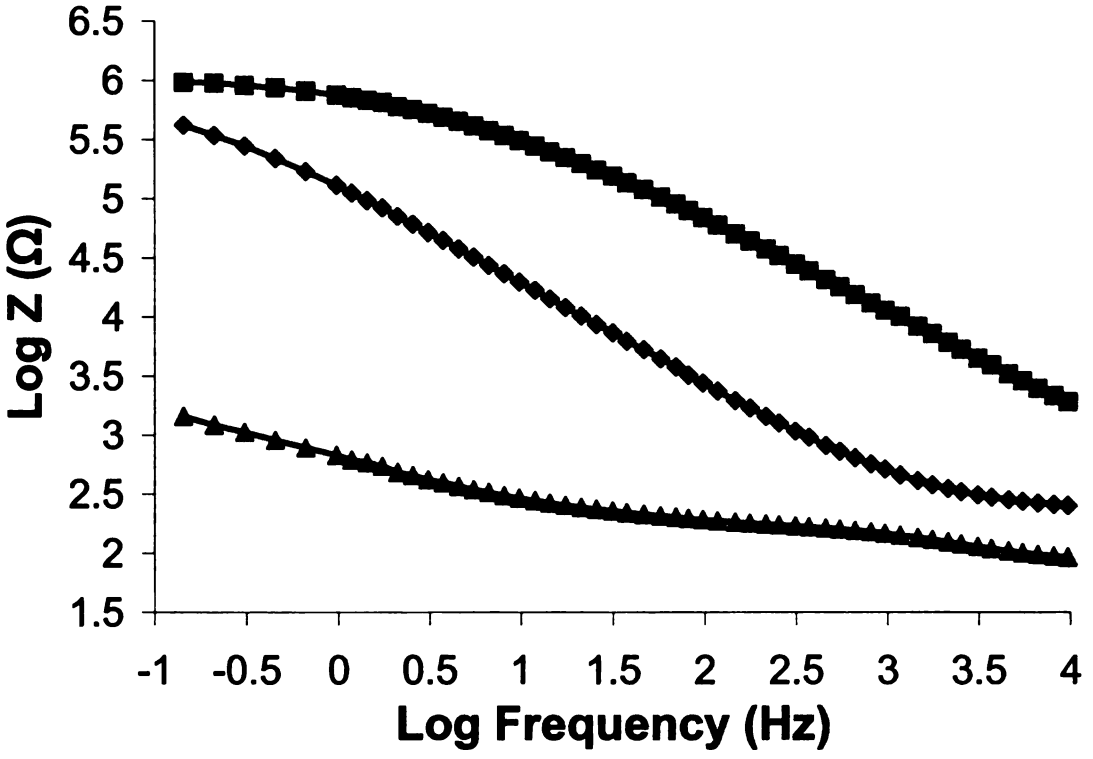

Figure 6.4: Impedance (Log Z) data were plotted as a function of Log frequency for a bare GCE surface (triangles), sBLM (squares), and sBLM after interaction with PAMAM G5 dendrimers (diamonds). An equivalent circuit shown in Figure 2.9 was used to fit the impedance data. The disruption of sBLM by PAMAM G5 increased the membrane capacitance and decreased the membrane resistance. [Electrode area: 7.064 mm^2]

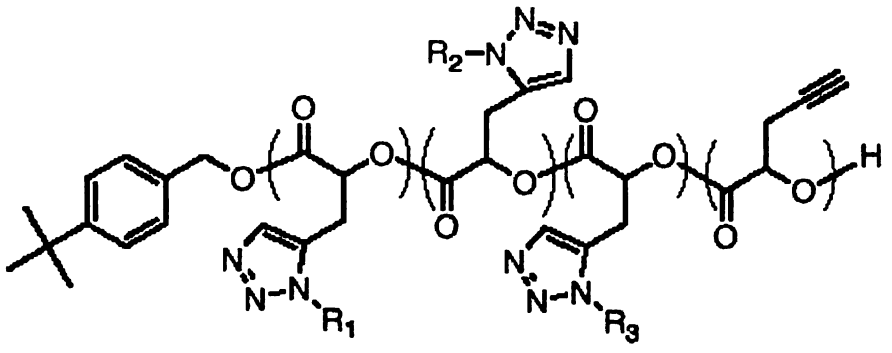

NPs	R_1	R_3	Molecular weight
PEG	$-(CH_2OCH_2)_5-$	-H	98000
PEG-amine		$-(CH_2)_5-NH_2$	87000
PEG-guanidine		$-(CH_2)_5-NHCHNHNH_2$	68800
PEG-acid		$-(CH_2)_6-OCO-(CH_2)_2-COOH$	82100

Figure 6.5: Structures of new PEG NPs synthesized using 'click' chemistry by Dr. Baker group in Department of Chemistry at MSU. The basic backbone of the structure is shown above the table. The group $-R_2$ is hydrogen (-H) in all NPs.

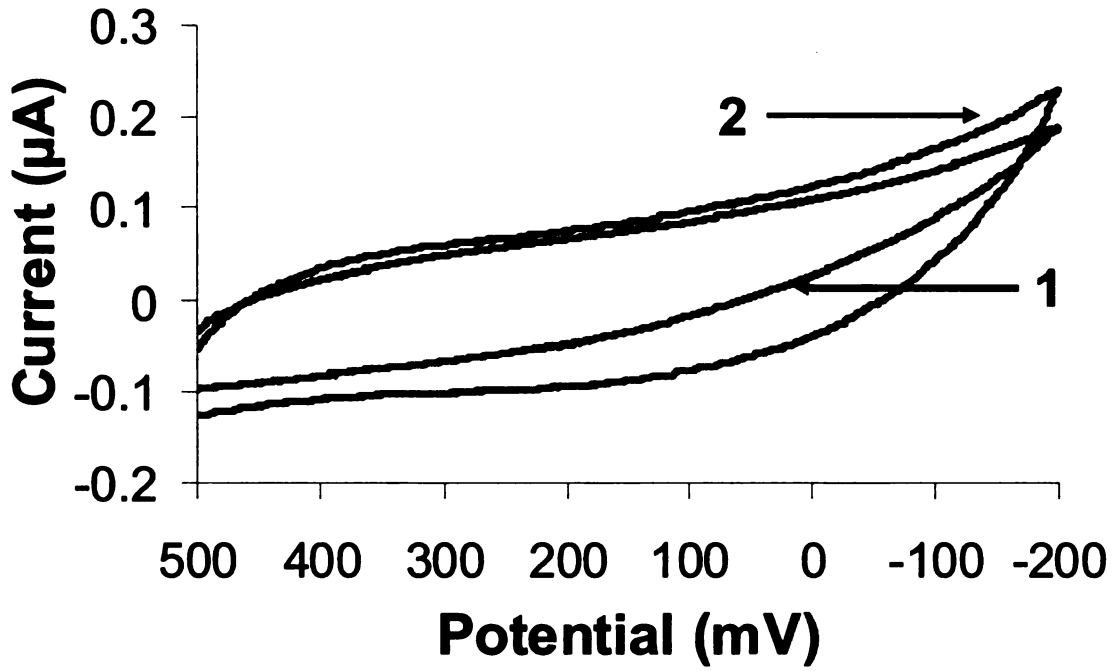

Figure 6.6: Cyclic voltammograms showing the effect of uncharged PEG NPs on sBLM: sBLM (curve 1), and sBLM after interaction with PEG uncharged NPs (curve 2). [Electrode area: 7.064 mm^2]

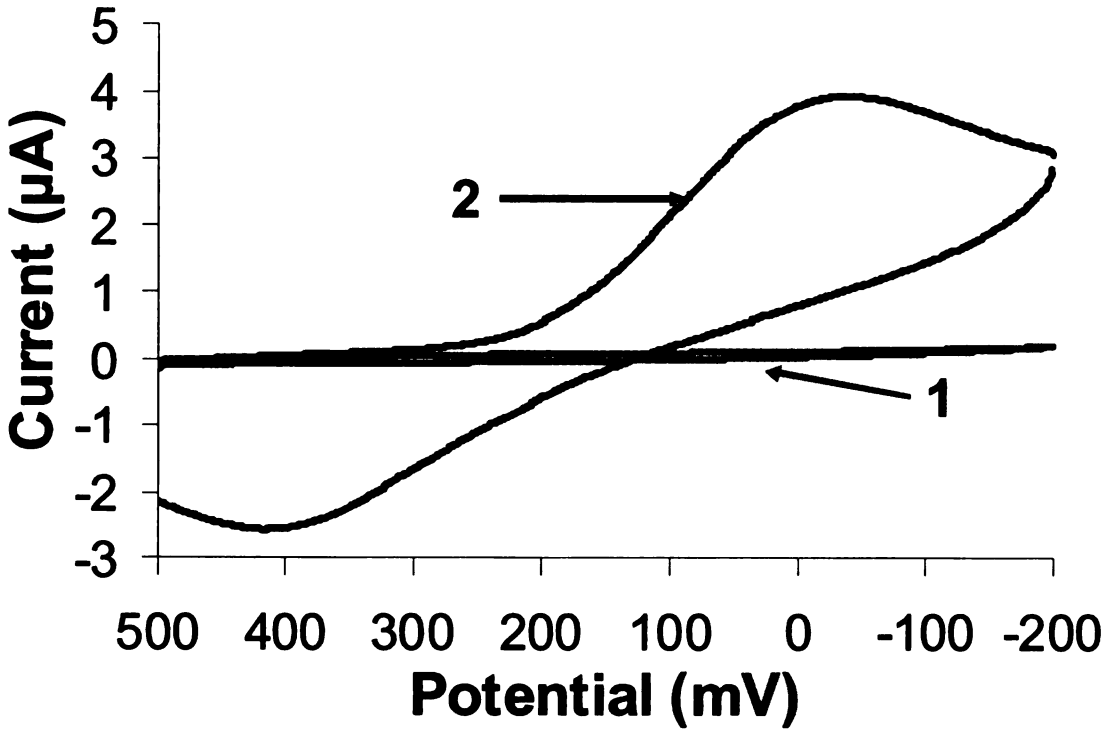

Figure 6.7: Cyclic voltammograms showing the effect of PEG amine NPs on sBLM: sBLM (curve 1), and sBLM after interaction with PEG amine NPs (curve 2). [Electrode area: 7.064 mm^2]

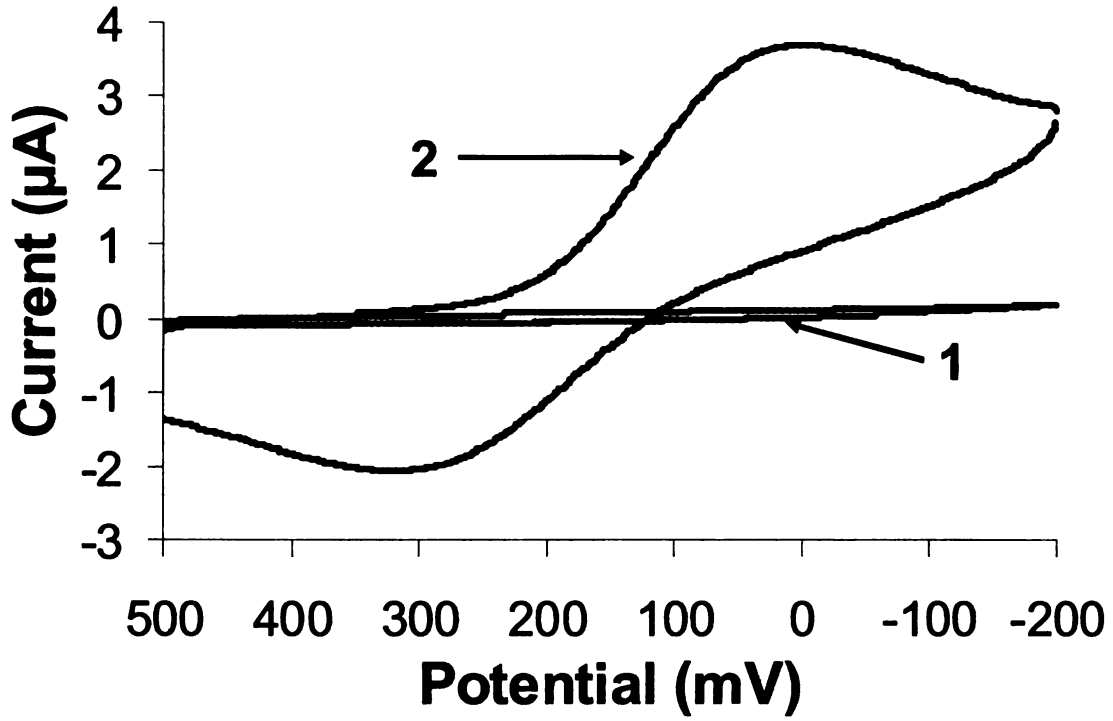

Figure 6.8: Cyclic voltammograms showing the effect of PEG acid NPs on sBLM: sBLM (curve 1), and sBLM after interaction with PEG acid NPs (curve 2). [Electrode area: 7.064 mm^2]

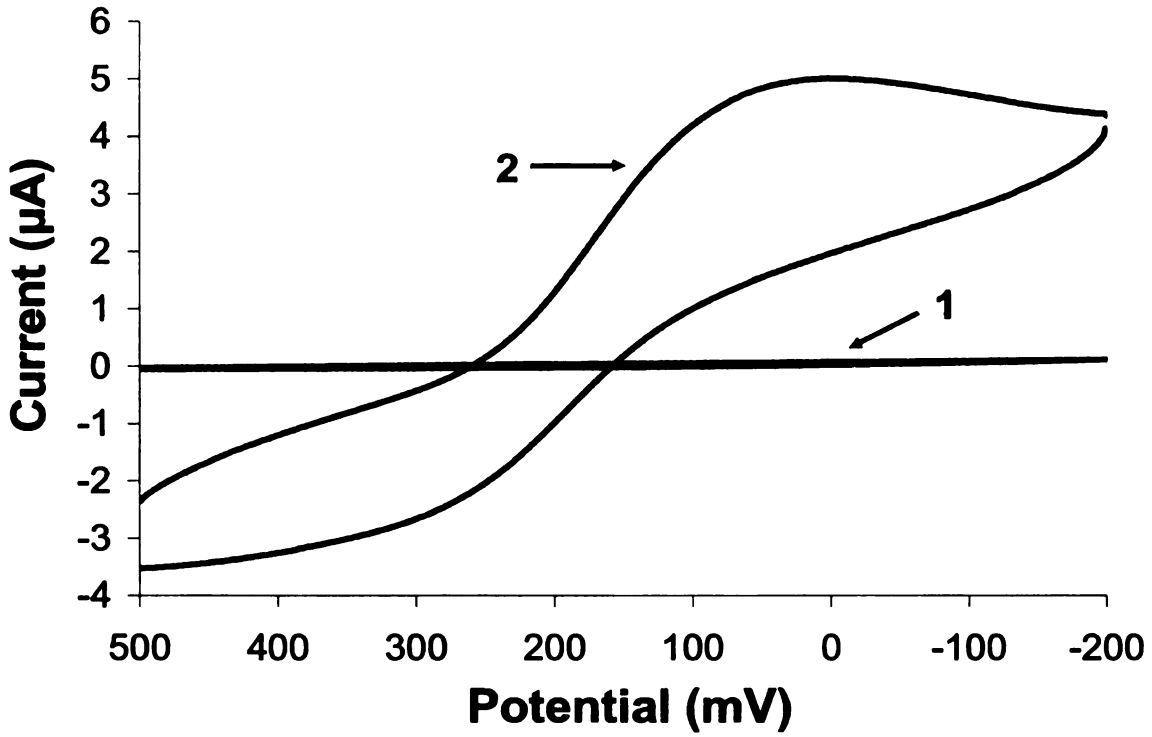

Figure 6.9: Cyclic voltammograms showing the effect of PEG guanidine NPs on sBLM: sBLM (curve 1), and sBLM after interaction with PEG guanidine NPs (curve 2). [Electrode area: 7.064 mm^2]

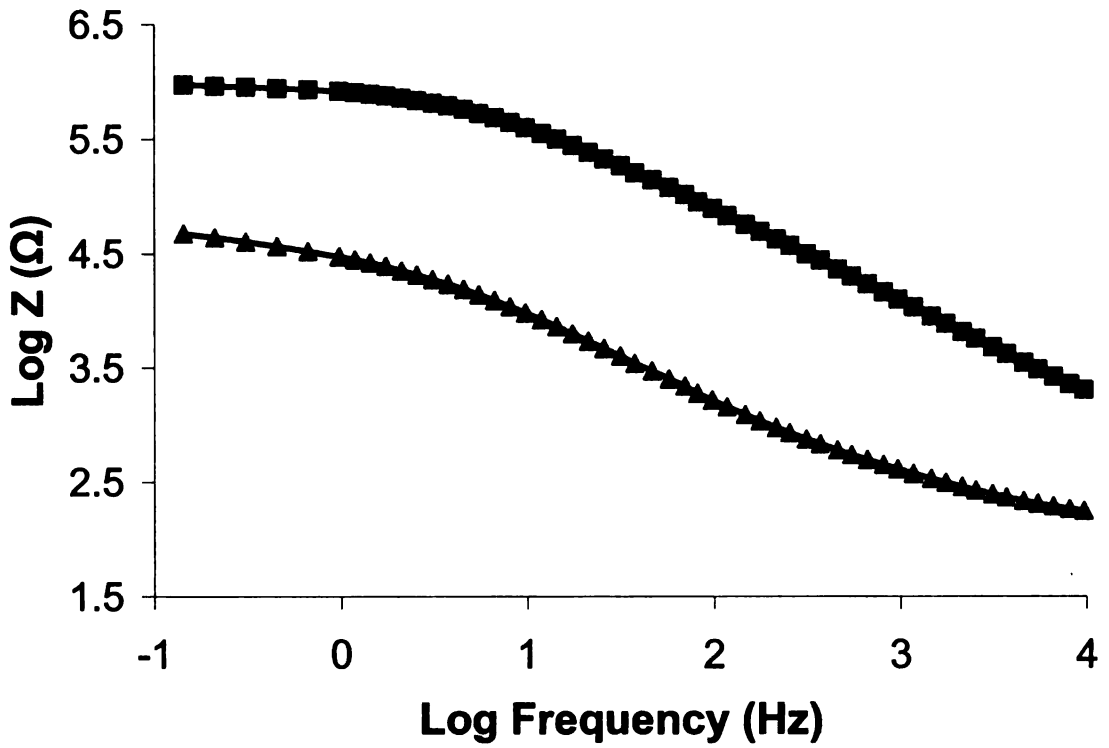

Figure 6.10: Impedance (Log Z) data were plotted as a function of Log frequency for a sBLM on GCE (squares), and sBLM after interaction with PEG guanidine NPs (triangles). An equivalent circuit shown in Figure 2.9 was used to fit the impedance data. The disruption of sBLM by PEG guanidine NPs increased the membrane capacitance and decreased the membrane resistance. [Electrode area: 7.064 mm^2]

7. INTEGRATION OF BIOMIMIETIC INTERFACES WITH GOLD ELECTRODE ARRAYS

7.1. Abstract

Recent advances in the recombinant DNA technology have led to the expression of novel soluble and membrane proteins in bacterial and mammalian cells. These proteins can be incorporated into biomimetic interfaces that allow the proteins' activities to be expressed and rapidly characterized, thereby advancing functional proteomics research To facilitate these applications, there is a need for development of tools that will allow a rapid, cost-effective, multi-parameter, simultaneous high-throughput characterization of multiple classes of proteins. In this study, development of a microelectrode array system for the characterization of membrane proteins is reported. Gold microlectrode arrays were fabricated on glass or silicon substrate using photolithography. The arrays were covered with insulating layer of silicon nitride to define the electrode size. Tethered bilayer lipid membrane (tBLM) interfaces were deposited on microelectrode arrays. Electrochemical techniques were used to characterize tBLM properties using a commercial potentiostat as well as novel custom-made circuits developed specifically for array microsystem. Highly insulating tBLMs with near-gigaohm membrane resistances were obtained on gold microelectrodes. Incorporation of synthetic ionophores and a channel peptide decreased membrane resistance significantly, thereby confirming the suitability for carrying out ion channel assays. The dependence of tBLM fluidity on temperature was also investigated. The membrane resistance value of a 1,2-dipalmitoyl-*sn*-glycero-3-phosphothioethanol (DPPTE)-1,2-dipalmitoyl-*sn*-glycero-3-phosphocholine (DPPC) tBLM stabilized above a 40°C corresponding to a phase transition temperature (PTT) of the lipid. Below PTT,

incorporation of gramicidin peptides did not mediate ion transport. Above PTT, gramicidin mediated ion transport decreased the membrane resistance indicating the fluid nature of a tBLM. In addition to tBLMs, a biosensor interface for measuring the esterase activity of a membrane protein, NEST, was deposited on microelectrode arrays. NEST sensor response was decreased by 26% after addition of 1 mM phenylmethylsulfonyl fluoride (PMSF) indicative of NEST inhibition. The dependence of the functional activity of NEST on temperature was investigated. NEST activity increased with increase in temperature in the range of 21°C to 31°C. Above 31°C, the activity decreased amost linearly with increase in temperature.

7.2. Introduction

With completion of Human Genome Project, the focus has now shifted towards structural and functional characterization of new proteins. Novel soluble and membrane proteins are being identified and expressed using recombinant DNA technology. There is a need for development of cost-effective, high-throughput tools for rapid characterization of the newly identified proteins. Biosensor arrays, in which multiple biomimetic interfaces are fabricated on miniaturized electrodes onto a single device, will allow simultaneous characterization of multiple proteins or enable a single assay to be performed on many samples in parallel. Biosensor arrays could greatly reduce screening times and increase throughput in a drug discovery process. These biosensor arrays can be easily adapted to array microsystem that allows multi-channel measurements. Center for Nanostructured Biomimetic Interfaces (CNBI) at MSU has developed sensor interfaces for several soluble proteins such as tyrosinase, glucose oxidase (Lu, J. *et al.*, 2007) and dehydrogenases (Hassler, B. L. and Worden, R. M., 2006; Kohli, N. *et al.*, 2006a;

Hassler, B. L. *et al.*, 2007a; Hassler, B. L. *et al.*, 2007b; Kohli, N. *et al.*, 2007; Lu, J. *et al.*, 2007; Hassler, B. L. *et al.*, 2008). The progress made with biosensors for soluble proteins has not been matched with the progress in designing biosensors for membrane proteins, because of the difficulties associated with expression, purification and reconstitution of these proteins. Moreover, membrane proteins need to be embedded in BLM for expressing their activity. In this study, gold electrode arrays were designed and fabricated using photolithography. A microelectrode array platform was developed by Dr. Mason's group at the Department of Electrical and Computer Engineering at MSU. The array platform was used to deposit different protein interfaces. High impedance tBLMs were deposited on microelectrodes ranging in size from 3 mm in diameter down to 50 μm in diameter. Gramicidin peptide was incorporated in tBLMs and the ion transport across BLM was measured using EIS. Further, tBLM interface was used to study the effect of temperature on bilayer fluidity and gramicidin activity.

7.3. Methods

7.3.1. Microelectrode array fabrication

Microelectrode arrays were fabricated using a lift-off photolithography process. The silicon wafers were diced to required dimension and cleaned in acetone. Then, diced wafers were ultrasonicated in acetone and DI water for 15 min each. Finally, the wafers were thoroughly rinsed with deionized (DI) water and dried in a nitrogen stream. A negative photoresist AZ 5214E (Clariant, Sommerville, NJ) was spin coated (3000 rpm, 35 sec) on silicon wafers and pre-baked at 95°C for 1 min. This step deposits on wafers approximately 1.5 μm thick photoresist film. To pattern microelectrodes, the wafer covered with photoresist film was exposed to UV light through an optical mask. The

exposed area of the photoresist gets cross linked during a post-baking at 120 °C (for 2 min). The cross linked photoresist loses its photosensitivity. Then, the whole wafer was exposed to UV light (no mask) for 1 min to degrade the previously unexposed photoresist. The degraded photoresist pattern was dissolved and removed by treating the wafer with AZ MIF 300 developer solution (Microchem Corporation, Newton, MA). Finally, the wafers were thoroughly rinsed with DI water.

Physical vapor deposition (Edwards Auto306 thermal evaporator, Ceramisis Ltd., London) technique was used to deposit titanium and gold layers on the photoresist patterned silicon wafers. First, a 5 nm thick titanium film was deposited at a rate of 0.2 Å per sec as an adhesion layer prior to gold deposition. Then, a gold film of 100 nm in thickness was deposited at a rate of 0.5 Å per sec. After gold deposition, the electrodes were cleaned and ultrasonicated in acetone for 20 min. The electrodes were rinsed using DI water and dried in nitrogen stream.

7.3.2. Deposition of insulation layer over microelectrode arrays

A 200 nm thick insulation layer of silicon nitride was deposited on microelectrode arrays using plasma enhanced chemical vapor deposition (Plasma 80plus, Oxford Instruments, UK). The electrode sizes were defined by using photolithography. Briefly, 1.5 μm thick layer of a positive photoresist S1813 was spin coated on silicon nitride covered microelectrode array, followed by heating at 95 °C for 8-10 min for pre-baking of the photoresist. The area of required electrode sizes on an array was exposed to UV light for 10 sec through a patterned optical mask. The photoresist in the exposed areas gets degraded with UV light which can be dissolved and subsequently removed after treatment with 352 development solution. The unexposed area remains unaffected.

Finally, microelectrode array was rinsed with DI water and dried. The S1813 photoresist covered area (unexposed area in the previous UV light treatment) protects the underlying silicon nitride film during the subsequent reactive ion etching process. The exposed silicon nitride area was removed using dry reactive ion etching (Plasma Quest, UK) process. After etching, the S1813 photoresist film was dissolved and removed by ultrasonicating the electrodes in acetone. The final rinsing was done using DI water. The electrodes were cleaned in piranha solution, washed with DI water, dried in nitrogen stream, and stored at room temperature until used.

7.3.3. Fabrication of tBLM on microelectrode arrays

DPPTE-DOPC tBLM was fabricated on microelectrode arrays using a same procedure described in Section 2.3.5. Instead of an electrochemical cell, the measurements were done in a small reservoir (~500 μL) created using a polydimethoxysiloxane (PDMS) block.

7.3.4. Fabrication of NEST sensor

NEST was expressed in *E. coli* and purified using reported procedures (Atkins, J. and Glynn, P., 2000; Kohli, N. *et al.*, 2007). NEST sensor was deposited on macroelectrodes or microelectrode array using the procedure described by Kohli *et al.* (Kohli, N. *et al.*, 2007). Briefly, the electrodes were cleaned in piranha solution and dipped in 5 mM solution of thioctic acid in ethanol for 1 hr. The electrodes were washed with ethanol, dried under nitrogen and dipped in poly-L-lysine (PLL) solution for 30 min. PLL solution was prepared by adding 12 mg of PLL in 50 mL of 20 mM phosphate buffer (pH 8.5). The electrodes were then rinsed with water and dipped in a solution of tyrosinase (0.2 mg/ml) for 1 h. The last two steps were repeated 3.5 times to create 3.5

PLL-tyrosinase bilayers with PLL being the topmost layer. The electrodes were washed with water and dipped in a solution of NEST protein (0.1 mg/mL) in 0.1 M phosphate buffer, pH (7.0) for 1 h. The electrodes were then washed with water, dried under nitrogen and dipped in phosphate buffer (0.1 M, pH 7.0) for testing. Phenyl valerate was used as the substrate for NEST. To prepare phenyl valerate substrate solution, 15 mg of phenyl valerate was dissolved in 1 mL of dimethylformamide (DMF), and 15 mL of water containing 0.03% Triton X-100 was added slowly under vigorous stirring.

7.3.5. NEST solution assay

To 100 μL of 5.263 mM phenyl valerate solution, 50 μL of enzyme solution (with proper dilution) was added and incubated at the target temperature for 20 min. Then, 100 μL of reaction stopping solution (9.5 mg/mL of sodium dodecyl sulfate and 1.23 mM 4-aminoantipyrine) was added and incubated at room temperature for 5 min. Finally, 50 μL of 12.1 mM potassium ferricyanide solution was added to the the mixture and incubated at room temperature for 5 min. The absorbance of the solution was measured at 486 nm.

7.4. Results and discussion

7.4.1. tBLM on microelectrode arrays on glass

The first generation microelectrode arrays were fabricated on glass. SU8 photoresist was used as insulation layer to define the area of ten gold electrode elements with electrode size ranging from 3 mm diameter to 250 μm in diameter (Design Glass-I) [Figure 7.1A]. Tethered bilayer lipid membranes (tBLM) were deposited on these sensing elements as described previously (Raguse, B. *et al.*, 1998; Atanasov, V. *et al.*, 2005; Jadhav, S. R. *et al.*, 2008b). The tBLM acts as an insulating dielectric barrier for ion

transport, thereby increasing the impedance of the bio-interface. Gramicidin peptides selectively transported alkali metal ions through the tBLM and therefore lowered the impedance of the modified tBLM in the presence of alkali metal ions in the electrolyte solution. Dr. Mason's lab has developed a compact, low power, impedance extraction and digitization circuit (IDC) that can be installed under each element of a sensor array (Yang, C. *et al.*, 2009). The properties of IDC are listed in Table 7.1 IDC circuit was used to locally extract and digitize sensor impedance information. IDC can measure current response ranging from 78 fA to 100 nA, suitable for tBLM measurements (Yang, C. *et al.*, 2009). The experimental set-up for EIS measurements of tBLM using IDC is shown in Figure 7.2. A data acquisition card (Agilent E3630A) was used to generate the sinusoidal stimulus and collect output data from the IDC. Impedance measurements were conducted over the frequency range of 10 mHz to 100 Hz using IDC after formation of DPPTE monolayer, then tBLM, and finally after the incorporation of gramicidin peptides in tBLM bathed in 100 mM sodium (alkali metal) chloride solution. A Randles equivalent circuit shown in Figure 2.5 was used to model the impedance data obtained using IDC, with the membrane capacitance (C_M) and membrane resistance (R_M) representing the properties of the lipid bilayer membrane. For a DPPTE monolayer, the C_M and R_M values were measured to be 0.635 $\mu F/cm^2$ and 20 $k\Omega cm^2$ respectively. For the tBLM, a C_M and R_M of 0.505 $\mu F/cm^2$ and 425 $k\Omega cm^2$ were obtained [Figure 7.3]. The capacitance value for tBLM was in agreement with the values obtained for quality tBLMs in our studies with commericial gold. A slightly lower value of membrane resistance suggested that there might be imperfections in tBLM at the edges of the electrode.

Incorporation of gramicidin peptides in tBLM decreased the membrane resistance from 425 to 59 $k\Omega cm^2$ due to the passage of sodium (alkali metal) ions through the tBLM. These results demonstrate that the compact IDC circuit can successfully characterize the impedance spectra of sensor materials. A chip containing an array of IDC units coupled to on-top gold electrodes would allow simultaneous measurement of all sensor elements.

7.4.2. tBLM on microelectrode arrays on silica substrates

Two designs of second-generation microelectrode arrays were deposited on silicon substrates to provide flexibility in choosing the desired sizes and patterns of electrodes. Design Si-I had ten gold electrode elements (deposited in an area of 3 X 3 mm^2) on a 15 X 30 mm^2 size silicon substrate [Figure 7.1B], while Design Si-II had forty gold electrodes (deposited in a 3 X 3 mm^2 area) on a 12.5 X 12.5 mm^2 size silicon substrate. The size of gold electrodes on an array was varied and controlled by patterning silicon nitride insulation layer using photolithography. In one of the Design Si-I electrode arrays (Design Si-IA), five electrode sizes (800 μm, 400 μm, 200 μm, 100 μm and 50 μm in diameter) were patterned with two electrodes of each size. While in Design Si-IB, microelectrode array having five electrodes each of sizes 250 μm and 500 μm diameter were fabricated. The maximum diameter of a gold electrode that can be accommodated on Design Si-I electrodes was 1 mm. In case of Design Si-II electrodes [Figure 7.1C], four electrode sizes (200 μm, 150 μm, 100 μm, and 50 μm in diameter) were patterned with ten electrodes of each size. The maximum diameter of a gold electrode that can be accommodated on Design Si-II electrodes was 250 μm.

tBLM was deposited on gold microelectrode arrays in a two step process described in Section 2.3.5. After BLM deposition, the electrochemical properties of tBLM were measured using electrochemical impedance spectroscopy (EIS). Figure 7.4A and Figure 7.4B, show the impedance spectrum obtained for tBLM deposited on 250 μm and 500 μm diameter microelectrodes, respectively. For a tBLM deposited on a 500 μm diameter electrodes, a highly insulting tBLM was obtained with a membrane resistance of 1.29 $M\Omega cm^2$. The suitability of tBLM for ion channel assays was confirmed by measuring ion transport activity of gramicidin peptides. Incorporation of gramicidin in tBLM decreased the R_M value to 0.029 $M\Omega cm^2$, confirming ion transport across tBLM [Figure 7.4A]. Similarly for a 250 μm electrode, the tBLM resistance was decreased by almost three order of magnitude (from 0.9 $M\Omega cm^2$ to 0.0015 $M\Omega cm^2$) following gramicidin incorporation [Figure 7.5B]. Electrochemical properties of the tBLM deposited on different size microelectrodes are summarized in Table 7.2 (absolute values of the constants) and in Table 7.3 (normalized to 1 cm^2 electrode area). As the electrode size got smaller, the absolute value of membrane resistances increased, while the membrane capacitance values decreased. Compared to membrane capacitance value of 1.2 μF obtained using a gold macroelectrode 5 mm in diameter, the microelectrodes had a membrane capacitance in nanofarads (nf). Similarly, microelectrodes had higher absolute membrane resistance values compared to macrolectrodes, while electrodes below 500 μm in diameter had near-gigaohm resistances. During patch clamp experiments conducted using liposome vesicles, obtaining a gigaohm resistance is a pre-requisite for ion channel assays. Gigaohm resistance membranes are characteristic of

good quality BLMs; stray currents do not contribute significantly at such high resistance thereby permitting the measurement of small ion channel currents. Obtaining near-gigaohm resistances with tBLMs on microelectrodes offers the possibility of using these membranes for sensitive single channel activity measurements. The sealing property of tBLMs on microelectrodes was confirmed by measuring the ion conduction activity of gramicidin peptides. The membrane resistance of tBLMs on all microelectrodes (from 800 μm down to 50 μm diameter electrodes) decreased significantly following gramicidin incorporation [Figure 7.5].

The area-normalized electrochemical properties of tBLMs deposited on microlectrodes deviate somewhat from those obtained using macroelectrodes [Table 7.3]. For electrodes smaller than 500 μm diameter electrode, the area normalized membrane resistance was below 1 $M\Omega cm^2$, and it decreased as the electrode size got smaller. Similarly, the area normalized membrane capacitance values increased as the electrode size decreased. These trends are likely due to electrode-edge effects, arising from incompletely formed tBLM at the electrode edge. The increase in ratio of circumference to area as electrodes get smaller is consistent with this hypothesis. In addition to the edge effects, surface characteristics of electrode, such as surface roughness, also play a major role. Higher roughness might cause formation of unorganized monolayer of tethering lipids having defects at the areas with higher roughness. This, in turn, leads to formation of non-insulating tBLMs that are unsuitable for ion channel assays. A higher surface roughness can also be imparted during fabrication process of electrodes. Deposition of microelectrode arrays using photolithography involves multiple steps of photoresist coating and removal. Incomplete removal of photoresist leaves residues on the electrode

surface, which can lead to defects in tBLM, and hence non-ideal charge transfer across the bilayer.

7.4.3. NEST sensor on microelectrode arrays

In addition to tBLMs, a biosensor interface was fabricated on gold macro- and microelectrodes. The biosensor measures the esterase activity of NEST, a catalytically active fragment of a membrane protein Neuropathy Target Esterase (NTE) (Atkins, J. and Glynn, P., 2000; Forshaw, P. J. *et al.*, 2001; Wang, J. and Richardson, R. J., 2003; Kropp, T. J. *et al.*, 2004). NTE is an important membrane protein in nerve cells. Inhibition of NTE by organophosphorus compounds leads to neurological diseases, such as organophosphate-induced delayed neuropathy and motor neuron disease (Glynn, P., 2006b; Glynn, P., 2006a). In collaboration with Dr. Rudy J. Richardson at the University of Michigan, the CNBI has developed a biomimetic interface for NEST that can detect presence of organophosphorus compounds (Kohli, N. *et al.*, 2007). The biosensor contains two enzymes, NEST and tyrosinase, immobilized using the positively charged polyelectrolyte PLL. NEST's esterase activity hydrolyzes the substrate (phenyl valerate) to phenol, which is subsequently oxidized to catechol and then to *o*-quinone by tyrosinase. *o*-quinone diffuses through enzymatic layers and gets rapidly reduced to catechol at the electrode surface. In constant potential amperometry (CPA) experiments, the electrode is held at negative potential (-100 mV), which results in o-quinone being reduced to catechol at the electrode. The cyclic interconversion of catechol and *o*-quinone results in signal amplification by the interface.

One disadvantage of this design is that conversion of catechol to *o*-quinone can cause an irreversible suicide inactivation of tyrosinase (Chang, T. S., 2009; Ramsden, C.,

2009). Higher accumulation of catechol might result in deactivation of tyrosinase over time. To minimize this effect, we developed an approach that uses cyclic voltammetry (CV) for measuring sensor response. In CV experiments, the potential is applied for a brief period of time, thereby limiting the amount of catechol regenerated, compared to constant potential amperometry. Secondly, part of catechol liberated due to *o*-quinone oxidation during a forward scan is converted back to quinone during a reverse scan. These two factors may significantly improve biosensor lifetime. To test this hypothesis, a concentration-current relationship was obtained using CPA and CV for freshly tyrosinase modified electrode (3 layers of PLL and tyrosinase). After the experiment, the electrode was rinsed and used again to generate the concentration-current curve. The concentration-current plot obtained for the first use ($R^2 = 0.999$) and second use ($R^2 = 0.999$) of same catechol sensor after rinsing using CPA is shown in Figure 7.6A. The sensitivity ($\mu A \mu M^{-1} cm^{-2}$) of tyrosinase sensor was found to decrease by 34% after the first use, possibly due to suicide inactivation of enzyme activity. The same experiment carried out using CV showed a 7% decrease in the sensitivity, suggesting that the extent of enzyme deactivation almost half in CV which could be due to less regeneration of catechol [Figure 7.6B]. In addition to CV, we explored the possibility of using EIS to monitor the catechol sensor response. EIS study showed that increasing the catechol concentration decreased the charge transfer resistance (R_{CT}) values. R_{CT} is related to concentration of reduced species as follows (Bard, A. and Faulkner, L., 2001)

$$R_{CT} = \frac{RT}{nFi_0} \quad \text{..... Eq. (7.1)}$$

$$i_0 = nFAk^0 C_O^{*(1-\alpha)} C_R^{*\alpha} \quad \text{..... Eq. (7.2)}$$

where, i_0 is an exchange current (Amperes), k^0 is the electron transfer coefficient, C_O^* is the bulk concentration of oxidized species, and C_R^* is the bulk concentration of reduced species, and A is area of electrode. In Figure 7.7, R_{CT} was plotted as a function of $C_O^{-1/2}$. It follows a linear ($R^2 = 0.996$) relationship, indicating that R_{CT} can be used as a measure of sensor response.

The concentration-current response obtained for NEST activity on a macroelectrode (~1 cm^2 area) using CPA and CV are shown in Figure 7.8A and Figure 7.8B respectively. Using CV, the sensitivity of a NEST sensor was 2.08 ± 0.1 $\mu A \mu M^{-1} cm^{-2}$, which was 8.7 times higher than the sensitivity obtained using CPA (240 ± 10 $nA \mu M^{-1} cm^{-2}$). The sensor response increased linearly ($R^2 = 0.998$) with phenyl valerate concentration in a range of 0 – 20 μM, reaching saturation at around 30 μM. NEST sensor was deposited on gold microelectrode arrays on silicon wafer using the same method. On a 500 μm diameter electrodes, a current sensitivity of 1.02 ± 0.05 $\mu A \mu M^{-1} cm^{-2}$ was obtained using CV. EIS was used to monitor the change in R_{CT} after addition of phenyl valerate. R_{CT} of NEST sensor on 500 μm diameter electrode decreased from

4.58 $k\Omega cm^2$ to 1.58 $k\Omega cm^2$ after addition of 10 μM phenyl valerate, suggesting that R_{CT} can also be used as a measure of NEST activity. An equivalent circuit shown in Figure 7.9 was used to model the impedance data. The NEST sensor on the array was then used to measure an organophosphate-induced inhibition of NEST esterase activity. Addition of 1 mM of the non-neuropathic NEST inhibitor phenylmethylsulfonyl fluoride (PMSF) decreased the current response by 28% [Figure 7.10A]. PMSF inhibits NEST esterase activity, thereby lowering the phenol and subsequent *o*-quinone production, which leads to decrease in sensor response. EIS results showed that inhibition of NEST activity by PMSF leads to increase in the charge transfer resistance [Figure 7.10B], once again indicating that R_{CT} can be used as measure of NEST inhibition [Figure 7.10B].

7.4.4. Effect of temperature on biomimetic interfaces

7.4.4.1. Temperature dependence of tBLM impedance

The temperature dependence of a tBLM's electrochemical properties was investigated. The tBLM was fabricated on gold macroelectrodes by depositing a lower leaflet of DPPTE tethering lipids, and then the upper leaflet was deposited using liposome vesicles made from 1,2-dipalmitoyl-*sn*-glycero-3-phosphocholine (DPPC) phospholipids. Both leaflets of the resulting DPPTE-DPPC tBLM had lipids with saturated hydrophobic chains. The temperature was varied from 22°C to 60°C, with tBLM incubated at each temperature until a steady state response was achieved. Figure 7.11A shows the R_M values for tBLM plotted as a function of temperature. The membrane resistance decreased to 40°C, after which it remained essentially constant up to 60°C. These results indicate that after 40°C, there was no change in insulating property of

BLM. Phospholipids with palmitoyl hydrocarbon chains have a phase transition temperature (PTT), at which the bilayer undergoes a transition from a gel state to a fluid, liquid-crystalline phase, of 40°C. These results imply that, in the gel phase, as the temperature was increased from 22°C to PTT, the membrane resistance decreased. Then, above the PTT, the BLM's resistance is essentially independent of temperature.

The fluid nature of saturated BLM was further confirmed using gramicidin channels. For ion conduction, free diffusion of the monomers in fluid BLM is necessary. It was observed that addition of gramicidin to symmetric tBLM at 22°C did not decrease membrane resistance, indicating that BLM was in a gel state. However, addition of gramicidin to symmetric tBLM at 50°C, which is above PTT of palmitoyl chains, decreased the membrane resistance from 116 $k\Omega cm^2$ to 77 $k\Omega cm^2$, confirming the fluid nature of tBLM [Figure 7.12].

7.4.4.2. Temperature dependence of NEST activity

The effect of temperature on the NEST activity was studied using a solution assay and using electrochemical NEST sensor in a temperature range of 22°C to 60°C. Figure 7.13A shows the temperature dependence of NEST activity in a solution assay. NEST activity increased from 21°C to 31°C, and above 31°C, NEST activity decreased, suggesting inhibition of NEST at higher temperatures. Fitting the Arrhenius equation to the NEST activity data between 31°C to 60°C gave activation energy of -19.3 $kJmol^{-1}K^{-1}$ [Figure 7.13B]. Similar results were obtained using the electrochemical NEST sensor. NEST activity was found to increase with temperature in a range from 21°C to 31°C. Above 31°C, the activity gradually decreased [Figure 7.14A]. At 50°C, NEST showed

only 55% of the activity obtained at 21°C. Fitting the Arrhenius equation to the decrease in NEST activity provided an activation energy of -14.8 $kJmol^{-1}K^{-1}$ [Figure 7.14B], which is similar to the value obtained in solution.. Cooling down the temperature back to 20°C did not recover the NEST activity, suggesting that higher temperatures may cause irreversible denaturation of NEST.

7.5. Conclusions

This study described the integration of tBLM and NEST biosensor interfaces with gold microelectrode arrays on glass and silicon substrates. The results indicate that highly insulating tBLMs can be deposited on microelectrodes ranging in size from 3 mm in diameter down to 50 μm in diameter. High impedance tBLMs with near-gigaohm resistances were obtained and were found to be suitable for characterization of ion conduction activity of channel peptides. The microelectrode array were also suitable for studying other membrane proteins such as NEST. NEST sensor response decreased in the presence of PMSF, indicative of NEST inhibition. NEST was found to undergo a temperature dependent deactivation above 31°C. The resulting biosensor arrays have potential applications in functional proteomics, biosensor development, and high-throughput drug screening.

Technology	0.5 μm CMOS
Chip area	0.06 mm^2
Power supply	3 Volts
Power	6 μW
Amplitude conversion linearity	50 dB
Phase conversion RMS error	2.7%
Maximum current range	100 nA
Sensitivity	78 fA

Table 7.1: The properties of impedance extraction and digitization circuit (IDC) that can be installed under each element of a sensor array. CMOS: complementary metal–oxide–semiconductor.

Electrode diameter (μm)	C_M of tBLM (nF)	R_M of tBLM (MΩ)	R_M of tBLM with gramicidin (MΩ)
50	2	2390	754
100	1	490	334
200	2	391	166
250	2	1860	3.10
400	2	398	96.9
500	3	654	14.9
800	6	471	36.3

Table 7.2: The absolute values of electrochemical properties for tBLMs deposited on Design Si-I microelectrodes on silicon.

Electrode diameter (μm)	C_M of tBLM (μFcm^{-2})	R_M of tBLM ($M\Omega cm^2$)	R_M of tBLM with gramicidin ($M\Omega cm^2$)
50	138	0.047	0.015
100	24.2	0.039	0.026
200	6.38	0.12	0.052
250	3.66	0.91	0.002
400	1.94	0.50	0.122
500	1.55	1.29	0.029
800	1.26	2.36	0.182

Table 7.3: The area normalized values of electrochemical properties for tBLMs deposited on Design Si-I microelectrodes on silicon.

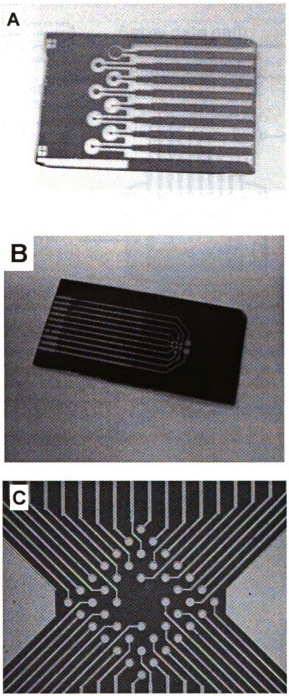

Figure 7.1: (A) First generation Design Glass-I microelectrode array deposited on glass substrate. SU8 photoresist was used as insulation layer to define the area of ten gold electrode elements. (B) Second generation Design Si-I microelectrode array deposited on silicon substrate. Silicon nitride was used as insulation layer to define the electrode size. (C) Design Si-II microelectrode array deposited on silicon substrate. Silicon nitride was used as insulation layer to define the electrode size.

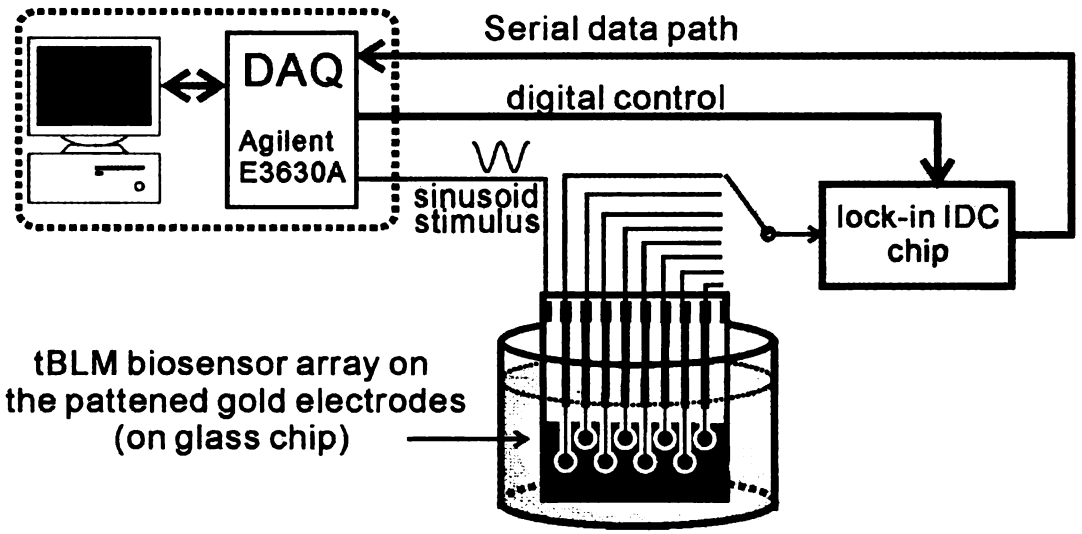

Figure 7.2: The experimental set-up for EIS measurements of tBLM using IDC (Yang, C. *et al.*, 2009).

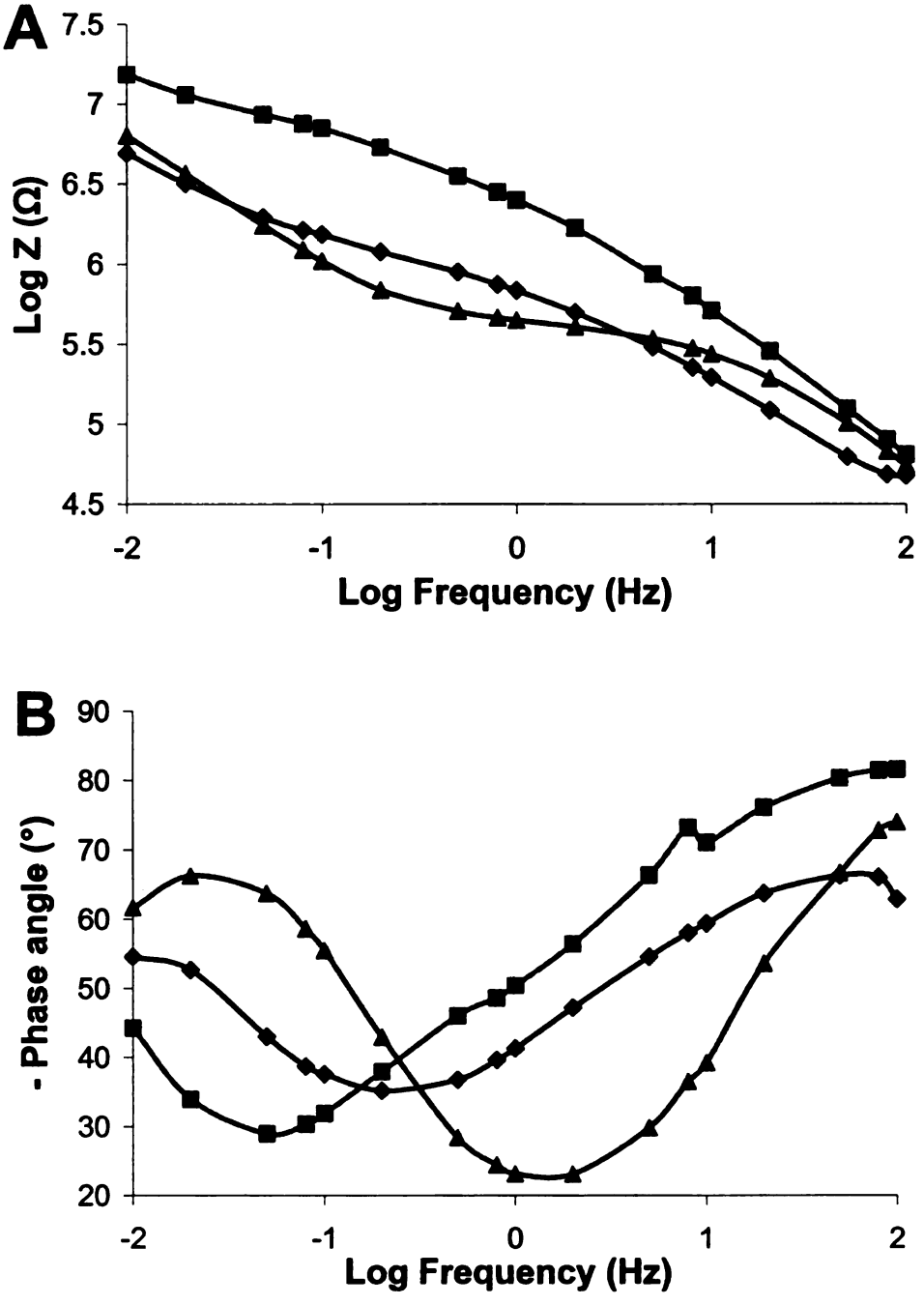

Figure 7.3: (A) Impedance (Log Z) data and (B) phase angle data were plotted as a function of Log frequency for tethering lipid monolayer (triangles) deposited on 3 mm diameter electrodes on Design Glass-I microelectrode array, tBLM formed using DOPC liposomes (squares), and for tBLM after gramicidin incorporation (diamonds) in 100 mM NaCl. Gramicidin was added to give a final concentration of 1 μM protein (monomer) in an electrolyte solution.

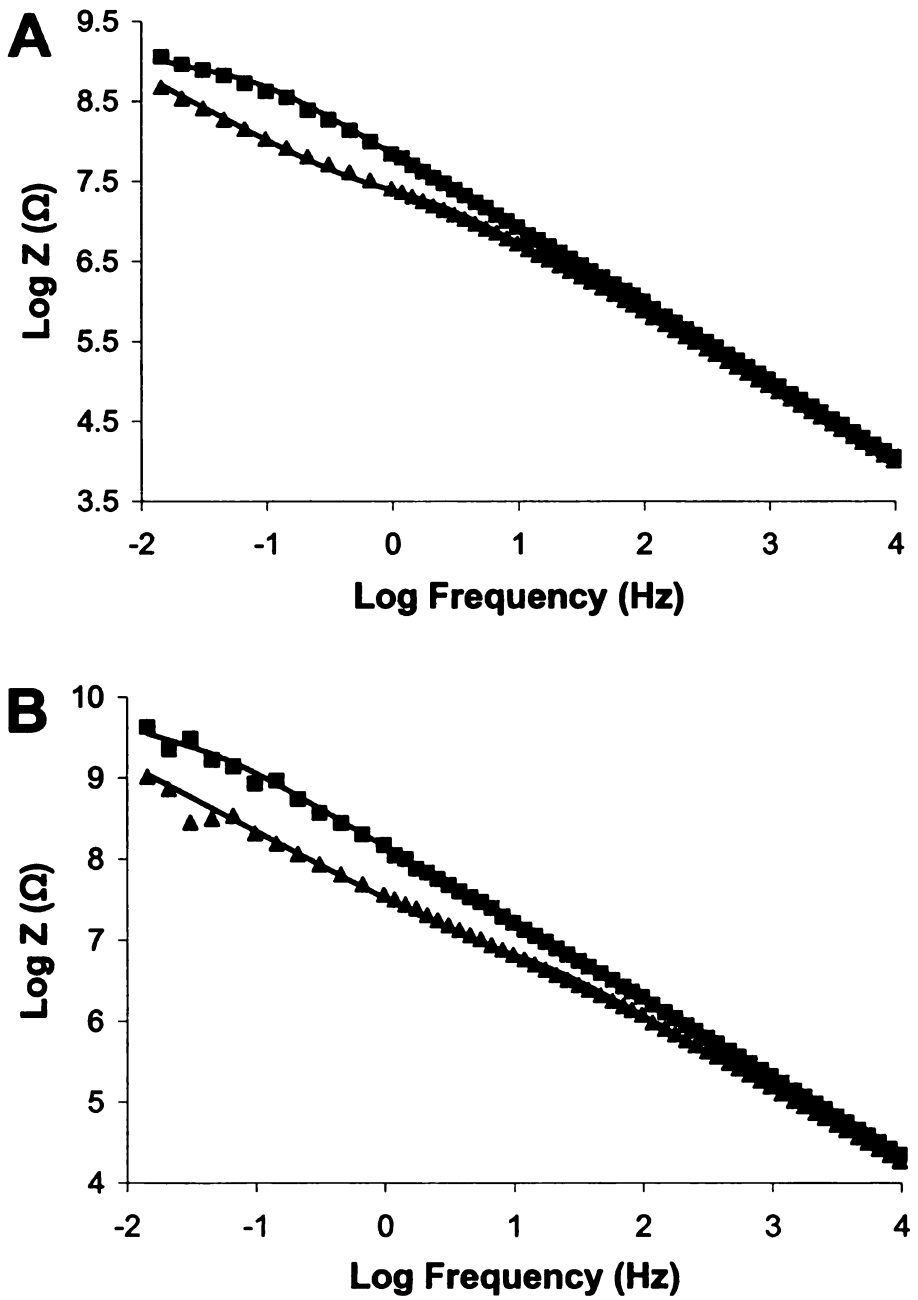

Figure 7.4: (A) Impedance (Log Z) data were plotted as a function of Log frequency for tBLM (squares) deposited on 500 μm diameter electrodes on Design Si-I microelectrode array, and for tBLM after gramicidin incorporation (triangles) in 100 mM NaCl. (B) Impedance (Log Z) data were plotted as a function of Log Frequency for tBLM (squares) deposited on 250 μm diameter electrodes on Design Si-I microelectrode array, and for tBLM after gramicidin incorporation (triangles) in 100 mM NaCl. Gramicidin was added to give a final concentration of 1 μM protein (monomer) in an electrolyte solution. An equivalent circuit shown in Figure 2.5 was fitted to the impedance data. The solid lines passing through the data points represent the model fit.

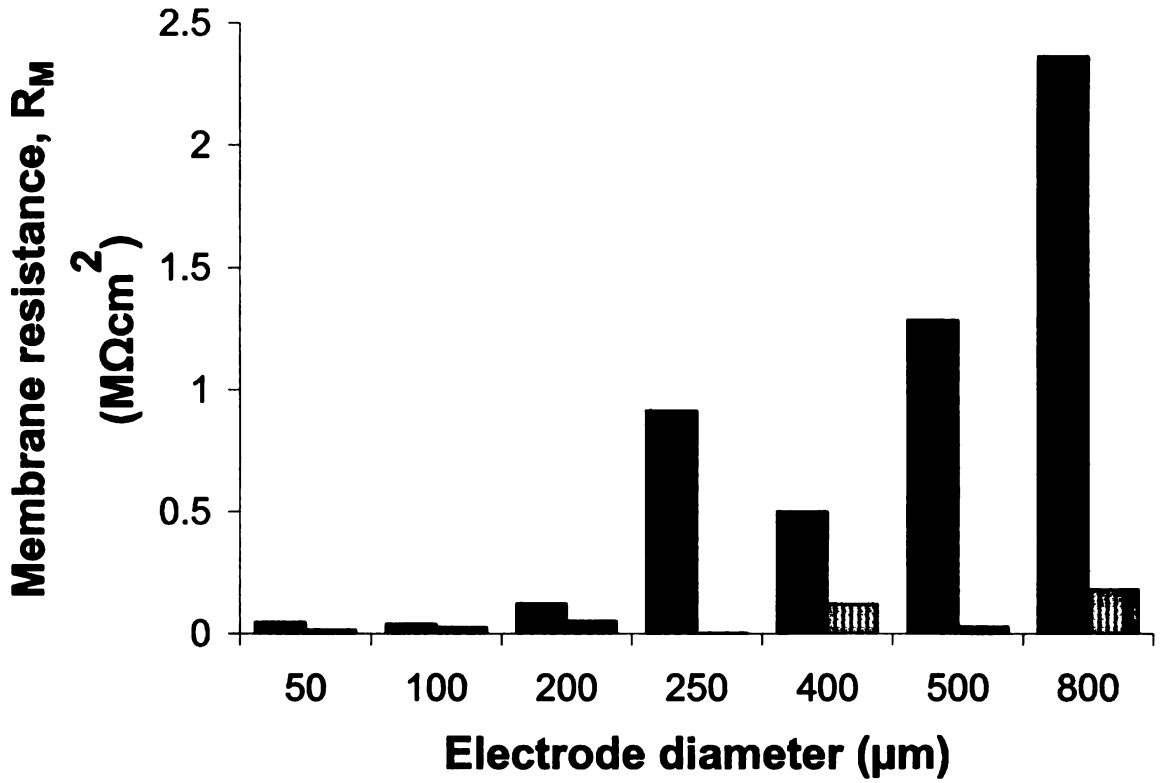

Figure 7.5: tBLM's area normalized membrane resistance before (bar with no vertical stripes) and after gramicidin incorporation (bar with vertical stripes) for tBLMs deposited on various size microelectrodes. The sealing nature of tBLMs was confirmed by the measurement of gramicidin-mediated ion conduction across tBLM.

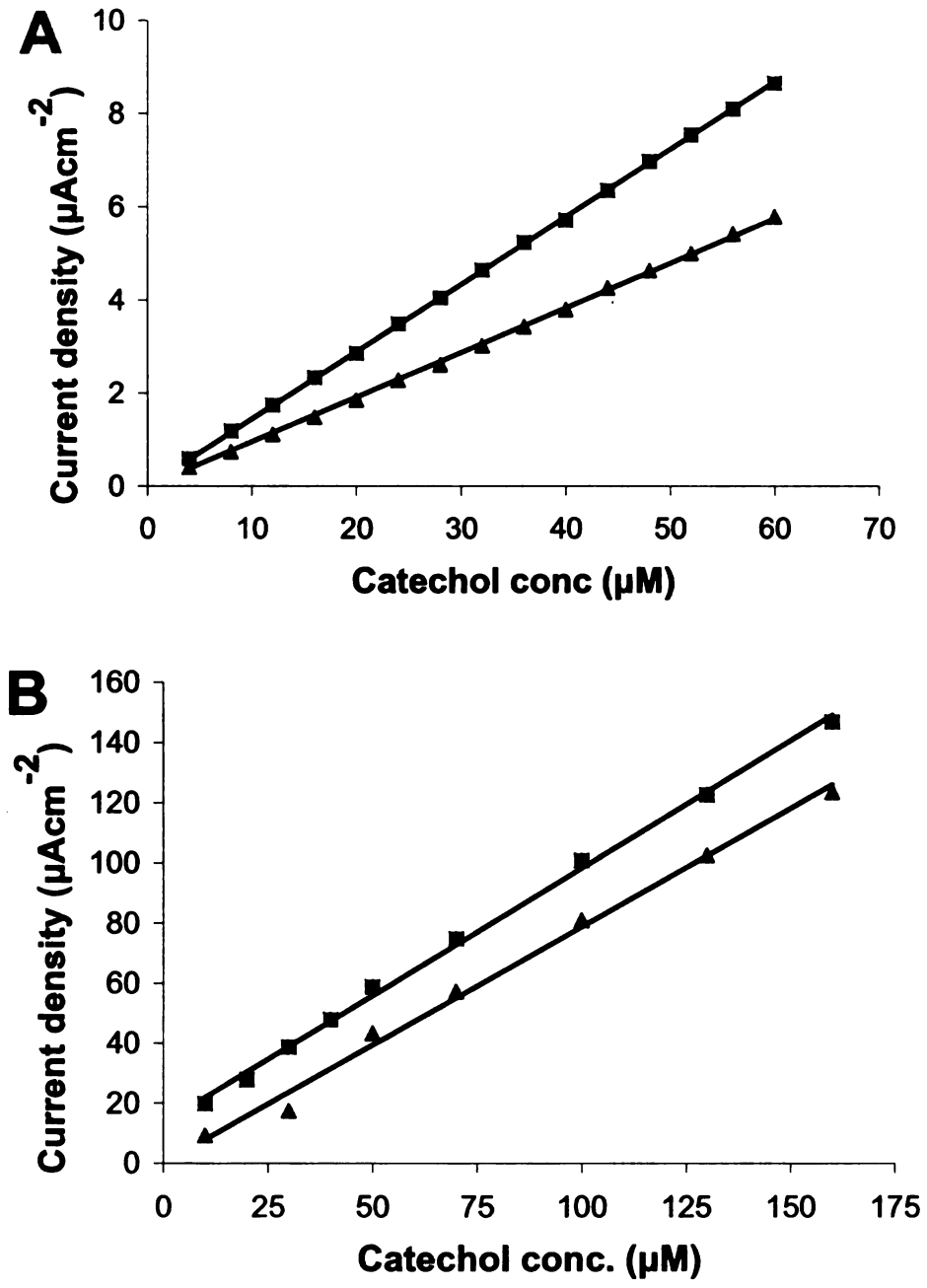

Figure 7.6: Current density of catechol sensor as a function of catechol concentration (conc.) obtained using (A) constant potential amperometry under stirring, and (B) using cyclic voltammetry.

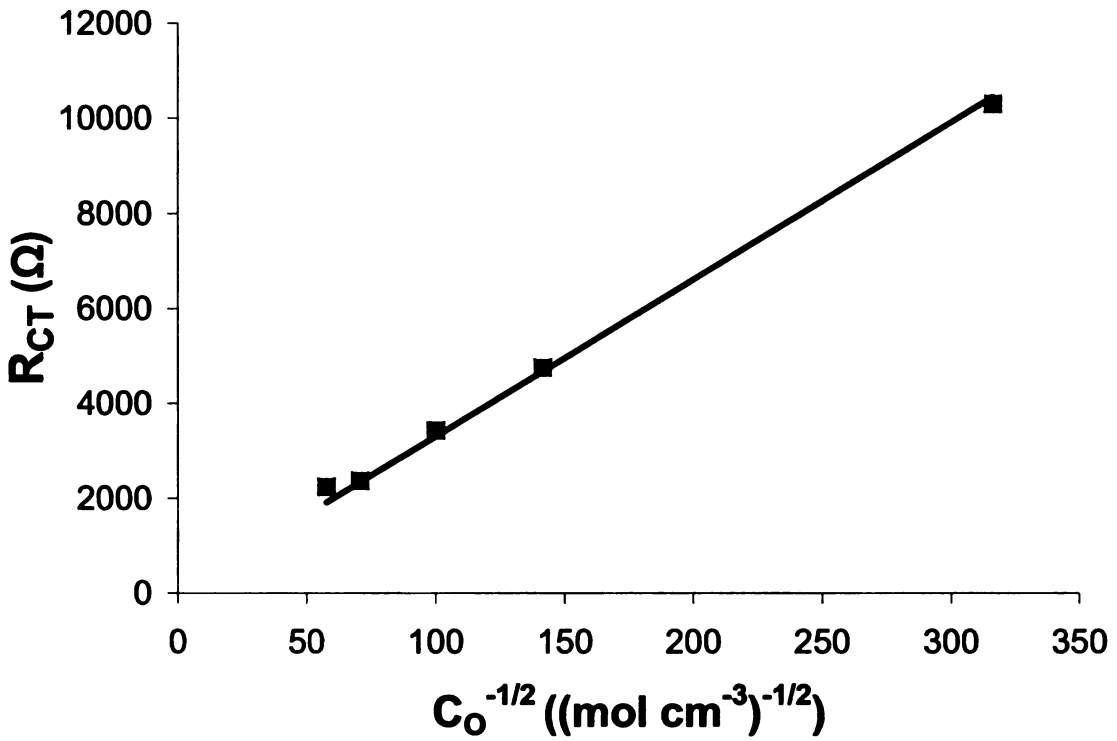

Figure 7.7: Charge transfer resistance (R_{CT}) obtained for catechol sensor as a function of catechol concentration.

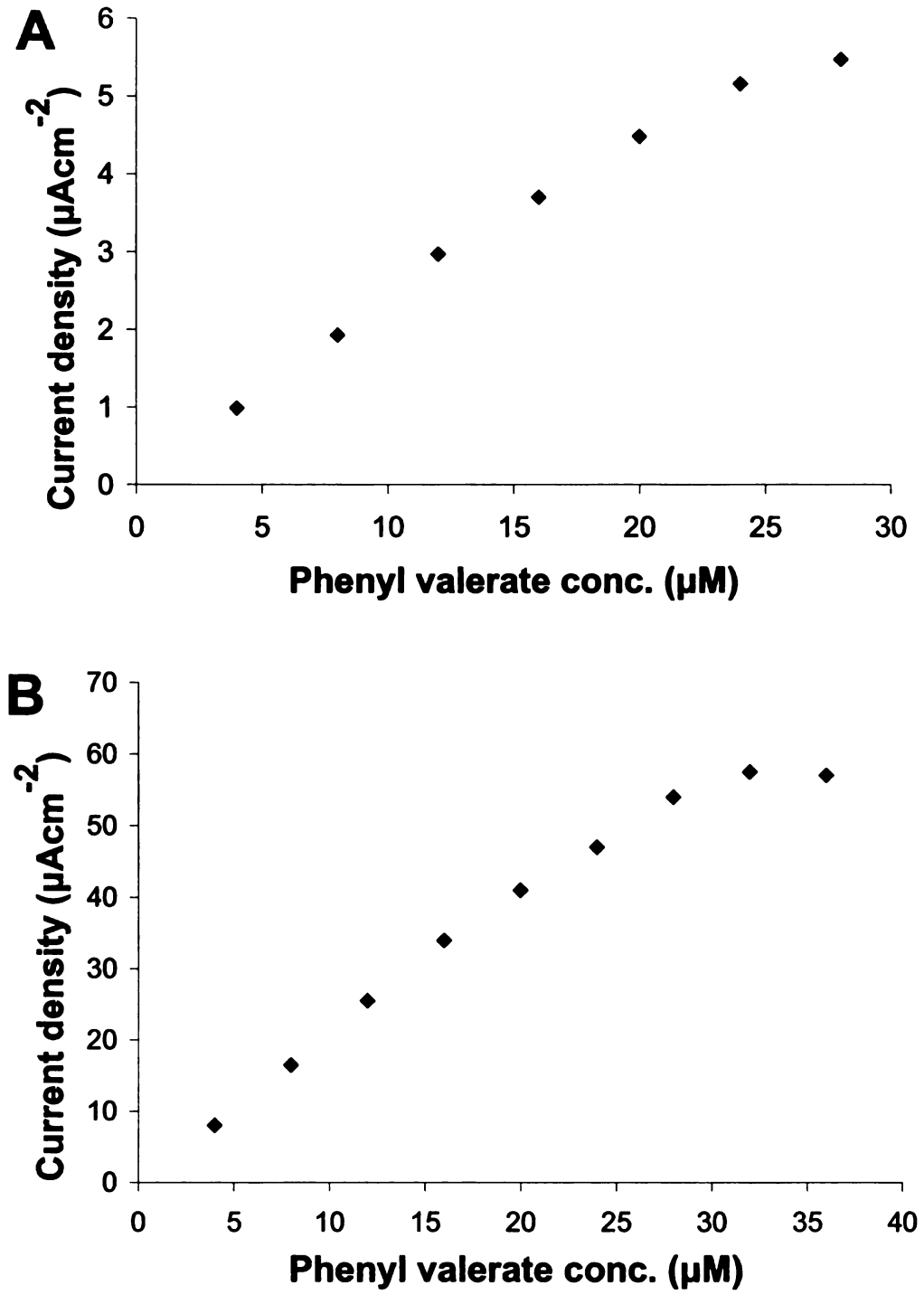

Figure 7.8: Current density of NEST sensor deposited on macroelectrode (5 mm in diameter) as a function of phenyl valerate concentration (conc.) obtained using (A) constant potential amperometry under stirring, and (B) using cyclic voltammetry.

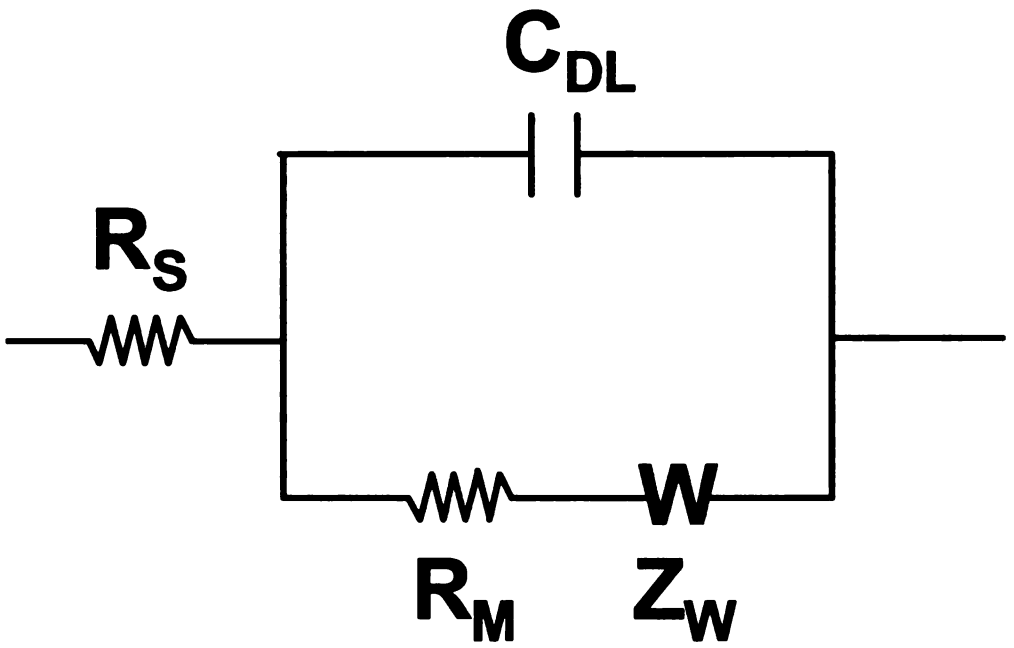

Figure 7.9: An equivalent circuit used to model impedance data from NEST sensor experiments. R_S represents the resistance of solution, C_{DL} is the double layer capacitance, R_M represents membrane resistance, and Z_W is the Warburg impedance.

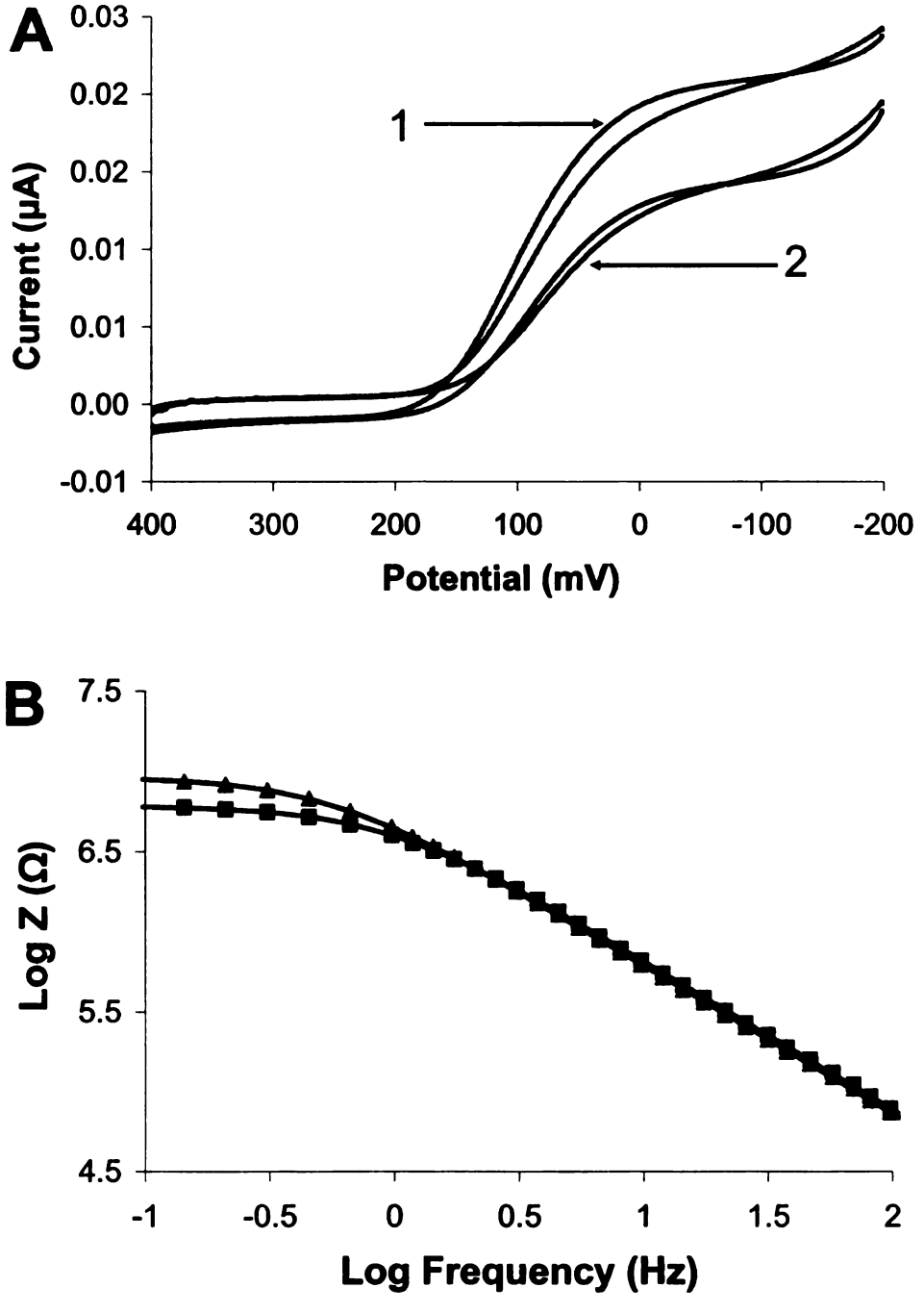

Figure 7.10: (A) Cyclic voltammogram obtained for NEST sensor on 500 μm microelectrode after addition on 10 μM phenyl valerate (curve 1), and after addition of 1 mM PMSF (curve 2). (B) Impedance data (Log Z) were plotted as a function of Log frequency for NEST sensor on 500 μm microelectrode after addition on 10 μM phenyl valerate (squares), and after addition of 1 mM PMSF (triangles). An equivalent circuit shown in Figure 7.9 was used to fit impedance data. The solid lines passing through the datapoints represents the fit.

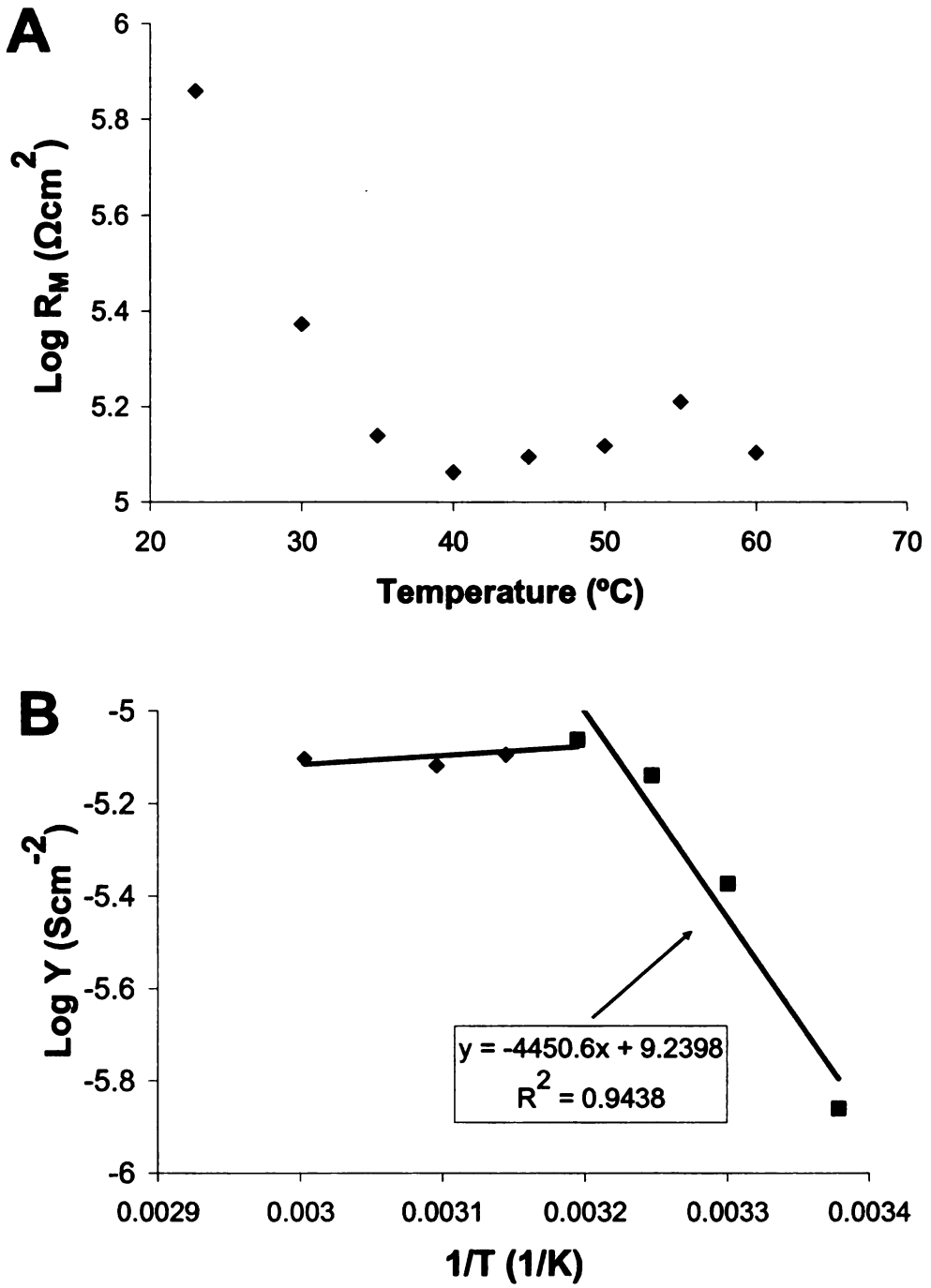

Figure 7.11: (A) Membrane resistance of DPPTE-DPPC tBLM was plotted as a function of temperature. Membrane resistance values stabilize after 40°C, which corresponds to the phase transition temperature of DPPC. (B) Admittance data (Log Y) of DPPTE-DPPC tBLM plotted as a function of 1/temperature to obtain activation energy.

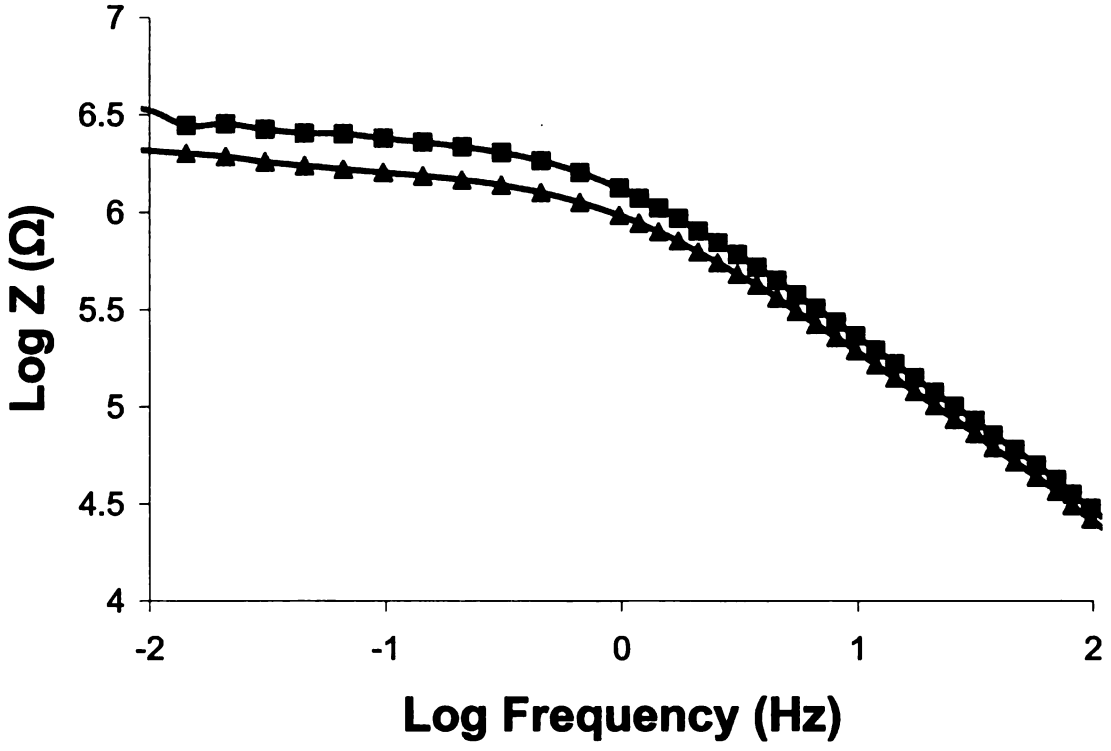

Figure 7.12: Impedance data (Log Z) was plotted as a function of Log frequency for DPPTE-DPPC tBLM at 50°C (squares), and after addition of 1 μM gramicidin at 50°C (triangles). [Electrode area is 0.2 cm^2]

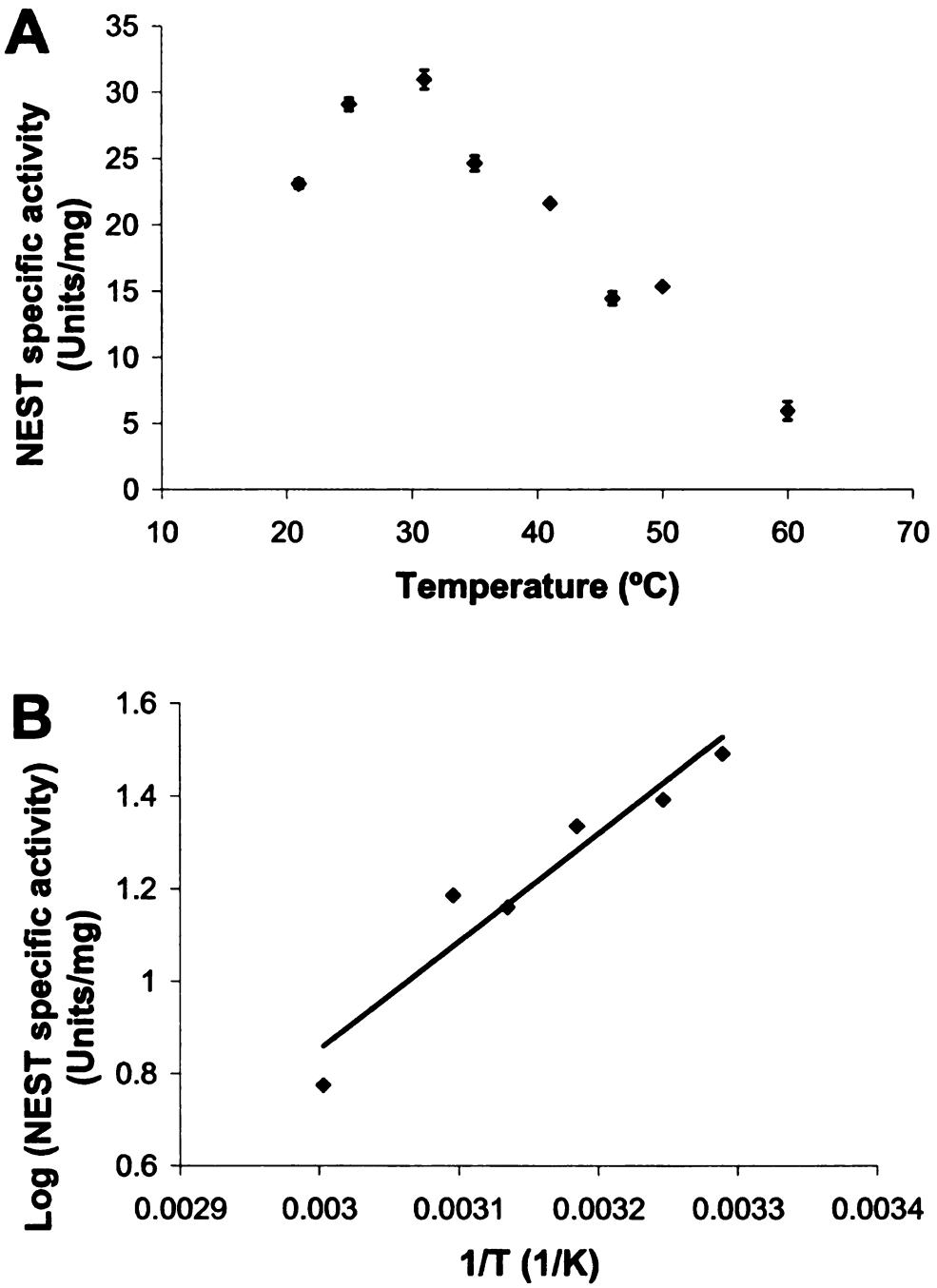

Figure 7.13: (A) NEST specific activity obtained using solution assay as a function of temperature. (B) Log(NEST specific activity) was plotted as a function of 1/temperature to obtain activation energy using solution assay of NEST.

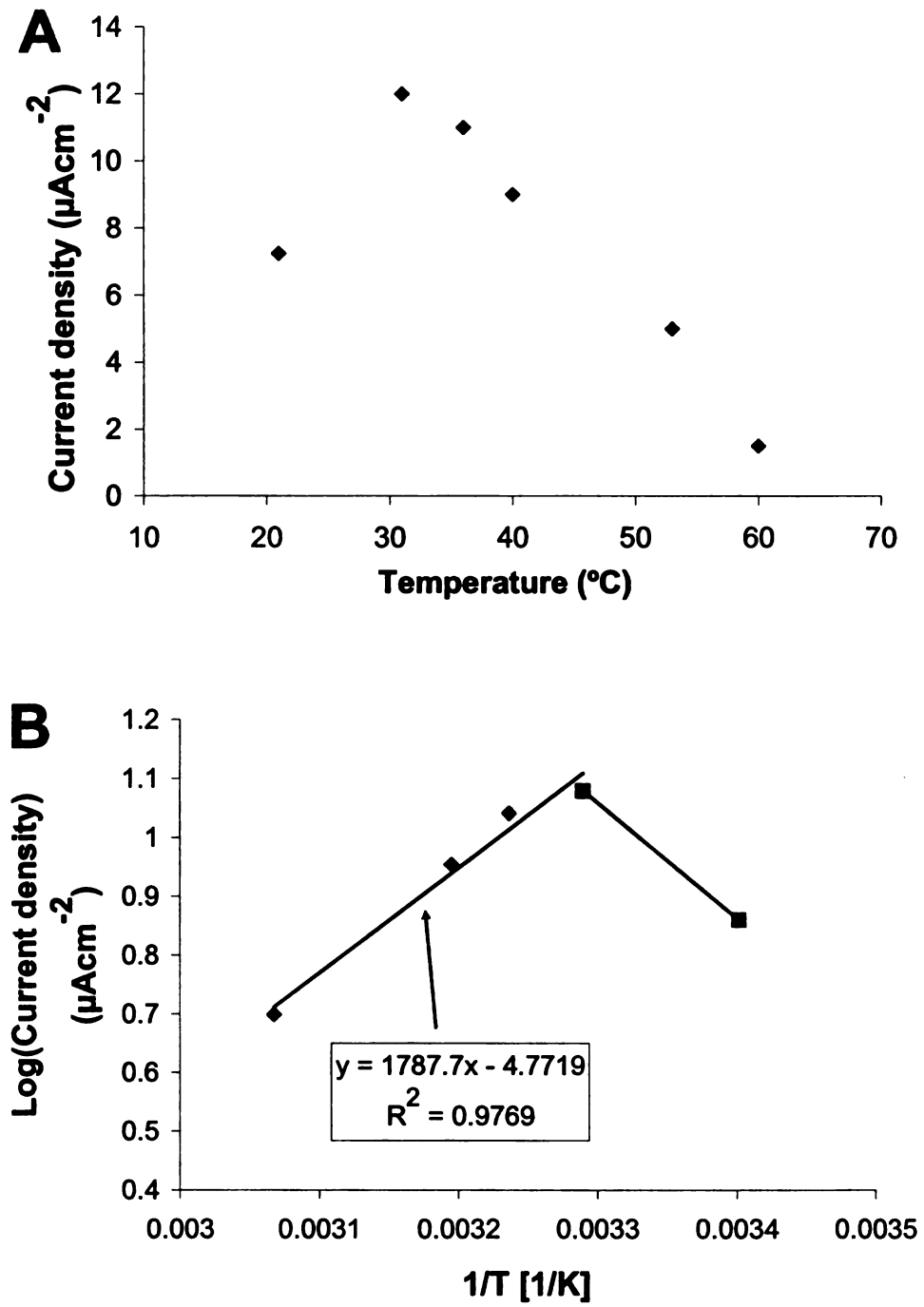

Figure 7.14: (A) Current density obtained using electrochemical sensor as a function of temperature. (B) Log(Current density) was plotted as a function of 1/temperature to obtain activation energy using electrochemical sensor of NEST.

8. REFERENCES

Andersson, M., Okeyo, G., Wilson, D., Keizer, H., Moe, P., Blount, P., Fine, D., Dodabalapur, A., and Duran, R.S. 2008. Voltage-induced gating of the mechanosensitive MscL ion channel reconstituted in a tethered lipid bilayer membrane. *Biosensors & Bioelectronics* 23(6):919-923.

Atanasov, V., Atanasova, P.P., Vockenroth, I.K., Knorr, N., and Koper, I. 2006. A molecular toolkit for highly insulating tethered bilayer lipid membranes on various substrates. *Bioconjugate Chemistry* 17(3):631-637.

Atanasov, V., Knorr, N., Duran, R.S., Ingebrandt, S., Offenhausser, A., Knoll, W., and Koper, I. 2005. Membrane on a chip: A functional tethered lipid bilayer membrane on silicon oxide surfaces. *Biophysical Journal* 89(3):1780-1788.

Atkins, J., and Glynn, P. 2000. Membrane association of and critical residues in the catalytic domain of human neuropathy target esterase. *Journal of Biological Chemistry* 275(32):24477-24483.

Bainbridge, G., Gokce, I., and Lakey, J.H. 1998. Voltage gating is a fundamental feature of porin and toxin beta-barrel membrane channels. *Febs Letters* 431(3):305-308.

Baker, G.L., Vogel, E.B., and Smith, M.R. 2008. Glass transitions in polylactides. *Polymer Reviews* 48(1):64-84.

Bard, A., and Faulkner, L. 2001. Electrochemical methods: Fundamentals and Applications. John Wiley and Sons, New York.

Becucci, L., and Guidelli, R. 2007. Kinetics of channel formation in bilayer lipid membranes (BLMs) and tethered BLMs: Monazomycin and melittin. *Langmuir* 23(10):5601-5608.

Becucci, L., Guidelli, R., Peggion, C., Toniolo, C., and Moncelli, M.R. 2005a. Incorporation of channel-forming peptides in a Hg-supported lipid bilayer. *Journal of Electroanalytical Chemistry* 576(1):121-128.

Becucci, L., Innocenti, M., Salvietti, E., Rindi, A., Pasquini, I., Vassalli, M., Foresti, M.L., and Guidelli, R. 2008. Potassium ion transport by gramicidin and valinomycin across a Ag(111)-supported tethered bilayer lipid membrane. *Electrochimica Acta* 53(22):6372-6379.

Becucci, L., Moncelli, M.R., and Guidelli, R. 2006. Impedance spectroscopy of OmpF porin reconstituted into a mercury-supported lipid bilayer. *Langmuir* 22(3):1341-1346.

Becucci, L., Moncelli, M.R., Naumann, R., and Guidelli, R. 2005b. Potassium ion transport by valinomycin across a Hg-supported lipid bilayer. *Journal of the American Chemical Society* 127(38):13316-13323.

Berquand, A., Mazeran, P.E., Pantigny, J., Proux-Delrouyre, V., Laval, J.M., and Bourdillon, C. 2003. Two-step formation of streptavidin-supported lipid bilayers by PEG-triggered vesicle fusion. Fluorescence and atomic force microscopy characterization. *Langmuir* 19(5):1700-1707.

Blake, M.S., and Gotschlich, E.C. 1982. Purification and Partial Characterization of the Major Outer-Membrane Protein of Neisseria-Gonorrhoeae. *Infection and Immunity* 36(1):277-283.

Blake, M.S., Gotschlich, E.C. 1987. Functional and immunological properties of pathogenic *Neisseria* surface proteins. Inouye M, editor. John WIley and Sons, Inc., New York.

Bunjes, N., Schmidt, E.K., Jonczyk, A., Rippmann, F., Beyer, D., Ringsdorf, H., Graber, P., Knoll, W., and Naumann, R. 1997. Thiopeptide-supported lipid layers on solid substrates. *Langmuir* 13(23):6188-6194.

Cevc, G., Svetina, S., and Zeks, B. 1981. Electrostatic Potential of Bilayer Lipid-Membranes with the Structural Surface-Charge Smeared Perpendicular to the Membrane-Solution Interface - an Extension of the Gouy-Chapman Diffuse Double-Layer Theory. *Journal of Physical Chemistry* 85(12):1762-1767.

Chang, T.S. 2009. An Updated Review of Tyrosinase Inhibitors. *International Journal of Molecular Sciences* 10(6):2440-2475.

Cornell, B.A., BraachMaksvytis, V.L.B., King, L.G., Osman, P.D.J., Raguse, B., Wieczorek, L., and Pace, R.J. 1997. A biosensor that uses ion-channel switches. *Nature* 387(6633):580-583.

Crampton, H.L., and Simanek, E.E. 2007. Dendrimers as drug delivery vehicles: non-covalent interactions of bioactive compounds with dendrimers. *Polymer International* 56(4):489-496.

Cremer, P.S., and Boxer, S.G. 1999. Formation and spreading of lipid bilayers on planar glass supports. *Journal of Physical Chemistry B* 103(13):2554-2559.

Diao, P., Jiang, D.L., Cui, X.L., Gu, D.P., Tong, R.T., and Zhong, B. 1999. Studies of structural disorder of self-assembled thiol monolayers on gold by cyclic voltammetry and ac impedance. *Journal of Electroanalytical Chemistry* 464(1):61-67.

Domanski, D.M., Klajnert, B., and Bryszewska, M. 2004. Influence of PAMAM dendrimers on human red blood cells. *Bioelectrochemistry* 63(1-2):189-191.

Du, L.W., Liu, X.H., Huang, W.M., and Wang, E.K. 2006. A study on the interaction between ibuprofen and bilayer lipid membrane. *Electrochimica Acta* 51(26):5754-5760.

Dufes, C., Uchegbu, I.F., and Schatzlein, A.G. 2005. Dendrimers in gene delivery. *Advanced Drug Delivery Reviews* 57(15):2177-2202.

Duncan, R., and Izzo, L. 2005. Dendrimer biocompatibility and toxicity. *Advanced Drug Delivery Reviews* 57(15):2215-2237.

Elie-Caille, C., Fliniaux, O., Pantigny, J., Maziere, J.C., and Bourdillon, C. 2005. Self-assembly of solid-supported membranes using a triggered fusion of phospholipid-enriched proteoliposomes prepared from the inner mitochondrial membrane. *Langmuir* 21(10):4661-4668.

Esfand, R., and Tomalia, D.A. 2001. Poly(amidoamine) (PAMAM) dendrimers: from biomimicry to drug delivery and biomedical applications. *Drug Discovery Today* 6(8):427-436.

Forshaw, P.J., Atkins, J., Ray, D.E., and Glynn, P. 2001. The catalytic domain of human neuropathy target esterase mediates an organophosphate-sensitive ionic conductance across liposome membranes. *Journal of Neurochemistry* 79(2):400-406.

Fortig, A., Jordan, R., Graf, K., Schiavon, G., Purrucker, O., and Tanaka, M. 2004. Solid-supported biomimetic membranes with tailored lipopolymer tethers. *Macromolecular Symposia* 210:329-338.

Gao, H., Feng, J., Luo, G.A., Ottova, A.L., and Tien, H.T. 2001. Some electrochemical features of supported bilayer lipid membranes. *Electroanalysis* 13(1):49-53.

Giess, F., Friedrich, M.G., Heberle, J., Naumann, R.L., and Knoll, W. 2004. The protein-tethered lipid bilayer: A novel mimic of the biological membrane. *Biophysical Journal* 87(5):3213-3220.

Ginzburg, V.V., and Balijepailli, S. 2007. Modeling the thermodynamics of the interaction of nanoparticles with cell membranes. *Nano Letters* 7:3716-3722.

Glynn, P. 2006a. A mechanism for organophosphate-induced delayed neuropathy. *Toxicology Letters* 162(1):94-97.

Glynn, P. 2006b. Neurodegeneration involving neuropathy target esterase (NTE). *Toxicology Letters* 164:S9-S9.

Graneli, A., Rydstrom, J., Kasemo, B., and Hook, F. 2003. Formation of supported lipid bilayer membranes on SiO2 from proteoliposomes containing transmembrane proteins. *Langmuir* 19(3):842-850.

Hassler, B.L., Amundsen, T.J., Zeikus, J.G., Lee, I., and Worden, R.M. 2008. Versatile bioelectronic interfaces on flexible non-conductive substrates. *Biosensors & Bioelectronics* 23(10):1481-1487.

Hassler, B.L., Dennis, M., Laivenieks, M., Zeikus, J.G., and Worden, R.M. 2007a. Mutation of Tyr-218 to Phe in Thermoanaerobacter ethanolicus secondary alcohol dehydrogenase: Effects on bioelectronic interface performance. *Applied Biochemistry and Biotechnology* 143:1-15.

Hassler, B.L., Kohli, N., Zeikus, J.G., Lee, I., and Worden, R.M. 2007b. Renewable dehydrogenase-based interfaces for bioelectronic applications. *Langmuir* 23(13):7127-7133.

Hassler, B.L., and Worden, R.M. 2006. Versatile bioelectronic interfaces based on heterotrifunctional linking molecules. *Biosensors & Bioelectronics* 21(11):2146-2154.

Hong, S.P., Leroueil, P.R., Janus, E.K., Peters, J.L., Kober, M.M., Islam, M.T., Orr, B.G., Baker, J.R., and Holl, M.M.B. 2006. Interaction of polycationic polymers with supported lipid bilayers and cells: Nanoscale hole formation and enhanced membrane permeability. *Bioconjugate Chemistry* 17(3):728-734.

Jadhav, S.R., Sui, D., Garavito, R.M., and Worden, R.M. 2008a. Fabrication of highly insulating tethered bilayer lipid membrane using yeast cell membrane fractions for measuring ion channel activity. *Journal of Colloid and Interface Science* 322(2):465-472.

Jadhav, S.R., Zheng, Y., Garavito, R.M., and Worden, R.M. 2008b. Functional Characterization of PorB class II Porin from Neisseria meningitidis using a Tethered Bilayer Lipid Membrane. *Biosensors and Bioelectronics* 24(4):831-835.

Janshoff, A., and Steinem, C. 2006. Transport across artificial membranes - an analytical perspective. *Analytical and Bioanalytical Chemistry* 385(3):433-451.

Jeuken, L.J.C., Connell, S.D., Henderson, P.J.F., Gennis, R.B., Evans, S.D., and Bushby, R.J. 2006. Redox enzymes in tethered membranes. *Journal of the American Chemical Society* 128(5):1711-1716.

Keller, C.A., and Kasemo, B. 1998. Surface specific kinetics of lipid vesicle adsorption measured with a quartz crystal microbalance. *Biophysical Journal* 75(3):1397-1402.

Klemic, K.G., Klemic, J.F., Reed, M.A., and Sigworth, F.J. 2002a. Micromolded PDMS planar electrode allows patch clamp electrical recordings from cells. *Biosensors & Bioelectronics* 17(6-7):597-604.

Klemic, K.G., Li, X.H., Klemic, J.F., Reed, M.A., and Sigworth, F.J. 2002b. Improved planar PDMS patch electrode array. *Biophysical Journal* 82(1):161A-161A.

Knoll, W., Koper, I., Naumann, R., and Sinner, E.K. 2008. Tethered bimolecular lipid membranes - A novel model membrane platform. *Electrochimica Acta* 53(23):6680-6689.

Kohli, N., Hassler, B.L., Parthasarathy, L., Richardson, R.J., Ofoli, R.Y., Worden, R.M., and Lee, I. 2006a. Tethered lipid bilayers on electrolessly deposited gold for bioelectronic applications. *Biomacromolecules* 7(12):3327-3335.

Kohli, N., Srivastava, D., Sun, J., Richardson, R.J., Lee, I.S., and Worden, R.M. 2007. Nanostructured biosensor for measuring neuropathy target esterase activity. *Analytical Chemistry* 79(14):5196-5203.

Kohli, N., Vaidya, S., Ofoli, R.Y., Worden, R.M., and Lee, I. 2006b. Arrays of lipid bilayers and liposomes on patterned polyelectrolyte templates. *Journal of Colloid and Interface Science* 301(2):461-469.

Krishna, G., Schulte, J., Cornell, B.A., Pace, R., Wieczorek, L., and Osman, P.D. 2001. Tethered bilayer membranes containing ionic reservoirs: The interfacial capacitance. *Langmuir* 17(16):4858-4866.

Krishna, G., Schulte, J., Cornell, B.A., Pace, R.J., and Osman, P.D. 2003. Tethered bilayer membranes containing ionic reservoirs: Selectivity and conductance. *Langmuir* 19(6):2294-2305.

Kropp, T.J., Glynn, P., and Richardson, R.J. 2004. The mipafox-inhibited catalytic domain of human neuropathy target esterase ages by reversible proton loss. *Biochemistry* 43(12):3716-3722.

Kugler, R., and Knoll, W. 2002. Polyelectrolyte-supported lipid membranes. *Bioelectrochemistry* 56(1-2):175-178.

Lang, H., Duschl, C., Gratzel, M., and Vogel, H. 1992. Self-Assembly of Thiolipid Molecular Layers on Gold Surfaces - Optical and Electrochemical Characterization. *Thin Solid Films* 210(1-2):818-821.

Lang, H., Duschl, C., and Vogel, H. 1994. A New Class of Thiolipids for the Attachment of Lipid Bilayers on Gold Surfaces. *Langmuir* 10(1):197-210.

Lapinski, M.M., Castro-Forero, A., Greiner, A.J., Ofoli, R.Y., and Blanchard, G.J. 2007. Comparison of liposomes formed by sonication and extrusion: Rotational and translational diffusion of an embedded chromophore. *Langmuir* 23:11677-11683.

Leroueil, P.R., Berry, S.A., Duthie, K., Han, G., Rotello, V.M., McNerny, D.Q., Baker, J.R., Orr, B.G., and Holl, M.M.B. 2008. Wide varieties of cationic nanoparticles induce defects in supported lipid bilayers. *Nano Letters* 8(2):420-424.

Lu, J., Drzal, L.T., Worden, R.M., and Lee, I. 2007. Simple fabrication of a highly sensitive glucose biosensor using enzymes immobilized in exfoliated graphite nanoplatelets Nafion membrane. *Chemistry of Materials* 19:6240-6246.

Lynch, E.C., Blake, M.S., Gotschlich, E.C., and Mauro, A. 1984. Studies of Porins - Spontaneously Transferred from Whole Cells and Reconstituted from Purified Proteins of Neisseria-Gonorrhoeae and Neisseria-Meningitidis. *Biophysical Journal* 45(1):104-107.

Malik, N., Wiwattanapatapee, R., Klopsch, R., Lorenz, K., Frey, H., Weener, J.W., Meijer, E.W., Paulus, W., and Duncan, R. 2000. Dendrimers: Relationship between structure and biocompatibility in vitro, and preliminary studies on the biodistribution of I-125-labelled polyamidoamine dendrimers in vivo. *Journal of Controlled Release* 65(1-2):133-148.

Mauro, A., Blake, M., and Labarca, P. 1988. Voltage Gating of Conductance in Lipid Bilayers Induced by Porin from Outer-Membrane of Neisseria-Gonorrhoeae. *Proceedings of the National Academy of Sciences of the United States of America* 85(4):1071-1075.

Mecke, A., Lee, D.K., Ramamoorthy, A., Orr, B.G., and Holl, M.M.B. 2005a. Synthetic and natural polycationic polymer nanoparticles interact selectively with fluid-phase domains of DMPC lipid bilayers. *Langmuir* 21(19):8588-8590.

Mecke, A., Majoros, I.J., Patri, A.K., Baker, J.R., Holl, M.M.B., and Orr, B.G. 2005b. Lipid bilayer disruption by polycationic polymers: The roles of size and chemical functional group. *Langmuir* 21(23):10348-10354.

Mecke, A., Uppuluri, S., Sassanella, T.M., Lee, D.K., Ramamoorthy, A., Baker, J.R., Orr, B.G., and Holl, M.M.B. 2004. Direct observation of lipid bilayer disruption by poly(amidoamine) dendrimers. *Chemistry and Physics of Lipids* 132(1):3-14.

Miller, C. 1986. Ion channel reconstitution. Plenum press, New York.

Minetti, C., Blake, M.S., and Remeta, D.P. 1998. Characterization of the structure, function, and conformational stability of PorB class 3 protein front Neisseria meningitidis - A porin with unusual physicochemical properties. *Journal of Biological Chemistry* 273(39):25329-25338.

Minetti, C., Blake, M.S., Tai, J.Y., and Remeta, D.P. 1997a. Characterization of native and recombinant forms of Por A and Por B gene products from Neisseria meningitidis. *Biophysical Journal* 72(2):THAM4-THAM4.

Minetti, C., Tai, J.Y., Blake, M.S., Pullen, J.K., Liang, S.M., and Remeta, D.P. 1997b. Structural and functional characterization of a recombinant PorB class 2 protein from Neisseria meningitidis - Conformational stability and porin activity. *Journal of Biological Chemistry* 272(16):10710-10720.

Moncelli, M.R., Becucci, L., and Schiller, S.M. 2004. Tethered bilayer lipid membranes self-assembled on mercury electrodes. *Bioelectrochemistry* 63(1-2):161-167.

Murakami, K., Gotschlich, E.C., and Seiff, M.E. 1989. Cloning and Characterization of the Structural Gene for the Class 2 Protein of Neisseria-Meningitidis. *Infection and Immunity* 57(8):2318-2323.

Naumann, C.A., Prucker, O., Lehmann, T., Ruhe, J., Knoll, W., and Frank, C.W. 2002. The polymer-supported phospholipid bilayer: Tethering as a new approach to substrate-membrane stabilization. *Biomacromolecules* 3(1):27-35.

Naumann, M., Rudel, T., and Meyer, T.F. 1999. Host cell interactions and signalling with Neisseria gonorrhoeae. *Current Opinion in Microbiology* 2(1):62-70.

Naumann, R., Schiller, S.M., Giess, F., Grohe, B., Hartman, K.B., Karcher, I., Koper, I., Lubben, J., Vasilev, K., and Knoll, W. 2003a. Tethered lipid Bilayers on ultraflat gold surfaces. *Langmuir* 19(13):5435-5443.

Naumann, R., Walz, D., Schiller, S.M., and Knoll, W. 2003b. Kinetics of valinomycin-mediated K+ ion transport through tethered bilayer lipid membranes. *Journal of Electroanalytical Chemistry* 550:241-252.

Neher, E., Sakmann, B., and Steinbach, J.H. 1978. Extracellular Patch Clamp - Method for Resolving Currents through Individual Open Channels in Biological-Membranes. *Pflugers Archiv-European Journal of Physiology* 375(2):219-228.

Niwa, O., and Tabei, H. 1994. Voltammetric Measurements of Reversible and Quasi-Reversible Redox Species Using Carbon-Film Based Interdigitated Array Microelectrodes. *Analytical Chemistry* 66(2):285-289.

Ohlsson, P.A., Tjarnhage, T., Herbai, E., Lofas, S., and Puu, G. 1995. Liposome and Proteoliposome Fusion onto Solid Substrates, Studied Using Atomic-Force Microscopy, Quartz-Crystal Microbalance and Surface-Plasmon Resonance - Biological-Activities of Incorporated Components. *Bioelectrochemistry and Bioenergetics* 38(1):137-148.

Ottovaleitmannova, A., and Tien, H.T. 1992. Bilayer Lipid-Membranes - an Experimental System for Biomolecular Electronic Devices Development. *Progress in Surface Science* 41(4):337-445.

Pantoja, R., Nagarah, J.M., Starace, D.M., Melosh, N.A., Blunck, R., Bezanilla, F., and Heath, J.R. 2004. Silicon chip-based patch-clamp electrodes integrated with PDMS microfluidics. *Biosensors & Bioelectronics* 20(3):509-517.

Peng, Z.Q., Tang, J.L., Han, X.J., Wang, E.K., and Dong, S.J. 2002. Formation of a supported hybrid bilayer membrane on gold: A sterically enhanced hydrophobic effect. *Langmuir* 18(12):4834-4839.

Qi, H.L., Tai, J.Y., and Blake, M.S. 1994. Expression of Large Amounts of Neisserial Porin Proteins in Escherichia-Coli and Refolding of the Proteins into Native Trimers. *Infection and Immunity* 62(6):2432-2439.

Radler, J., Strey, H., and Sackmann, E. 1995. Phenomenology and Kinetics of Lipid Bilayer Spreading on Hydrophilic Surfaces. *Langmuir* 11(11):4539-4548.

Raguse, B., Braach-Maksvytis, V., Cornell, B.A., King, L.G., Osman, P.D.J., Pace, R.J., and Wieczorek, L. 1998. Tethered lipid bilayer membranes: Formation and ionic reservoir characterization. *Langmuir* 14(3):648-659.

Ramsden, C. 2009. Suicide-inactivation of tyrosinase by catecholic substrates. *Febs Journal* 276:30-30.

Richter, R., Mukhopadhyay, A., and Brisson, A. 2003. Pathways of lipid vesicle deposition on solid surfaces: A combined QCM-D and AFM study. *Biophysical Journal* 85(5):3035-3047.

Richter, R.P., Berat, R., and Brisson, A.R. 2006. Formation of solid-supported lipid bilayers: An integrated view. *Langmuir* 22(8):3497-3505.

Richter, R.P., and Brisson, A.R. 2005. Following the formation of supported lipid bilayers on mica: A study combining AFM, QCM-D, and ellipsometry. *Biophysical Journal* 88(5):3422-3433.

Rudel, T., Schmid, A., Benz, R., Kolb, H.A., Lang, F., and Meyer, T.F. 1996. Modulation of Neisseria porin (PorB) by cytosolic ATP/GTP of target cells: Parallels between pathogen accommodation and mitochondrial endosymbiosis. *Cell* 85(3):391-402.

Sackmann, E. 1996. Supported membranes: Scientific and practical applications. *Science* 271(5245):43-48.

Sauerbrey, G. 1959. Verwendung Von Schwingquarzen Zur Wagung Dunner Schichten Und Zur Mikrowagung. *Zeitschrift Fur Physik* 155(2):206-222.

Schiller, S.M., Naumann, R., Lovejoy, K., Kunz, H., and Knoll, W. 2003. Archaea analogue thiolipids for tethered bilayer lipid membranes on ultrasmooth gold surfaces. *Angewandte Chemie-International Edition* 42(2):208-211.

Schneiter, R., and Daum, G. 2006. Extraction of yeast lipids. Xiao W, editor. Humana Press, Totowa, N.J. .

Sigworth, F.J., and Neher, E. 1980. Single Na+ Channel Currents Observed in Cultured Rat Muscle-Cells. *Nature* 287(5781):447-449.

Sinner, E.K., and Knoll, W. 2001. Functional tethered membranes. *Current Opinion in Chemical Biology* 5(6):705-711.

Snejdarkova, M., Rehak, M., and Otto, M. 1997. Stability of bilayer lipid membranes on different metallic supports. *Biosensors & Bioelectronics* 12(2):145-153.

Song, J.M., Minetti, C., Blake, M.S., and Colombini, M. 1998. Successful recovery of the normal electrophysiological properties of PorB (class 3) porin from Neisseria meningitidis after expression in Escherichia coli and renaturation. *Biochimica Et Biophysica Acta-Biomembranes* 1370(2):289-298.

Song, J.M., Minetti, C., Blake, M.S., and Colombini, M. 1999. Meningococcal PorA/C1, a channel that combines high conductance and high selectivity. *Biophysical Journal* 76(2):804-813.

Starr, T.E., and Thompson, N.L. 2002. Fluorescence pattern photobleaching recovery for samples with multi-component diffusion. *Biophysical Chemistry* 97(1):29-44.

Stora, T., Lakey, J.H., and Vogel, H. 1999. Ion-channel gating in transmembrane receptor proteins: Functional activity in tethered lipid membranes. *Angewandte Chemie-International Edition* 38(3):389-392.

Terrettaz, S., Mayer, M., and Vogel, H. 2003. Highly electrically insulating tethered lipid bilayers for probing the function of ion channel proteins. *Langmuir* 19(14):5567-5569.

Tien, H.T. 1995. Self-Assembled Lipid Bilayers as a Smart Material for Nanotechnology. *Materials Science & Engineering C-Biomimetic Materials Sensors and Systems* 3(1):7-12.

Tien, H.T., and Ottova, A.L. 2000. Membrane Biophysics as viewed from experimental bilayer lipid membranes. Elsevier, New York.

Tien, H.T., and Ottova, A.L. 2001. The lipid bilayer concept and its experimental realization: from soap bubbles, kitchen sink, to bilayer lipid membranes. *Journal of Membrane Science* 189(1):83-117.

Vockenroth, I.K., Atanasova, P.P., Long, J.R., Jenkins, A.T.A., Knoll, W., and Koper, I. 2007. Functional incorporation of the pore forming segment of AChR M2 into tethered bilayer lipid membranes. *Biochimica et Biophysica Acta (BBA) - Biomembranes* 1768(5):1114-1120.

Wang, J., and Richardson, R.J. 2003. Tentative models for the three-dimensional structure of the NTE esterase domain (NEST): Predictions from threading and docking. *Toxicological Sciences* 72:1487.

Wang, X.B., and Li, M. 2003. Automated electrophysiology: High throughput of art. *Assay and Drug Development Technologies* 1(5):695-708.

Weel, J.F.L., Hopman, C.T.P., and Vanputten, J.P.M. 1991. Bacterial Entry and Intracellular Processing of Neisseria-Gonorrhoeae in Epithelial-Cells -

Immunomorphological Evidence for Alterations in the Major Outer-Membrane Protein Pib. *Journal of Experimental Medicine* 174(3):705-715.

Weel, J.F.L., and Vanputten, J.P.M. 1991. Fate of the Major Outer-Membrane Protein-P.Ia in Early and Late Events of Gonococcal-Infection of Epithelial-Cells. *Research in Microbiology* 142(9):985-993.

Weiss, M.S., Abele, U., Weckesser, J., Welte, W., Schiltz, E., and Schulz, G.E. 1991. Molecular Architecture and Electrostatic Properties of a Bacterial Porin. *Science* 254(5038):1627-1630.

Weiss, M.S., and Schulz, G.E. 1992. Structure of Porin Refined at 1.8 Angstrom Resolution. *Journal of Molecular Biology* 227(2):493-509.

Woodhouse, G., King, L., Wieczorek, L., Osman, P., and Cornell, B. 1999. The ion channel switch biosensor. *Journal of Molecular Recognition* 12(5):328-334.

Yang, C., Jadhav, S.R., Worden, R.M., and Mason, A.J. 2009. Compact low-power impedance extractor and digitizer for sensor array microsystems. *IEEE Journal of Solid-State Circuits* 44(10):2844-2855.

Yin, P., Burns, C.J., Osman, P.D.J., and Cornell, B.A. 2003. A tethered bilayer sensor containing alamethicin channels and its detection of amiloride based inhibitors. *Biosensors & Bioelectronics* 18(4):389-397.

Young, J.D.E., Blake, M., Mauro, A., and Cohn, Z.A. 1983. Properties of the Major Outer-Membrane Protein from Neisseria-Gonorrhoeae Incorporated into Model Lipid-Membranes. *Proceedings of the National Academy of Sciences of the United States of America-Biological Sciences* 80(12):3831-3835.

Zebrowska, A., and Krysinski, P. 2004. Incorporation of Na+,K+-ATP-ase into the thiolipid biomimetic assemblies via the fusion of proteoliposomes. *Langmuir* 20(25):11127-11133.

Zeng, F.W., and Zimmerman, S.C. 1997. Dendrimers in supramolecular chemistry: From molecular recognition to self-assembly. *Chemical Reviews* 97(5):1681-1712.

Zhou, J.H., Wu, J.Y., Hafdi, N., Behr, J.P., Erbacher, P., and Peng, L. 2006. PAMAM dendrimers for efficient siRNA delivery and potent gene silencing. *Chemical Communications* (22):2362-2364.